



**FACULTY
OF MATHEMATICS
AND PHYSICS**
Charles University

DOCTORAL THESIS

Anna Kuzminova

**Modification of polymeric substrates by means of
non-equilibrium plasma**

Department of Macromolecular Physics

Supervisor of the doctoral thesis: doc. RNDr. Ondřej Kylián, Ph.D.

Study programme: Physics

Specialization: Biophysics, Chemical and Macromolecular Physics

Prague 2018

I declare that I carried out this doctoral thesis independently, and only with the cited sources, literature and other professional sources.

I understand that my work relates to the rights and obligations under the Act No. 121/2000 Coll., the Copyright Act, as amended, in particular the fact that the Charles University has the right to conclude a license agreement on the use of this work as a school work pursuant to Section 60 paragraph 1 of the Copyright Act.

In..... date.....

signature

Název práce: Modifikace polymerních substrátů pomocí nízkoteplotního plazmatu

Autor: Anna Kuzminova

Katedra: Katedra makromolekulární fyziky

Vedoucí doktorské práce: doc. RNDr. Ondřej Kylián, Ph.D.

Abstrakt: Úprava povrchů polymerních materiálů pomocí nízkoteplotního plazmatu je téma, které si získává rostoucí pozornost, což je dáno širokým spektrem možných aplikací. Jako příklad je možné uvést úpravu polymerních fólií používaných v potravinářském průmyslu, kde je možné pomocí plazmatu výrazně vylepšit funkčnost těchto materiálů (např. zlepšit možnost jejich potisku nebo zvýšit jejich bariérové vlastnosti). V rámci této disertační práce byly studovány dvě možné strategie modifikace polymerů. První z nich byla založena na opracování polymerů atmosférickým plazmatem. Hlavní pozornost byla věnována studiu vlivu atmosférického plazmatu na povrchové vlastnosti 8 běžně používaných polymerů, zejména na jejich chemické složení, morfologii a smáčivost. Mimo to bylo prokázáno, že vystavení polymerů atmosférickému plazmatu vede ke změně jejich mechanických vlastností, k jejich nezanedbatelnému odleptávání a v určitých případech i ke zvýšení jejich biokompatibility. Druhou studovanou strategií bylo povlakování polymerů tenkými funkčními nanokompozitními vrstvami obsahujícími kovové nanočástice. Byly vyvinuty povlaky s regulovatelným antibakteriálním účinkem, laditelnou smáčivostí i povlaky, které zvyšují bariérové vlastnosti polymerních fólií.

Klíčová slova: dielektrický bariérový výboj, plazmová úprava, nanočástice, nanokompozitní tenké vrstvy, plazmový polymer, antibakteriální povrchy.

Title: Modification of polymeric substrates by means of non-equilibrium plasma

Author: Anna Kuzminova

Department: Department of Macromolecular Physics

Supervisor of the doctoral thesis: doc. RNDr. Ondřej Kylián, Ph.D.

Abstract: Processing of polymeric materials by means of non-equilibrium plasma is a topic that reaches increasing attention, which is due to the wide range of possible applications. As an example can be mentioned processing of polymeric foils used for

food packaging, where plasma treatment enables to improve their functional properties (e.g. increase their printability or enhance their barrier properties). In the frame of this PhD. thesis two different strategies suitable for the modification of polymeric materials were followed. The first one was based on treatment of polymers by atmospheric plasma. The main attention was devoted to the investigation of influence of atmospheric pressure plasma on surface properties of 8 commonly used polymers, namely on their chemical composition, morphology and wettability. In addition, it was observed that plasma treatment causes also alteration of their mechanical properties, may lead to their substantial etching and in some cases improves their biocompatibility. The second studied strategy was based on coating of polymers with thin functional nanocomposite films based on metal nanoparticles. Coatings with controllable antibacterial character, tailor-made wettability or with improved barrier properties were developed.

Keywords: dielectric barrier discharge, plasma treatment, nanoparticles, nanocomposite thin film, plasma polymer, antibacterial surfaces.

Acknowledgments

First of all I would like to thank my supervisor Doc. RNDr. Ondřej Kylián PhD. for giving me the opportunity to do this interesting doctorate work, for his advices, help and patience. I am also grateful to Prof. RNDr. Hynek Biederman DrSc, doc. Ing. Andrey Shukurov PhD. and Doc. Danka Slavínská CSc for their interest and consultations in the course of my doctorate.

I am very thankful to my colleagues Mgr. Jan Hanuš PhD., Mgr. Martin Petr PhD., Mgr. Artem Shelemin Ph.D., Mgr. Jiří Kratochvíl and Mgr. Mykhailo Vaidulych for invaluable assistance in experimental work and XPS measurements. I would like to thank to RNDr. Pavel Solar PhD. for his assistance in all computer-related issues and Mgr. Jaroslav Kousal PhD. for consultations concerning ellipsometry measurements. Thanks go too other current and former members of Department of Macromolecular Physics: Mgr. Iurii Melnichuk PhD., Mgr. Ivan Gordeev PhD., Mgr. Anton Serov PhD., Mgr. Daniil Nikitin, Mgr. Pavel Pleskunov, Mgr. Marcela Búryová and Mgr. Vratislava Dvořáková.

I am very indebted to Mgr. Ivan Khalakhan PhD. (Department of Surface and Plasma Physics) for SEM measurements and RNDr. Jana Beranová PhD. (Faculty of Science, Charles University) for performance of biological tests.

Special thanks to the group of Prof. Dr. Franz Faupel from Christian Albrechts University at Kiel for the possibility of short-term research stay in their laboratory. At this point I have to acknowledge specifically Mgr. Oleksandr Polonskyi PhD. for his help in organization of ICP-MS measurements and assistance in experiments during my research stay in Germany.

I would like to thank RNDr. Milan Šimek PhD. from the Institute of Plasma Physics of the Czech Academy of Sciences for the opportunity to be in his team as well as to other group members: Mgr. Vladislava Fantova, Ing. Eva Doležalová PhD. and Ing. Václav Prukner PhD. for their contribution and involvement within my work.

Certainly, a lot of thanks are addressed to my parents, my brother Andrei and all friends for their untold support and encouragement. And finally I am incredibly grateful to my son Illia and husband Sergii for their love and just for that they are with me.

Objectives of the Doctoral Thesis This

This work is focused on modification of surfaces of polymeric materials by two ways:

- 1) dielectric barrier discharge (DBD) treatment at atmospheric pressure in ambient air;
- 2) deposition of functional thin films.

The first part of this thesis represents a completely new scientific topic at the Department of Macromolecular Physics. The aim was to develop, test and optimize process of surface modification of common polymers by means of dielectric barrier discharge. Detail investigation of influence of atmospheric pressure air plasma on 8 selected polymers was performed with intention to elucidate changes in their surface properties (wettability, surface energy, morphology, chemical composition, mechanical and bioadhesive properties) induced by the plasma treatment. In addition, the etching rates of polymers by DBD plasma were determined in order to understand etching of more complex pathogenic microorganisms.

The second part of this thesis is dedicated to the development of thin functional coatings and their characterization by various techniques. The main attention was paid to the preparation of silver-based nanocomposite coatings with tunable antibacterial activity. Besides this, coatings with tailorable wettability as well as barrier thin films were also studied.

Contents

Acknowledgments	iv
Objectives of the Doctoral Thesis This.....	v
1 Introduction.....	1
1.1 Plastic materials: brief history and current state-of-the-art	1
1.2 Modification of polymers by plasmas	4
1.2.1 DBD plasma treatment of polymers.....	5
1.2.2 Functional coatings	9
1.2.2.1 Plasma polymerization and plasma polymers.....	10
1.2.2.2 Plasma polymer based nanocomposites.....	14
2 Experimental	18
2.1 DBD treatment of polymers	18
2.2 Deposition systems.....	20
2.2.1 Deposition of pHMDSO and SiO _x thin films.....	20
2.2.2 Deposition of Ag nanoparticles.....	21
2.2.3 Fabrication of Ag-based nanocomposites	22
2.3 Plasma diagnostics methods and methods for physico-chemical characterization of samples	23
2.3.1 Optical emission spectroscopy (OES).....	23
2.3.2 Atomic Force microscope (AFM)	24
2.3.3 Scanning Electron Microscopy (SEM)	26
2.3.4 X-ray Photoelectron Spectroscopy (XPS).....	27
2.3.5 Ellipsometry	28
2.3.6 Inductively coupled plasma mass spectroscopy (ICP-MS).....	29
2.3.7 Nano Dynamic Mechanical Analysis (nanoDMA)	30
2.3.8 Permeability measurements	32

2.3.9	UV-VIS Spectrophotometry.....	34
2.3.10	Wettability measurements.....	34
2.3.11	Mass loss measurements	37
2.4	Protocols of biological tests	38
2.4.1	Cell growth on polymeric foils	38
2.4.2	Evaluation of sporicidal effect of DBD plasma	39
2.4.3	Antibacterial activity of nanocomposites.....	41
3	Results and discussion	43
3.1	DBD treatment of polymers	44
3.1.1	DBD plasma characterization	44
3.1.2.1	<i>Chemical composition</i>	<i>48</i>
3.1.2.2	<i>Surface morphology</i>	<i>54</i>
3.1.2.3	<i>Wettability and surface energy.....</i>	<i>58</i>
3.1.2.4	<i>Mechanical properties of Nylon and PET foils</i>	<i>62</i>
3.1.2.5	<i>Plasma etching of conventional polymers.....</i>	<i>63</i>
3.1.3	Application of DBD plasma.....	65
3.1.3.1	<i>Influence of DBD plasma on cell growth</i>	<i>65</i>
3.1.3.2	<i>Effect of DBD plasma on bacterial spores of B. Subtilis</i>	<i>68</i>
3.2	Preparation of functional thin films.....	71
3.2.1	SiO _x and plasma polymerized HMDSO.....	71
3.2.2	Antibacterial nanocomposites	76
3.2.2.1	<i>Characterization of silver nanoparticles.....</i>	<i>76</i>
3.2.2.2	<i>Characterization of Ag/pHMDSO and Ag/SiO_x nanocomposites</i>	<i>79</i>
3.2.2.3	<i>Ion release from Ag/pHMDSO and Ag/SiO_x nanocomposites</i>	<i>83</i>
3.2.2.4	<i>Antibacterial activity of Ag/pHMDSO and Ag/SiO_x nanocomposites.....</i>	<i>88</i>

3.2.2.5	<i>Final remarks and preliminary results related to the role of Ag nanoparticles oxidation.....</i>	91
3.2.3	Coatings with tailorable wettability	95
3.2.4	Investigation of barrier properties	99
4	Conclusions	103
	Bibliography	107
	List of tables.....	123
	List of abbreviations	124
	Author's contribution	125
	List of publications.....	126

1 Introduction

1.1 Plastic materials: brief history and current state-of-the-art

It is very difficult to imagine a modern life without plastics, i.e. materials that use man-made polymers. Plastic as a material surrounds us everywhere and represents an integral part of today's world. Over the last decade, worldwide plastic production has reached 300 million tons per year¹ - around 59 million tons are manufactured only in Europe each year. Evaluation of positive extra EU-28² trade balance of plastics manufacturing was estimated to be approximately 16.5 billion euros for year 2015. These values continue to grow with rate of 4% annually that is associated with an increase in public demand [1].

The first documentation on the use of polymers dates since around 1600 BC [2]. Initially, the manufacture of plastics included natural materials such as natural rubber or caoutchouc, eggs, treated cattle corn or processed milk proteins [3]. Since the nineteenth century natural polymers began to be replaced by synthetic ones. In the early of twentieth century, the term 'plastic' for synthetic polymers was first introduced by L.H. Beakeland during the development of Bakelite [4].

The term 'plastic' is derived from the Greek word 'plastikos', meaning 'ability to be formed or molded' and refers to ability of synthetic polymers to acquire different forms and shapes, such as for example foils, bottles, blocks, granules or fibers. Development of synthetic polymers has led to the emergence of a variety of plastic types, including thermoplastics, elastomers, thermosets [5], or recently even biodegradable polymers [6]. Synthetic polymeric materials, depending on their structure, may exhibit unique and advantageous properties (e.g. flexibility, relatively high thermal resistance and stability, high strength-to-weight ratio, mechanical resistance, optical transparency, stiffness or barrier properties) as compared to other

¹ In the text presented data were collected by PlasticEurope for year 2015.

² Extra EU-28 refers to transactions with all countries except of Europe Union (EU) countries, consisting of 28 Member States.

materials. Because of this fact, plastics have become widely employed in diversity of industries in the last century, that range for instance from food packaging to flexible electronics, or from textile industry to biomedical field. The PlasticEurope statistics reported that the largest percentage of consumption of polymer materials is achieved in the packaging industry that is estimated to be about 39 % of all market sectors in 2015.

Nowadays, the most demanded and utilized modern plastics are thermoplastics. This is due to the fact that thermoplastic can be easily moulded under heating and since they become liquid at the melting point and hard again after cooling, they can be easily recycled.

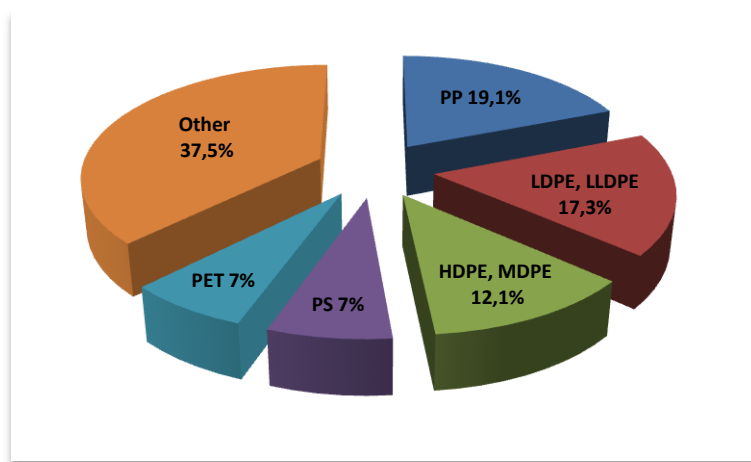


Figure 1.1 Statistics of European plastic demand. Data were collected by the Association of Plastics Manufacturers in Europe.

As can be seen in **Figure 1.1**, the most often used plastic material is **polypropylene (PP)** that was discovered in 1954. PP has numerous functional advantages such as lightness, stability, recycling ability or chemical resistance. However, apart from these, popularity of polypropylene is also connected with its low production costs making it widely used in many fields, e.g. in food industry, for packaging, production of house hold items, building industry and others.

The second place on demand takes **polyethylene (PE)**. First synthesis of polyethylene dates back to 1933. Polyethylene materials are graded depending on branching degree and their density. The most popular types of PE are high density polyethylene (HDPE), medium density polyethylene (MDPE), low density polyethylene (LDPE) and linear low-density polyethylene (LLDPE). HDPE, MDPE and LDPE are different kinds of PE that exhibit different average density. HDPE has density from $0.945 \text{ g}\cdot\text{cm}^{-3}$ to $0.965 \text{ g}\cdot\text{cm}^{-3}$ and low degree of branching. These parameters determine the high strength of HDPE. LDPE has higher level of branching than HDPE and lower density (around $0.930\text{-}0.935 \text{ g}\cdot\text{cm}^{-3}$), so it is weaker, but more flexible than HDPE. Both HDPE and LDPE are extensively used in packaging industry, including production of food containers or wrapping foils.

Polyethylene terephthalate (PET) was licensed in year 1941. PET, which combines unique properties such as lightweight, transparency and ability to prevent moisture and gases from penetrating, is one of the worthy candidates for storing beverages and drinking water and thus to replace glass bottles. In Europe the annual demand of PET reaches 7% of the main applied field, which corresponds to approximately 3 million tons of produced PET, where the largest part is used for production of bottles.

Not less significant in the history of polymers is **nylon**. It was invented in the 30s of the last century and then started to be used for production of synthetic fibers in textile industry and in military industry. Nylon is chemically and thermally resistant (the highest melting point is 256°C), elastic, durable and has good gas barrier properties. These properties are behind the successful use of nylon in the food field, including for example food packaging or heat-resistant bags for ovens.

However, apart from the above-mentioned well-known plastics, other polymers are also in demand on the market and receive an increasing interest. The first example represents **polyethylene naphthalate (PEN)** that belongs to the same polyester group as PET, but has better thermal resistance and better barrier characteristics against oxygen, carbon dioxide or vapor transition. In spite of its higher cost, PEN is nowadays considered as the best option for packaging of beer and carbonated beverages. **Polyether ether ketone (PEEK)** and **polymethyl methacrylate (PMMA)** belong to group of so-called engineering thermoplastics that are applied in the fields that require high mechanical strength and high resistance to temperature or

chemical exposure (e.g. in automotive or aerospace industries). Moreover, PEEK can be used in medicine for manufacturing of medical instruments to be capable to withstand sterilization procedures or as substitute of metals in the case of medical implants. PMMA is due to its properties (transparency, hardness) that are close to the ones of conventional silica like glass also called acrylic glass. However, in contrast to silica glass PMMA is light, unbreakable and mechanically processable and thus represents a clear alternative to silica glass.

Finally, the great interest is recently devoted to biodegradable plastics, i.e. polymers that can be decomposed over the time [6], [7]. This popularity is connected with environment pollution by plastic wastes connected with intensive human consumption. **Polylactic acid (PLA)** is one of the representatives of such polymers. Biodegradable properties of PLA occur as a consequence of degradation of ester functional groups that are under the action of hydrolysis converted into non-toxic components. Among diversity of PLA applications are agricultural foils, food and waste packaging, wound and skin protective coverage, drainage in stomatology and medicine in general.

To summarize, a wide choice of polymers is available on the market. These materials offer unique characteristics and may be use, depending on a particular application, to replace other materials such as glasses or metals.

1.2 Modification of polymers by plasmas

Though polymeric materials have numerous advantages mentioned in the previous chapter their use is in some cases limited by their improper surface properties. This relates for instance to their low surface energy/wettability, which in turn causes a poor printability or dye-uptake needed for food or beverage packaging or textile industry, low adhesion of additional functional coatings important for instance for printable electronics, insufficient chemical reactivity making them hard to be functionalized by different kinds of biomolecules, or unsatisfactory biocompatibility that is crucial for biomedical applications. In addition, common polymers often

exhibit relatively high oxygen, carbon dioxide or water vapor permeability that may be determinative in the case of food packages for the shelf-life of the foodstuff and its quality. Because of this there is a clear demand on improving surface characteristics of polymers and thus different strategies were proposed. They can be divided into two main groups:

- Surface treatment
- Coating of polymers with thin films with desired properties

As it will be briefly discussed in the subsequent subchapters, plasma-based techniques may be used in both cases.

1.2.1 DBD plasma treatment of polymers

There are different possible ways how to modify surface properties of polymers, such as processes based on wet chemistry, flame treatment or biological processing [8]. Among them the surface treatment based on the use of non-equilibrium plasma experienced an increasing interest in the last decades [9]. This is connected with the fact that plasma-based methods are in general time and cost effective, due to the absence of hazardous solvents they are environmentally friendly, suitable for treatment of temperature sensitive materials like polymers and last, but not least, plasma treatment affects only the top most layers of treated objects and does not compromise their bulk properties. Thanks to these characteristics plasma treatment is highly interesting for treatment and functionalization of polymers widely used in biomedicine or tissue engineering [10].

The common way of plasma generation is based on the application of external electric field to a gas at reduced or atmospheric pressure [11], [12]. This field accelerates light electrons to energies sufficient for ionization of neutral atoms and molecules of a gas. By this way new electron-ion pairs are formed. As soon as the production of charged species counterbalances their losses (recombination), self-sustained plasma is ignited. Since the majority of species in laboratory plasma are neutrals (typical level of ionization in such plasmas reaches 1 electron or ion per 10^6

neutrals) whose temperature stays close to the room temperature such produced plasmas are often termed low-temperature. Naturally, accelerated electrons may cause not only ionization, but they may also excite both atoms and molecules or dissociate molecules presented in the plasma bulk. Products of these reactions may subsequently interact with each other that lead to formation of species originally not presented in the working gas. As a result of this, plasma is rather complex medium consisting of electrons, positively and negatively charged ions, radicals, neutral particles as well as photons that are emitted during radiative de-excitation of excite species. All of these may interact with an object that is introduced to the plasma and alter its surface properties via various routes. In general, different processes may be activated such as grafting (insertion of a specific functional group on the surface through chemical bonding), activation (generation of free radicals on the surface), film deposition (deposition of a thin layers adherent to the surface) or etching (chemical or physical ablation of the material surface). The above mentioned processes obviously may act simultaneously and their contribution is strongly linked with particular process parameters (pressure, power, geometry, working gas mixture etc.).

There are numerous options how to modify polymer surfaces using low-temperature plasmas. In this work an atmospheric pressure air **dielectric barrier discharge (DBD)** was selected as this kind of plasma enables low-cost operation compatible with the low-cost nature of common polymers.

First DBD was ozone discharge tube developed by W.Siemens in 1857 that served as a device for ozonizing air [13]. Initially researches were mainly dedicated to oxygen and nitrogen oxide generation in DBDs for water treatment. Lately, further investigations were focused on the physical processes of micro-discharges occurring in DBDs and on their possible applications for surface modifications, oxidation of CO₂ laser, pollution control [14], generation of UV-radiation [15], flat plasma displays [16], or recently in medicine for sterilization [17].

Dielectric barrier discharges may have different configurations (both planar and cylindrical arrangement of electrodes), but their common feature is the presence of at least one dielectric layer, preferably glass, ceramic materials or thin polymer film, between powered electrodes (see **Figure 1.2**) that limits a DC current in the inter-

electrode gap space and prevents thus an arc transition. Due to the presence of dielectric barrier alternating voltage has to be applied for the plasma generation. The usual driving voltage in DBD with discharge gap of several millimeters is around 3-15 kV at frequencies ranging from 500 Hz to 500 kHz.

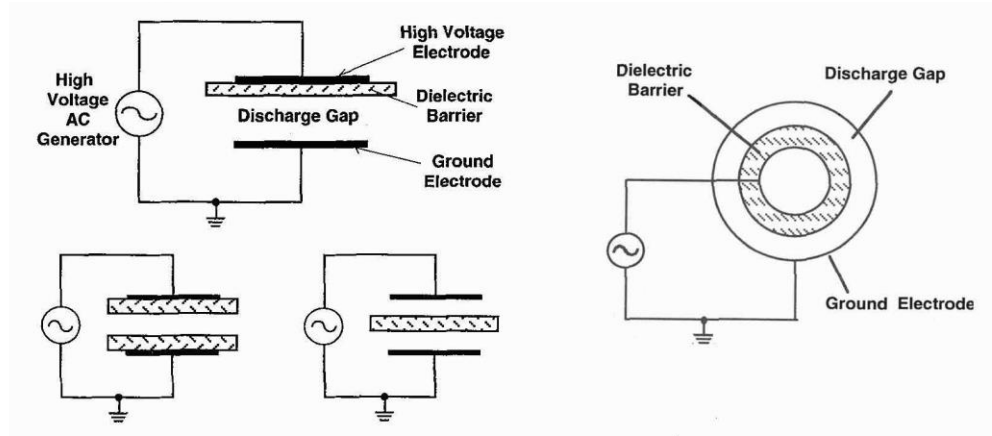


Figure 1.2 DBD setups with different configurations. *Adopted from [18].*

As soon as the applied voltage exceeds certain value (so-called *breakdown voltage*), ions and electrons are generated in the space between the electrodes and plasma is ignited. The breakdown in a gas at atmospheric pressure leads in most of cases to the appearance of numerous individual micro-discharges [12]. Gas composition, pressure, dielectric material and electrode geometry influence only the properties of micro-discharges such as filament radius, charge transfer density, etc. In contrast, the number of micro-discharges per unit of time depends on the applied power: higher the power the larger number of micro-discharges is generated at the same electrode parameters. This allows scale-up of DBD configuration from small laboratory setups to industrial large-scale devices, which makes DBDs highly suitable for technological applications [19],[20].

There are already many publications devoted to polymer surface modification by DBDs operated in different gas mixtures (e.g. argon, oxygen, nitrogen, helium or their combinations) (e.g. [21], [22]). However, the use of these gases is relatively expensive and not profitable for real industrial applications and thus there is a clear

demand to employ laboratory air as working gas. It was demonstrated by different groups that dielectric barrier discharges sustained in air at atmospheric pressure are capable to effectively modify polymeric surfaces (e.g. polypropylene [23], poly(ethylene terephthalate) [24], [25], [26], polyurethane [25], polyimides [27], polyethylene [28], [29], poly(ethylene naphthalate) [30], poly(methyl methacrylate) [31] or polyamides [32]–[34]). Based on these studies it was clearly proved that DBD treatment in most of cases causes oxidation of polymeric substrates that in turn enhances their surface energy and with it connected wettability. However, it is worth noting that these changes are not temporally stable: with increasing storage time the surface energy and wettability of plasma treated polymers gradually decrease. This effect, which is termed **ageing** or **hydrophobic recovery**, is due to the reorientation of polar functional groups on polymeric surfaces, outward-diffusion of low-weight oligomers or additives and/or by accumulation of air-born impurities [35], [36]. The typical time scale of these processes is several days or weeks, at a maximum.

Besides the oxidation and alteration of wettability induced by DBD treatment, exposure of polymers to atmospheric pressure plasma commonly results also in changes of their surface morphology - DBD treated polymers often exhibit higher roughness as compared to untreated ones (e.g. [24], [27], [31]). Modification of morphology of polymeric materials is frequently ascribed to their etching that is not spatially homogeneous (e.g. due to different etching rates of crystalline and amorphous regions in polymeric structure [37]). The etching is, however, not important only for surface nano-roughening, but it can be used for sterilization/decontamination of surfaces as well. As highlighted in literature [38], the strategy based on etching may be in many cases more favorable as compared to plasma-based inactivation of biological pathogens as it assures complete removal of biological contamination from the surface and thus guarantees the safety of treated materials.

To conclude, DBD plasmas operated in air at atmospheric pressure were shown in the last two decades to be valuable tool for modification of surfaces of polymeric materials as well as for their sterilization/decontamination. This was documented in numerous works (e.g. [23]–[27], [39]–[41]). However, in these studies different DBD set-ups and operational conditions were implemented that make the comparison of

reached results for different polymers almost impossible. Thus, the main aim of this study is to investigate and compare the effect of DBD treatment on wider range of common polymers. For this purpose, the treatment of different polymers (PP, PE, nylon 6,6, PEN, PEEK, PMMA, PLA) introduced in *subchapter 1.1* was performed in the same DBD system and under identical operational conditions. Main attention was devoted to changes of chemical composition, surface energy and morphology induced by plasma treatment. In addition, etching rates of all polymers were evaluated as well that was followed by experiments focused on the possibility to etch also biomolecules or bacteria. Finally, the possibility to use plasma treatment for improving cell adhesion was tested.

1.2.2 Functional coatings

The second strategy for improvement of properties of commonly used polymeric foils is their coating. Among techniques that were developed for this purpose considerable attention is paid to the deposition of functional coatings by plasma based methods at low pressures. Typical examples are barrier coatings that lowers permeability of gases through polymeric foils (e.g. [42]–[45]), bio-adhesive or bio-repellent coatings that assure required biocompatibility (e.g. [46]–[49]), coatings with adjustable wettability including the possibility to produce super-hydrophilic or super-hydrophobic surfaces [50]–[52] or antibacterial thin films (e.g. [53]–[55]). Important classes of materials for above-listed examples are **plasma polymers**, i.e. macromolecular solids formed during plasma polymerization, or their **nanocomposites** with metal nanoparticles. These two types of materials will be briefly introduced in the following two subchapters.

1.2.2.1 Plasma polymerization and plasma polymers

Plasma polymerization is a process, which occurs as the result of introduction of organic precursor into the plasma³. There are different models of plasma polymerization kinetics [56]–[60]. In general, polymerization process is described by three stages similar to conventional radical polymerization: (i) **initiation**, (ii) **propagation** and (iii) **termination** (**Figure 1.3**) [58].

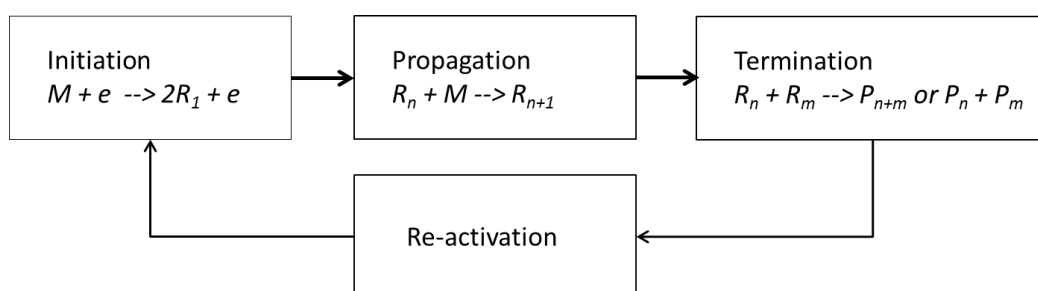


Figure 1.3 Illustration of polymerization process, where M is monomer, e stands for electron, R is a radical and P means polymer or neutral molecule [58].

The initiation takes place in the plasma volume predominantly through collisional processes between energetic electrons and organic molecules. The most probable reaction is in this case dissociation of precursor that leads to formation of radicals. Created radicals are highly reactive toward addition reactions with other bi-radicals or with unsaturated molecules that leads to propagation of polymeric chain or toward recombination with other radicals (termination reaction). In contrast to conventional polymerization scheme the formed molecules may be re-activated via additional electron impact and thus the plasma polymerization may be viewed as a sequence of termination reactions and re-activation of the products. Formed species subsequently condense on a substrate introduced into the plasma that gives rise to a solid organic thin film. However, it is important to stress that, re-activation and termination reactions may occur not only in the gas phase [58], but also on the surface of growing films [59].

³ In this case the process is also called plasma-enhanced chemical vapor deposition (PE-CVD).

More complex model of plasma polymerization was suggested by Yasuda and co-workers [56]. In this model, the synthesis of the coating is supposed to result from a balance between deposition processes and simultaneous film etching, i.e. via competitive ablation and polymerization (CAP, see **Figure 1.4**). The ablation occurs through highly reactive radicals that can be produced in the plasma volume and react at the plasma-growing film interface to form stable molecules (e.g., water, CO₂, CO) that desorb from the film. As these molecules cannot take part in the growth of the film anymore they are either pumped-out of the reactor or are re-activated through electron collisions in the plasma bulk.

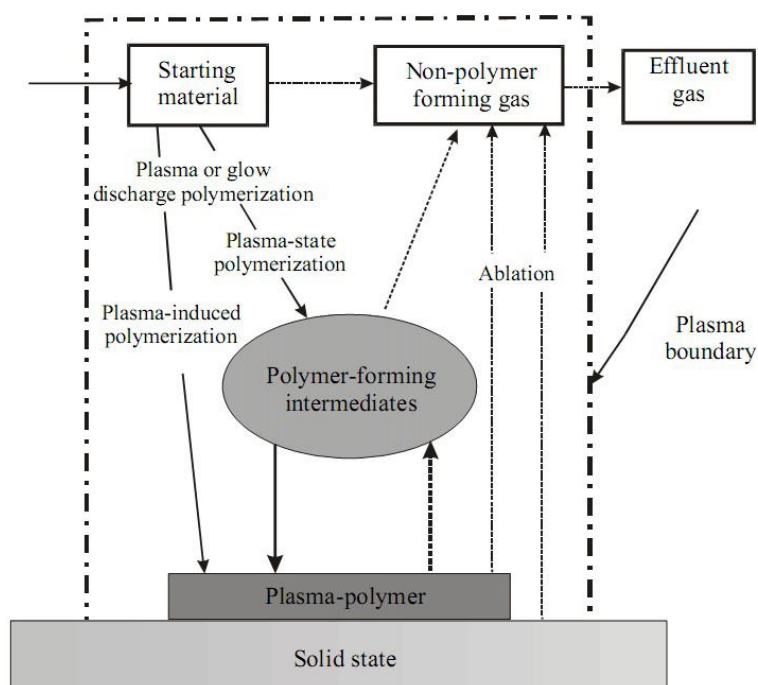


Figure 1.4 Overall model of plasma polymerization in glow discharge by H. Yasuda.
Taken from [56].

The plasma polymerization scheme was further extended by D'Agostino [57] who included ions as important species for the film growth. In his model, which is termed ion Activated Growth Model (AGM), it is assumed that surfaces of growing films are

continuously exposed to impinging ions. As the ions may have energies reaching several tens of eV they may induce chemical bond breaking. This leads to the formation of surface dangling bonds which can act as preferential adsorption sites for reactive species coming from the plasma. In other words, the precursor can be incorporated in the growing film through a surface reaction with a radical site (e.g. via the opening of a double bond). This process is termed plasma-induced polymerization.

Despite the differences in proposed models of plasma polymerization, the common point is that this process is highly stochastic. As a result of this plasma polymers have, in contrast to conventional polymers that are composed of regularly repeating units (**Figure 1.5, a**), irregular chemical structure that is characterized by randomly distributed short chains, frozen radicals and with more or less cross-linked structure (**Figure 1.5, b**). The structure, chemical and physical properties of produced plasma polymers may be tailored by many operational parameters [61]. The main parameters that may be used for control of the properties of plasma polymers are type and geometrical configuration of the deposition reactor (for examples of different configuration, please see **Figure 1.6**), feeding gas, flow rate of the monomer and delivered power⁴, pressure of working gas, frequency of the RF discharge excitation voltage, substrate temperature and its position.

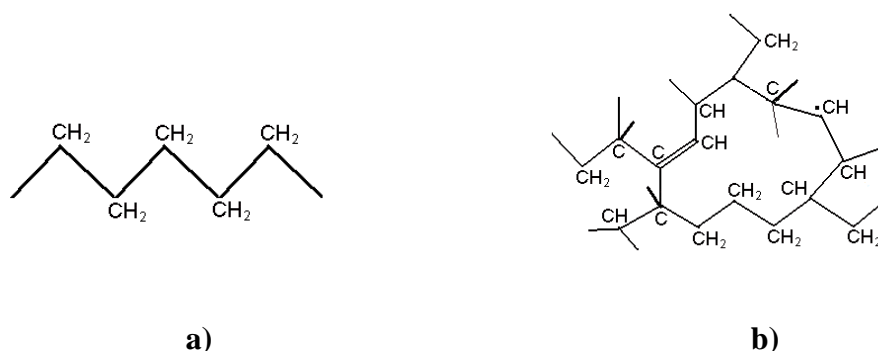


Figure 1.5 Chemical structure of conventional PE (**a**) and hypothetical structure of hydrocarbon plasma polymer (**b**) *Taken from [62].*

⁴ Flow rate and delivered power determine the energy deposited per monomer, i.e. so called Yasuda parameter.

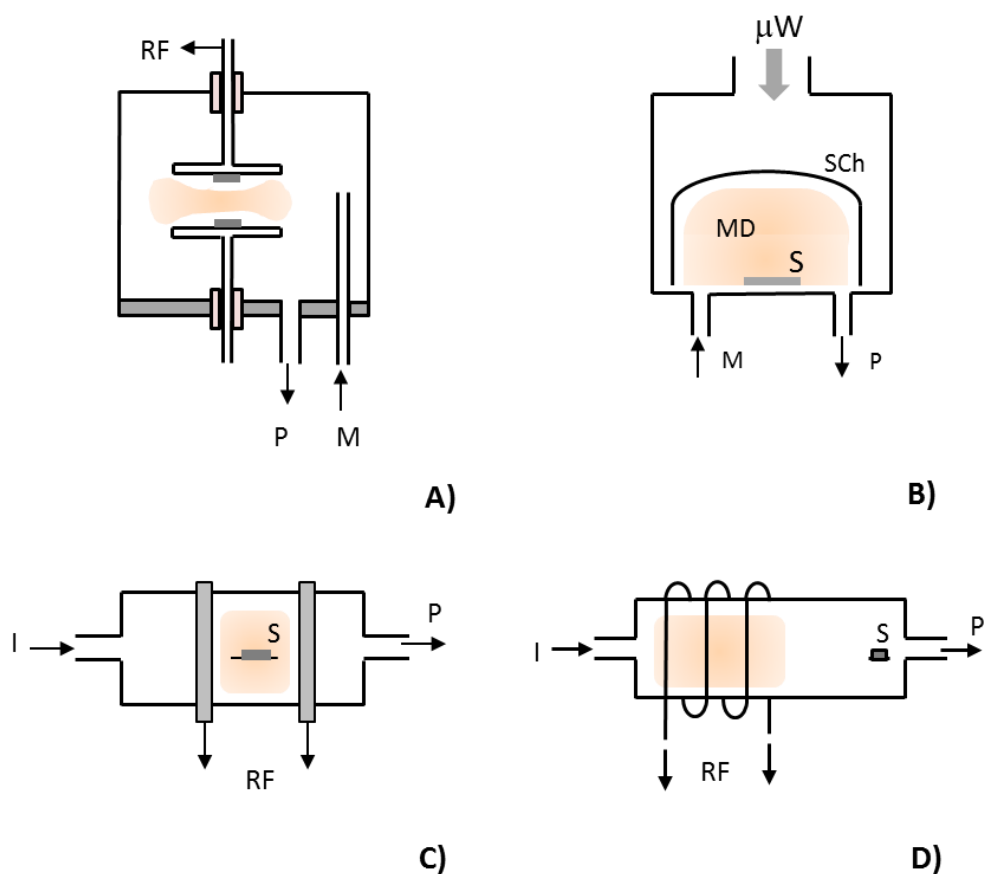


Figure 1.6 Different deposition systems for plasma polymerization:
a) parallel plate electrode reactor, **b)** microwave reactor,
c) and **d)** external electrode reactors. *Taken from [62].*

In addition, under certain conditions the plasma polymerization may result in coatings that have inorganic character. Typical example of this is plasma polymerization of organosilicon precursor, such as hexamethyldisiloxane (HMDSO, chemical structure is presented in **Figure 1.7**), in presence of oxygen. In the case when oxygen is not introduced to the deposition chamber the important film forming species are carbonated radicals that are formed by partial fragmentation of HMDSO molecule. Because of this, growing films exhibit organic character with high abundance of hydrocarbon groups. Addition of oxygen at sufficient amount leads to dramatic change in the deposition process: oxygen either reacts in the plasma bulk with carbon in CH_x radicals that leads to formation of species that do not contribute to plasma polymerization (e.g. CO , CO_2) or etches carbon from the growing films [63]. This in turn leads to lowering of fraction of hydrocarbon groups in the films

that thus tend to have to inorganic silica-like character. Obviously, the differences in the chemical structure of the coatings prepared without and with oxygen change dramatically the physical properties of resulting films (wettability, mechanical, optical or barrier properties). Such high flexibility that enables to produce either hydrophilic or hydrophobic films, barrier coatings or bioadhesive coatings alongside with the non-toxic and non-flammable character of HMDSO, its sufficient vapor pressure, availability and price, makes plasma polymerization of hexamethyldisiloxane one of the most studied system (e.g. [64]–[70]).

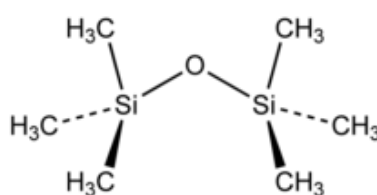
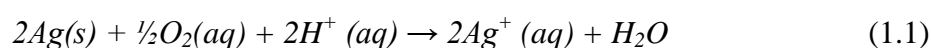


Figure 1.7 Chemical structure of hexamethyldisiloxane (HMDSO).

1.2.2.2 Plasma polymer based nanocomposites

Another classes of materials that are recently in focus are nanocomposites. These are multi-component materials with distinguishable phases among which one has at least one dimension of less than 100 nm. The interest in these materials is connected with the fact that they offer unique properties needed for various kinds of applications. For example, nanocomposites based on metal nanoparticles embedded into polymer or plasma polymer matrix may be used as optical coatings, sensors for organic vapors, switching applications or as antibacterial materials [71]. The latter is important in light of recent data that clearly showed increasing resistance of certain bacterial strains to common antibiotics. Because of this there is an urgent demand to develop alternative bactericides. One of the materials that experiences renewed and increasing attention is (nano)silver, whose good antibacterial properties are known since ancient times [72]. Although the exact bactericidal mechanism of silver is still not fully understood, it is supposed that the antibacterial nature of silver is

predominantly connected with its ability to release silver ions that subsequently interact with vital enzymes or bacterial DNA or are capable to destroy irreversibly cell membranes of pathogenic organisms and hence inhibit their growth [73]–[75]. Recently, various nanocomposite coatings consisting of silver nanoparticles (Ag NPs) inside a matrix of plasma polymers (e.g. SiO_x matrix synthesized by plasma polymerization performed in HMDSO/O₂ mixture) have been intensively investigated [53], [76]–[79]. In this case the plasma polymers serve as a reservoir for the out-diffusion of silver ions that are produced in aqueous environment by oxidative dissolution process involving protons and dissolved oxygen [80]:



The advantage of use of plasma polymers as matrix material is connected both with their very good adhesion to various substrates and possibility to regulate Ag⁺ ion release by properties of plasma polymerized matrix, e.g. its cross-link density, wettability or chemical structure [54].

Since a wide range of types of both plasma polymer and metal nanoparticles can be produced, plasma polymer/nanoparticles nanocomposites are considered as valuable in many modern applications that include biomedicine, food packaging or ultrasensitive bio-sensing or bio-recognition [81]. As consequence, different strategies were developed for production of metallic nanoparticles and for their embedding into plasma polymer matrix by means of vacuum based methods. This is due to series of advantages of such physical way of nanocomposites fabrication: vacuum based methods are in comparison to strategies that utilize wet chemical process environmental friendly, easy to implement, relatively low-cost and offer good control over the properties of both metallic nanoparticles and plasma polymer matrix. One of the most promising methods for metal NPs production is magnetron-based gas aggregation source (GAS) of nanoparticles or gas aggregation cluster⁵ source, which was first experimentally realized by Haberland and co-workers [82], [83]. The

⁵ In the literature both terms ‘nanoparticle’ and ‘cluster’ may be found, which have in general same meanings. In this work only the term ‘nanoparticle’ will be used.

principle scheme of deposition machine is presented in **Figure 1.8**. These authors, in contrast to previously used aggregation sources that utilized thermal evaporation as a primary source of material from which NPs were created [84]–[86], proposed to use magnetron sputter discharge. This made it possible to produce NPs from metals with high melting points. In addition, important fraction of NPs that leave the aggregation chamber is electrically charged (both positively or negatively (e.g. [87])) that in turn enables their mass/size filtration or acceleration towards the substrate.

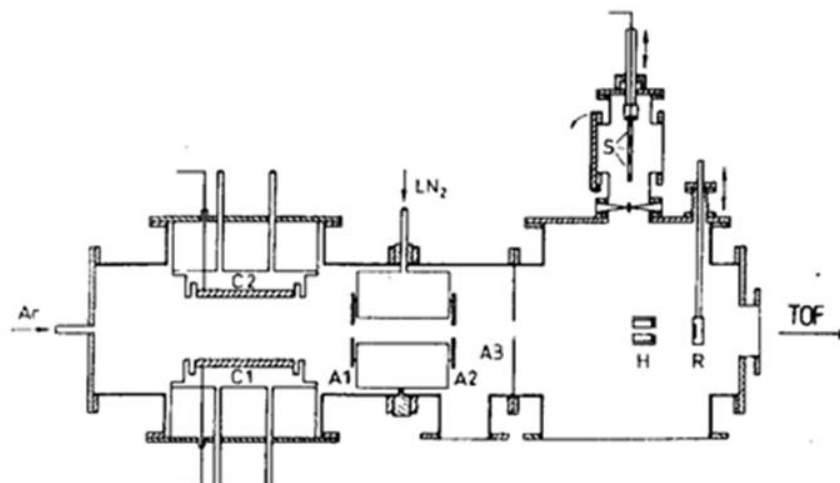


Figure 1.8 Scheme of deposition set-up for preparation of nanoparticles, where Ar – argon, LN₂ – liquid nitrogen, TOF – time-of-flight mass spectrometer, C1 and C2 – magnetron cathodes, A1, A2 and A3 – apertures, H – heater, R – crystal microbalance, S – substrate holder). *Taken from [82].*

In general, the principle of nanoparticle deposition in GAS based on magnetron sputtering may be described shortly as follows. The atoms sputtered from the metal target are introduced to the flow of noble gas (typically argon). At sufficiently high pressure (tens of Pa), stable dimmers start to be formed through the three body collisions:



where M is metal atom and Ar is rare gas atom. Subsequently dimers are cooled down as a result of their collisions with the working gas and they begin to grow by addition of metal atoms from the gas phase. Formed nanoparticles are simultaneously

dragged by the working gas and transported through a small exit aperture into the main low-pressure deposition chamber, where they are deposited on a substrate.

Deposition conditions such as working gas composition or pressure, applied power, target material, temperature in the aggregation chamber and its size may influence the formation and growth of NPs and hence their properties: size, deposition rate, chemical composition, etc.

Haberland concept of magnetron-based aggregation source has become a basis for development of new models and constructions of GAS systems. By the group of prof. Biederman a simple and compact GAS with a planar magnetron similar to the Haberland's aggregation source has been developed. The new design of GAS integrates movable magnetron or electrode without the magnetic circuit driven by DC or RF power. This enables to vary the aggregation length. Moreover, the GAS consists of stainless steel chamber equipped by water cooled system for better stabilization of the nanoparticles deposition rate. Finally, no mass filtration element is used that significantly enhances the deposition rate of NPs. This GAS design was proved to enable deposition of wide spectrum of nanoparticles including not only metallic ones, but also NPs of metal-oxides, plasma polymer NPs or even core-shell nanoparticles (for selected examples refer to following publications [88]–[94]).

The great advantage of GAS systems is not only the range of materials from which NPs may be prepared, but also the possibility to combine them with other vacuum based deposition systems (PE-CVD, magnetron sputtering) to produce nanocomposites with different architectures (e.g. nanocomposites, in which NPs are randomly distributed in the matrix [95], sandwiched structures [90] or in the form of coatings that have lateral gradients in the amount of embedded NPs [96]). In addition, in contrast to other vacuum based methods (co-sputtering, sputtering with simultaneous plasma polymerization) the process of NPs formation occurs solely in the aggregation chamber of GAS and thus it is decoupled from the deposition of matrix.

2 Experimental

2.1 DBD treatment of polymers

A schematic diagram of DBD system used for the treatment of polymeric foils is depicted in **Figure 2.1, a**. The plasma was generated in between two asymmetric parallel planar electrodes spaced at a distance of 2.0 mm, one conductive (stainless steel) and the other one covered with a dielectric layer (1 mm thick sintered alumina). The powered rectangular top electrode with dimensions of 20 mm \times 20 mm \times 50 mm can be moved in one direction along the length of the bottom electrode (dimensions 72 mm \times 160 mm), which enables the treatment of a larger sample area. **Figure 2.1, b** represents a photo of DBD system with ignited plasma between the upper movable electrode and the bottom grounded electrode.

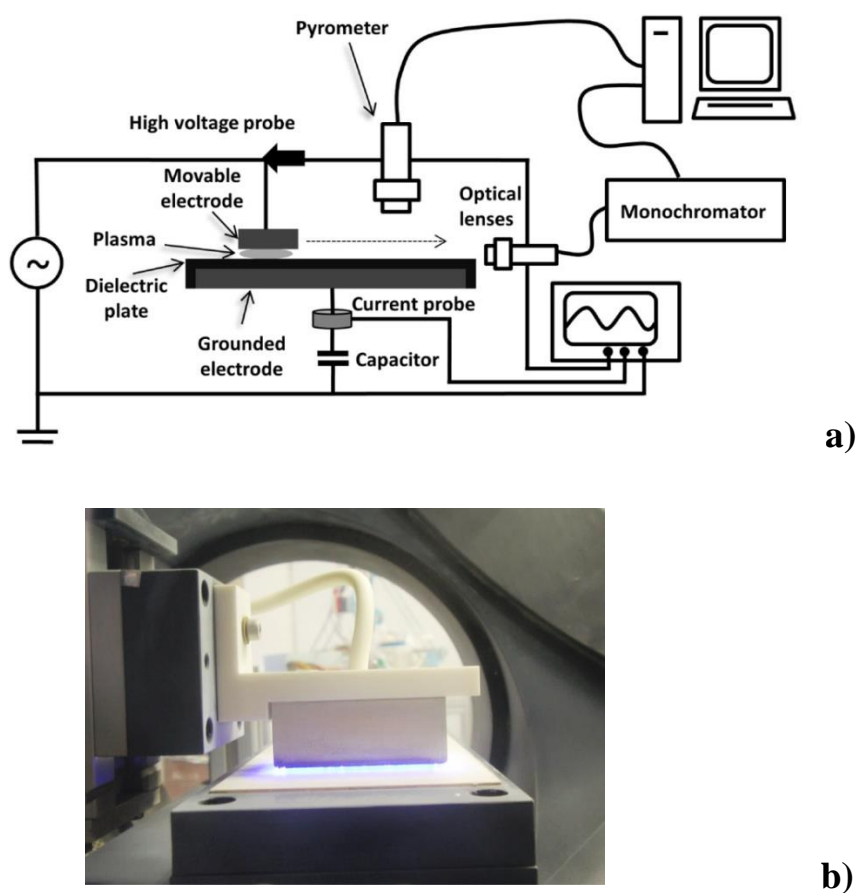
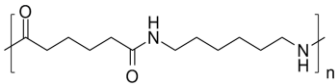
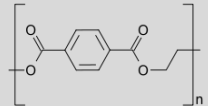
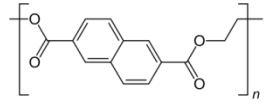
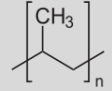
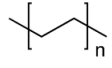
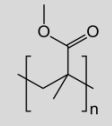
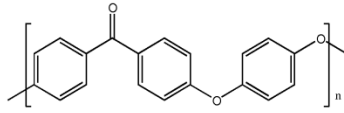
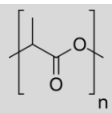


Figure 2.1 Schematic illustration of DBD system used for treatment of polymeric foils (a) and photography of a DBD plasma reactor (b)

Table 2.1 Polymers used in this study with their chemical structure.

Chemical formula	Name
	Nylon 6,6
	Polyethylene terephthalate (PET)
	Polyethylene naphthalate (PEN)
	Polypropylene (PP)
	Polyethylene low density (LDPE)
	Poly(methyl methacrylate) (PMMA)
	Polyether ether ketone (PEEK)
	Polylactic acid (PLA)

The powered top electrode was driven by a high-voltage, low-frequency AC power supply. The applied voltage was in the range 9.6 kV–10.8 kV. The DBD frequency was automatically tuned and decreased slightly (from 21 kHz to 18 kHz) with an increasing applied AC voltage. Laboratory air was used as the working gas at the pressure of one atmosphere. The humidity was in the range of 30–40%. The samples to be treated were placed on the bottom grounded electrode.

Different polymeric foils were used for modification by DBD plasma in this work. The list of used polymers, which were selected as representative examples of hydrocarbon polymers, polymers with oxygen and nitrogen functional groups and polymers that contain aromatic rings, is presented in **Table 2.1**. All foils were sourced from Goodfellow and had thickness of 50 μm except PP foils, which were 30 μm thick. For the experiments, polymeric foils were cut into the strips approximately 2.5 cm wide and about 7 cm long. All foils were used as received without any pretreatment.

2.2 Deposition systems

2.2.1 Deposition of pHMDSO and SiO_x thin films

Polymerized hexamethyldisiloxane (pHMDSO) and silicon oxide (SiO_x) thin films were prepared by means of low-pressure plasma-enhanced chemical vapor deposition (PE-CVD) method. The deposition took place in a stainless steel vacuum chamber that was equipped with 3-inch, planar, water cooled electrode (see **Figure 2.2**). The electrode was capacitively coupled through a matchbox to an RF generator working at a frequency of 13.56 MHz. The working RF power was fixed at 40 W. The precursor HMDSO (Sigma, chemical structure is depicted in **Figure 1.7**) was thermally stabilized and vaporized outside the apparatus. The flow rate of HMDSO precursor into the deposition chamber was regulated by a needle valve and was 0.25 sccm in all experiments. HMDSO was used either alone or with oxygen addition that enabled to vary chemical structure of produced coatings from the one typical for plasma polymers to the one that corresponds to SiO_2 -like films. The flow rate of oxygen was varied from 0 sccm up to 15 sccm, which corresponded to O_2 :HMDSO ratio 60:1. The pressure inside the deposition chamber was regulated by a butterfly valve and was kept at 4 Pa.

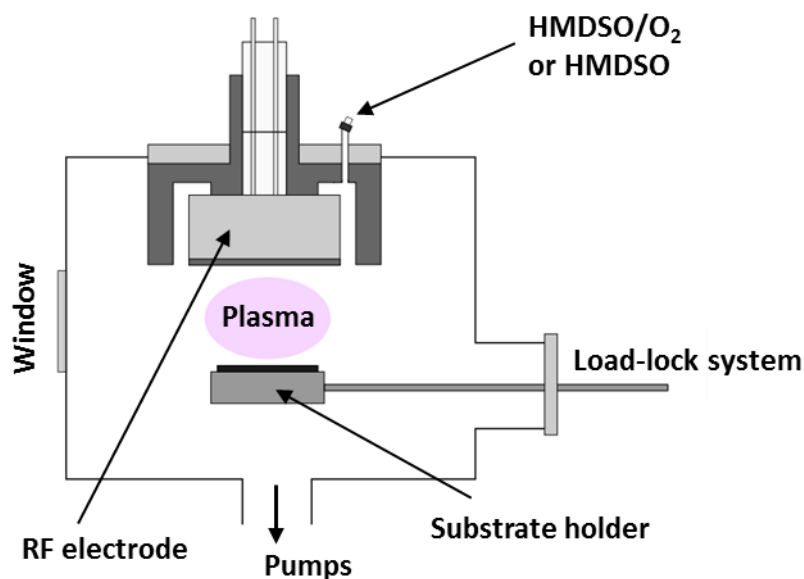


Figure 2.2 Experimental set up used for deposition of thin films.

2.2.2 Deposition of Ag nanoparticles

Gas aggregation source (GAS) schematically depicted in **Figure 2.3** was used for the fabrication of Ag nanoparticles. This GAS system of original construction consisted of water cooled, cylindrical aggregation chamber ended with a conical lid with an orifice 2 mm in diameter. DC planar magnetron equipped with a silver target (Safina a.s., declared purity 99.99%) was placed into the gas aggregation chamber. Ar was used as working gas, the pressure inside the gas aggregation chamber was 30 Pa and DC magnetron current was 100 mA. No mass or size filtration of produced nanoparticles was applied in this study.

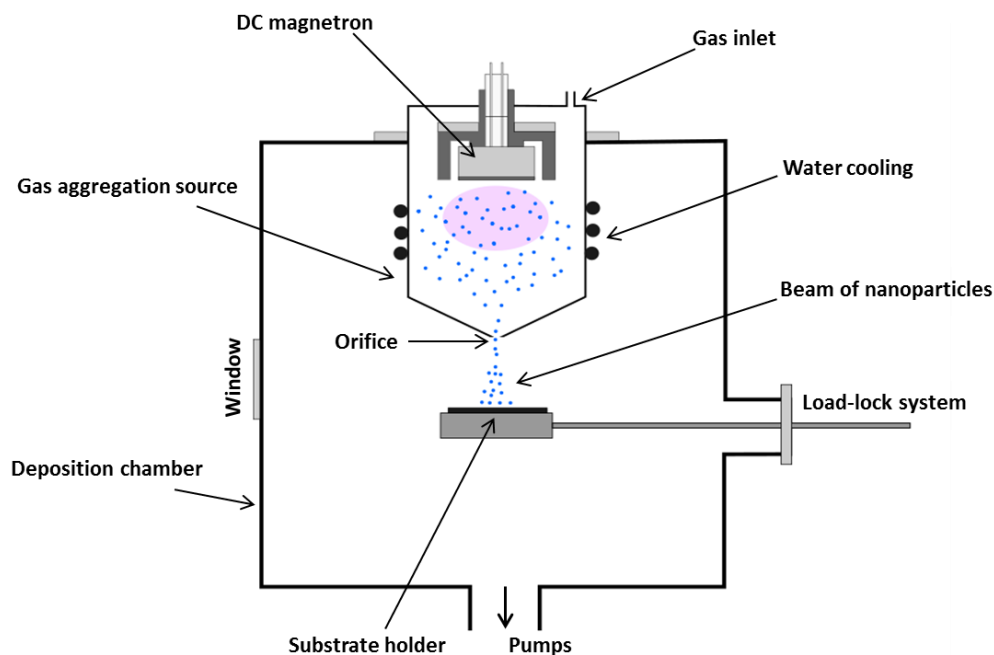


Figure 2.3 Experimental set-up for deposition of silver nanoparticles.

2.2.3 Fabrication of nanocomposite coatings

This work was focused on a novel strategy suitable for preparation of functional nanocomposites using combination of GAS and PE-CVD.

Nanocomposites based on silver nanoparticles embedded into different matrixes (plasma polymerized HMDSO and SiO_x matrix) were prepared in the form of sandwich structures by sequential deposition of Ag NPs and matrix. The steps of fabrication of nanocomposites are schematically shown in the **Figure 2.4**. The main attention was devoted to the evaluation of the effect of the number of silver NPs in produced nanocomposites, role of matrix material and influence of architecture of produced coatings on their wettability, Ag ions release, antibacterial efficiency and barrier properties.

Similar approach was used for production of coatings with tunable roughness and wettability. In this case C:H NPs were used instead of Ag NPs. They were prepared using protocol described in [97].

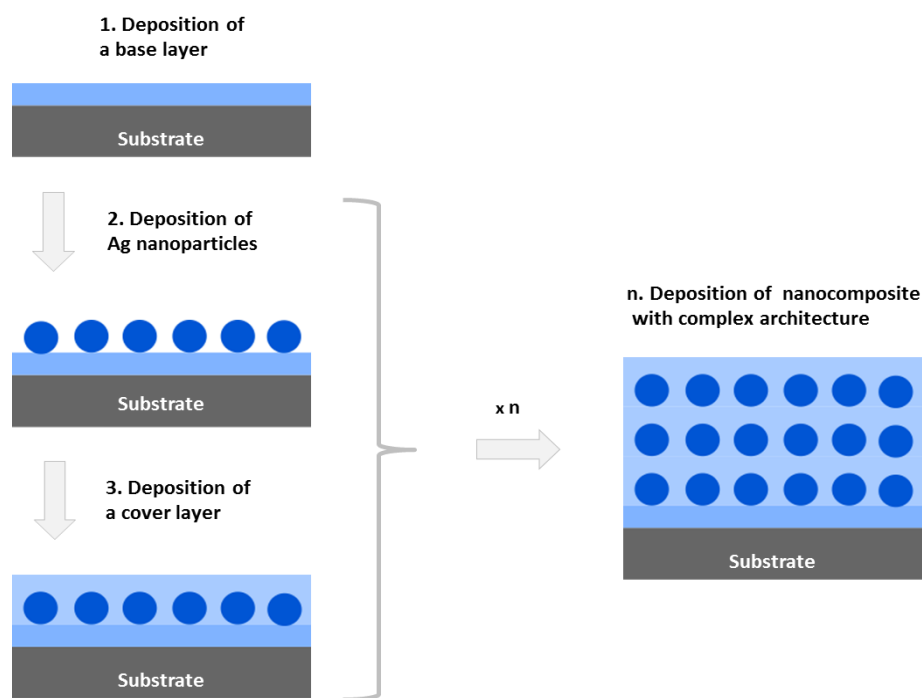


Figure 2.4 Schematic illustration of nanocomposites preparation.

2.3 Plasma diagnostics methods and methods for physico-chemical characterization of samples

2.3.1 Optical emission spectroscopy (OES)

Optical emission spectroscopy (OES) is a common diagnostic method for detection of excited atoms and molecules (both neutral and ionized) presented in the low temperature plasma. This method is based on analysis of light emitted by plasma during the radiative de-excitation of excited species to lower energy states. The wavelength of emitted radiation is given by the energy difference between the upper and lower energy levels and thus is characteristic for a given atom or molecule. Thus, optical emission spectra as a collection of different spectral lines may provide the information about the composition of the plasma.

In this study, OES was used for characterization of processing plasma. In the case of DBD plasma time-averaged emission spectra collected from the whole DBD volume were recorded by the Andor iStar ICCD DH740i-18U-03 camera through the iHR-320 spectrometer in collaboration with Dr. M. Šimek. In the case of plasma polymerization of HMDSO the optical signal emitted by the plasma was collected through the diagnostics window and analyzed by Avantes spectrometer (AvaSpec 3648) in the range of 250–850 nm according to [98].

2.3.2 Atomic Force microscope (AFM)

Characterization of the surface morphology was done using Atomic Force microscope (AFM). The AFM enables to image almost all types of surfaces, for example polymers, biological objects, nanoparticles, composites and etc. The AFM consists of sharp tip on the end of cantilever that scans a sample surface and a laser beam deflection system. Schematic illustration is depicted in **Figure 2.5**.

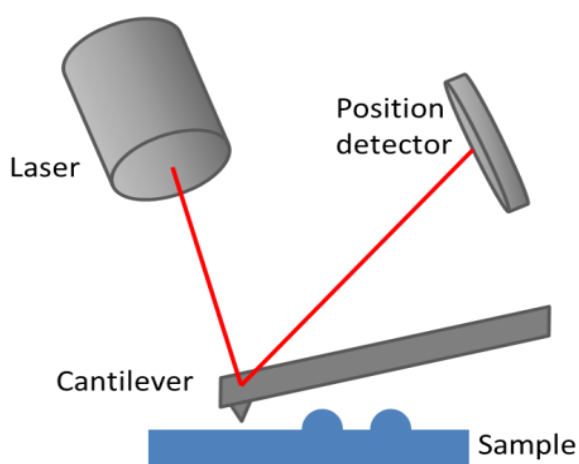


Figure 2.5 AFM schematic illustration.

When the cantilever interacts with the sample surface, the forces that occur between the tip and sample are measured and controlled by electronic feedback loop

employing a laser deflection. Position of laser beam reflected from the cantilever is monitored by detector to track the surface for imaging.

Different measuring modes may be used that can be divided into static and dynamic ones. In the static (or contact) mode the tip is in constant contact with the substrate, whereas in the dynamic (or non-contact) mode the cantilever is oscillated near its resonance frequency (typically from several kHz to 400 kHz) up and down near the surface by adding an extra piezoelectric element. In the most common mode, so-called tapping or intermittent contact mode, the tip touches the sample and moves completely away from the sample in each oscillation cycle. The interaction between the tip and the sample causes the change in amplitude of the cantilever's oscillation. The feed-back loop is then used to adjust the height of the cantilever above the sample in order to maintain constant cantilever oscillation amplitude. Recorded heights for different positions on the sample are then used for construction of an AFM image of sample surface.

Information obtained by the AFM is a set of discrete values of heights $Z(x)$ for each of n measured points on the sample. This enables statistical analysis of recorded AFM images [99]. One of the most common studied parameters is the root-mean-square (RMS) roughness w that describes the standard deviation of the surface height and is defined as:

$$w = \sqrt{\frac{1}{n} \sum Z(x)^2} \quad (2.1)$$

In this work, AFM (Quesant Q-scope 350 AFM) was used for the measurements of the morphology of polymeric foils and deposited films. The AFM was operated in the intermittent contact mode (scan rate 2 s, resolution 512 x 512 points) using ACLA-10 Si probes (tip radius of 10 nm, nominal spring constant 58 Nm⁻¹, AppNano). Each reported value of RMS roughness represents an average over at least three 10 µm x 10 µm scans performed on randomly selected positions on the measured samples.

2.3.3 Scanning Electron Microscopy (SEM)

Scanning electron microscope (SEM) is used to visualize the surface topography by scanning with a beam of electrons. The work principle of SEM is as follows: electrons emitted by an electron gun are accelerated (accelerating voltage is typically in the range of hundred volts to tens of kilovolts) and focused onto the sample (see **Figure 2.6**). As a result of interaction between the electron beam and sample, low-energy secondary electrons, backscattered electrons, Auger electrons, X-rays, etc. are generated. Special detectors collect information depending on the type of come-off signal. For imaging of the sample, secondary and backscattered electrons are generally used.

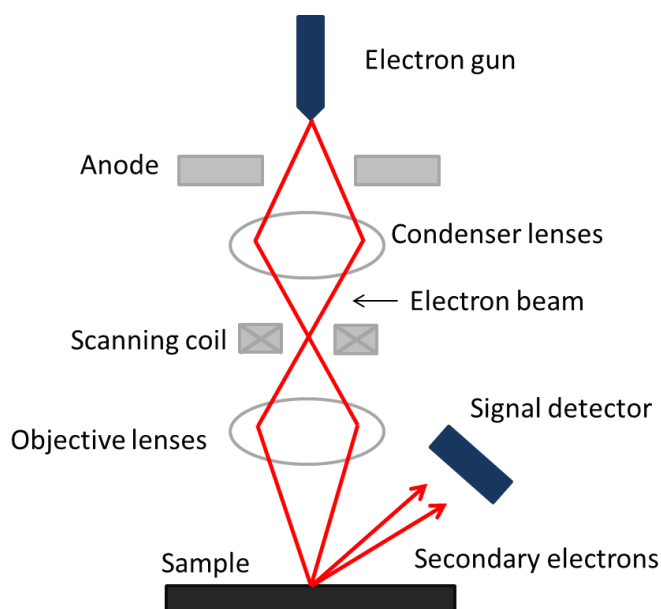


Figure 2.6 Simplify scheme of the SEM.

In this work, morphology of prepared samples was measured by the scanning electron microscope Tescan Mira III using maximum acceleration energy at 30 kV. As substrates for SEM analysis of Ag NPs and Ag containing nanocomposites one-side polished silicon wafers were used. Size distribution of Ag NPs was determined by means of software Solarius Particles [100]. Diameters of at least 100 NPs from

each SEM image with the view field of 1 μm were used to determine the particle size distribution.

Since the samples during their scanning are bombarded by high-energy electrons either positive or negative potential can appear in the case of non-conductive materials. This charging leads to distortion of obtained data and quality of analysis. Common approach to the mitigation of charging is covering of the sample by thin metallic film (gold, silver, etc.) [101], [102]. This strategy was employed in our case for the characterization of bacterial spores. Untreated and plasma treated spores of *B. subtilis* were dried for 1 hour after the DBD plasma exposure and then covered by a thin layer of magnetron sputtered gold. The dimensions of spores were deduced from SEM images. In this case the lengths and widths of at least 70 spores were measured.

2.3.4 X-ray Photoelectron Spectroscopy (XPS)

X-ray photoelectron spectroscopy (XPS) is a surface sensitive technique (information depth around 5-10 nm depending on the material) that provides information about chemical composition of the samples. The XPS can detect any elements with atomic weight equal to or higher than 6.9 (i.e. from lithium beyond). The main principle of XPS is based on irradiation of the material surface by X-ray beam. Due to the photon interaction with the matter electrons are ejected from the inner orbitals with kinetic energy:

$$E_{kinetic} = h\nu - \phi - E_{binding} \quad (2.2)$$

where h is Planck constant, ν is frequency of incident X-ray beam, ϕ is work function of spectrometer (provided by calibration of the device, typically few eV) and $E_{binding}$ is binding energy of the electron [103]. According to this equation, from known photon energy and measured electron's kinetic energy it is possible to calculate electron binding energy, which is unique for each element.

In addition, oxidation, surface charging, contamination of the surface influences the position and intensity of XPS peaks, so in all cases the calibration of binding energy of peaks according to known element is needed.

In this work chemical analysis was carried using an XPS spectrometer equipped with a hemispherical analyzer (Phoibos 100, Spec). The XPS scans were acquired at constant take-off angle of 90^0 using Al Ka X-rays source (1486.6 eV, 200 W, Specs). Survey spectra were acquired for binding energies in the range of 0-1100 eV at a pass energy of 40 eV (dwell time 100 ms, step 0.5 eV). All the XPS spectra were referenced to the binding energy of aliphatic C-C bonds at 285.0 eV [104]. The fitting of high resolution XPS spectra of selected peaks (C1s, O1s and N1s) was performed after Shirley background subtraction with mixed Gauss-Lorentzian lines (70% Gaussian and 30% Lorentzian) using the CasaXPS program.

2.3.5 Ellipsometry

Ellipsometry is a versatile non-contact method for characterization of properties of thin films such as thickness and optical constants. Ellipsometry is based on monitoring changes of the polarization of light reflected by the surface of the sample (see **Figure 2.7**) that are expressed by phase difference Δ of p- and s- polarizations and amplitude ratio upon reflection $\tan(\psi)$. Δ and $\tan(\psi)$ are connected with a complex reflection coefficient ρ through the equation:

$$\rho = \frac{R_p}{R_s} = \tan(\Psi)e^{i\Delta} \quad (2.3)$$

where R_p and R_s are Fresnel coefficients corresponding to p- and s- polarization, respectively, that are dependent on the optical constants of studied samples (thickness, refractive index and extinction coefficient). Since the optical constants cannot be directly derived from the measured data, iterative fitting of recorded ellispometric data by a model has to be used that solves Fresnel equations using optical constants that describe the analyzed sample as fitting parameters [105], [106].

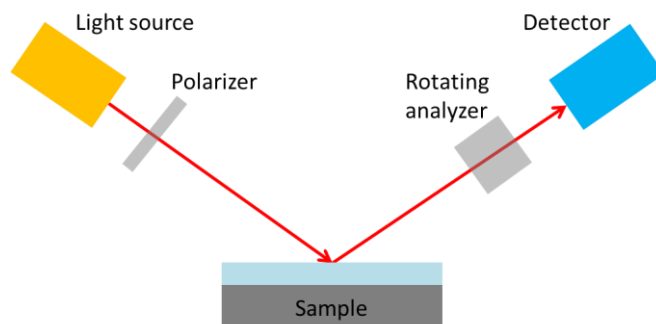


Figure 2.7 Schematic illustration of ellipsometry measurements.

In this work, spectroscopic ellipsometer Woolam M-2000DI was applied for measurement of thickness of deposited coatings. During all experiments the incident angle was varied from 55 to 75° at the wavelength range of 192–1690 nm at room temperature in laboratory air. Silicon wafers were used as substrates for ellipsometry measurements.

2.3.6 Inductively coupled plasma mass spectroscopy (ICP-MS)

ICP-MS is a sensitive technique, which is capable to detect and quantify amount of most of elements in the periodic table in solutions down to concentration of ppt (parts per trillion; ng/l). The ICP-MS device consists of sample introduction system, inductively coupled plasma as an ionization source that uses argon gas, mass spectrometer with a quadrupole filter and detector. First, the sample solution is sprayed into the argon plasma where it subsequently evaporates, decomposes and eventually ionizes. Produced ions are then separated according to their mass/charge ratios by a high resolution magnetic sector mass analyzer. Finally, the ions are detected and counted [107].

The ICP-MS (NexION® 300 ICP-MS system) was employed for monitoring of silver ion release kinetics from silver based coatings into the aqueous environment in this study. For measurements the samples were immersed into 10 ml distilled water in small bottles made of high density polyethylene (HDPE) at room temperature for different time intervals. The values of silver ion release were converted into the release per area taking into account the volume of the supernatant and the size of samples (1.13 cm^2 in this study). Each reported value is the average from 2 independent measurements.

2.3.7 Nano Dynamic Mechanical Analysis (nanoDMA)

Dynamic Mechanical Analysis, also known as DMA, is an indentation technique used to measure mechanical properties of thin films (hardness, storage modulus, loss modulus, complex modulus etc.) by applying a sinusoidal deformation that results in response of material. NanoDMA is a technique that performs such mechanical measurements at the nanoscale.

The common nanoindentation methods to measure mechanical properties of material are based on data recorded during a cycle of the loading and unloading of the indenter [108], [109] (see **Figure 2.8**). These recorded data are subsequently modeled taking into account both elastic and plastic deformation during the loading that facilitates the determination of the hardness of the material. However, during the unloading, it is assumed that only elastic deformation is recovered ignoring plasticity reverses. This assumption may be applied in case of ceramics or metals showing only elastic recovery but not in case of polymers, which have additionally viscoelastic behavior. Thus, for polymers dynamic mechanical analysis is commonly applied. Characterization of the viscoelastic properties of polymers is defined by complex modulus, which is in turn comprised of storage and loss modulus. Storage modulus represents the stiffness of the material. Loss modulus describes the damping behavior of the material.

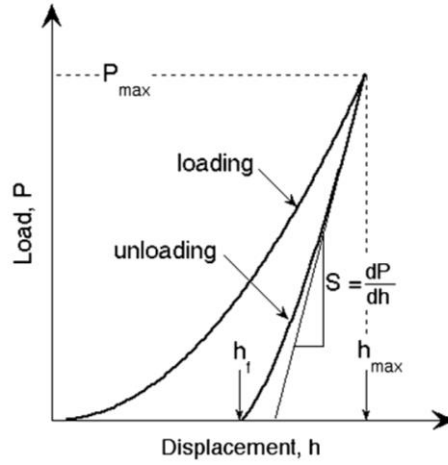


Figure 2.8 A load-displacement curve; h_{\max} maximum displacement at the maximum load P_{\max} , S is elastic unloading stiffness. *Taken from [109].*

NanoDMA measurements use a quasi-static force and a much smaller dynamic load at established frequencies, which may be ramped from 0.1Hz up to 300Hz. Displacement amplitude and phase shift are analyzed according to resulting signal measured by lock-in amplifier (see **Figure 2.9**).

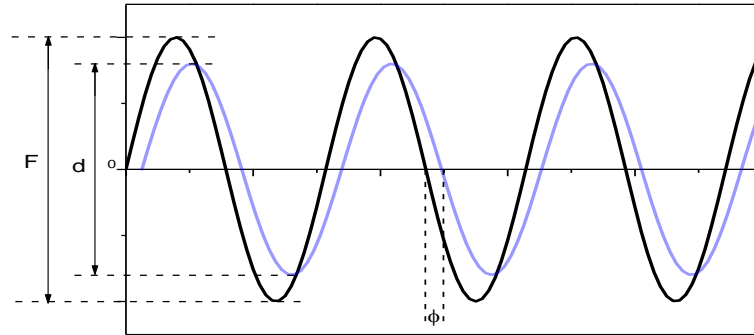


Figure 2.9 Dynamic input signal; F is applied dynamic force, d is dynamic displacement, and ϕ is phase shift. *Taken from [110].*

The storage (loss and complex) modulus is defined with equation:

$$E = \frac{k \cdot \sqrt{\pi}}{2 \cdot \sqrt{Ac}} \quad (2.4)$$

where k is function of frequency (measured in nanoDMA test) and given as the storage, loss or complex stiffness, respectively; Ac is contact area.

Hardness is calculated by the following equation:

$$H = \frac{P+Fact}{Ac} \quad (2.5)$$

where P is maximum force and $Fact$ is the dynamic actuation force.

The complex Young's modulus was assessed via nanoDMA (Hysitron, Triboscope 75 with a nano-DMAIII module combined with an AFM microscope Ntegra Prima, NT-MDT) with a standard Berkovich-type indenter. Prior to each measurement, the indenter was brought to contact with the sample under the constant force of 0.4 μN . Linearly increasing load function was applied immediately afterwards to indent the surface with superimposed dynamic load (with variable amplitude and a frequency of 220 Hz). For measurements of polymers, the maximal quasi-static force reached 100 μN and, in case of plasma polymerized coatings, it was 500 μN .

2.3.8 Permeability measurements

An original set-up of own construction was used for the evaluation of barrier properties of the coatings deposited on PET foils. This system, which is schematically presented in **Figure 2.10**, is based on measuring the temporal pressure rise in an ultra-high-vacuum (denoted as $V1$ in **Figure 2.10**) chamber evacuated before the measurements to the base pressure of 3×10^{-6} Pa and separated from the surrounding environment (denoted as $V2$ in **Figure 2.10**) by the tested polymeric foil. Before each measurement the UHV chamber $V1$ was pumped by turbo-molecular pump to the base pressure. At the same time, the volume $V2$ above the foil was pumped by a scroll pump to pressure of 1 Pa. After this pumping stage, which was in all cases 24 hours in order to reach reproducible results, the volume $V2$ was filled by testing gas (water vapor in our case) and the pumping of UHV part was stopped. The rising pressure in the UHV chamber was measured by an ionization

gauge. The slope of the pressure rise is proportional to the permeability coefficient of a tested gas through a polymeric foil.

The calculation of permeability coefficient P was performed using the equation [111]:

$$P = \frac{\left(\frac{V \cdot \Delta p}{T}\right)_{T_s}}{P_s} \cdot \frac{l}{A_m \cdot t \cdot \Delta P_u} \quad (2.6)$$

where V is the permeate side volume given in cm^3 , Δp stands for the pressure increment in time t in Pa , t is the time of permeation in sec , T and T_s are operating and standard temperatures in K , P_s is the standard pressure in Pa , l is the membrane thickness in cm , A_m is the membrane area in cm^2 and ΔP_u represents the pressure difference across the membrane, which is given in Pa . More details regarding the set-up and measuring protocol may be found in the previous study [45]. The samples were measured at least two times.

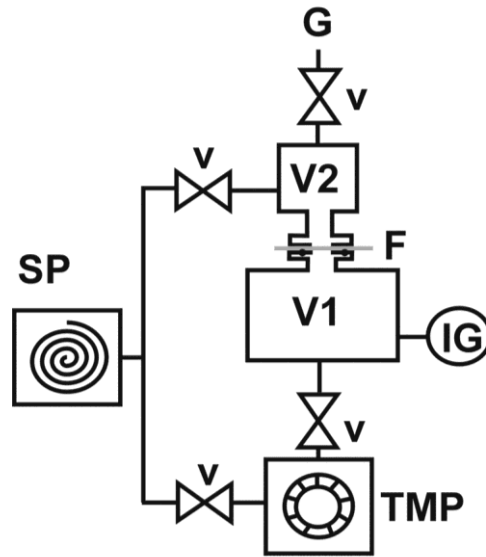


Figure 2.10. Schematics of set-up used for permeability measurements: SP – scroll pump, TMP – turbomolecular pump, v – valves, IG – ionization gauge, F – tested foil, V1 – ultra-high vacuum part, V2 - upstream part, G – gas inlet.

2.3.9 UV-VIS Spectrophotometry

Ultraviolet-visible spectrophotometry (UV-VIS) is a type of absorption spectroscopy in the ultraviolet and visible region of light spectra. This method is based on the measurement of changes of intensity of light at given wavelength in an absorbing media that follows the Beer-Lambert law [112]:

$$A = \log \left(\frac{I_0}{I} \right) = \epsilon cl \quad (2.7)$$

where A is the absorbance of the sample, I_0 and I are intensities of light before and after it passed the sample, respectively, l is the path length through the sample, c is the concentration of the absorbing species and ϵ is the extinction coefficient.

The common UV-VIS spectrophotometer consists of a light source (deuterium and tungsten lamps for UV and VIS spectral regions), monochromator, beam-splitter that splits the beam of light into two separated beams: the first one passes through the sample and the second one that passes through a blank sample is used as a reference, and detector. This configuration had also the UV-VIS spectrophotometer that was used in this study (Hitachi U-2900) that enabled absorption measurements in the spectral range from 200 nm up to 1100 nm.

Although UV-VIS spectrophotometry is predominantly used in analytical chemistry for the quantitative determination of different analytes and biomolecules, in this study it was used for the characterization of polymeric foils and for investigation of localized surface resonance peak of Ag NPs [113].

2.3.10 Wettability measurements

The wettability and surface energy of polymeric foils and produced coatings was measured by means of sessile drop technique using home-build goniometer. Wettability was characterized by water contact angle θ , i.e. angle (tangent) of a liquid drop with a solid surface at the base (see **Figure 2.11**). According to the

recommendation on wettability measurements by Strobel et al. [114] both static and dynamic (i.e. advancing and receding) water contact angles were measured. In order to measure dynamic water contact angles the water droplets were inflated and deflated with a needle-syringe without the contact line moving. The advancing and receding angles were then evaluated as maximal and minimal contact angle values, within which the triple line did move – see **Figure 2.12**. Each reported contact angle value is the average of three independent measurements performed on randomly selected positions on the sample.

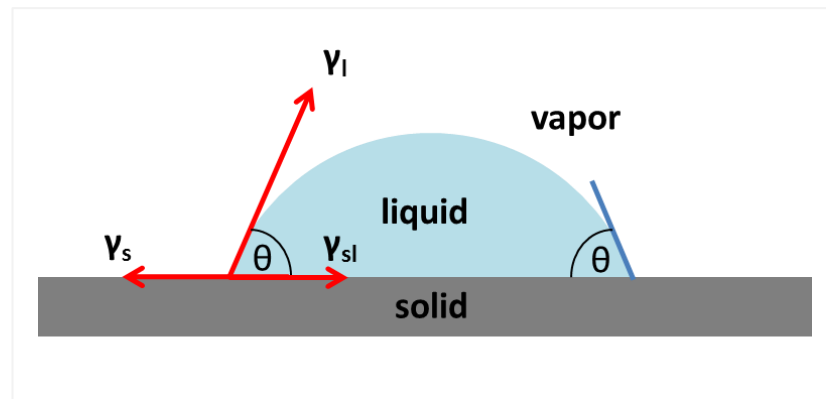


Figure 2.11 Illustration of the measurement of contact angle of liquid.

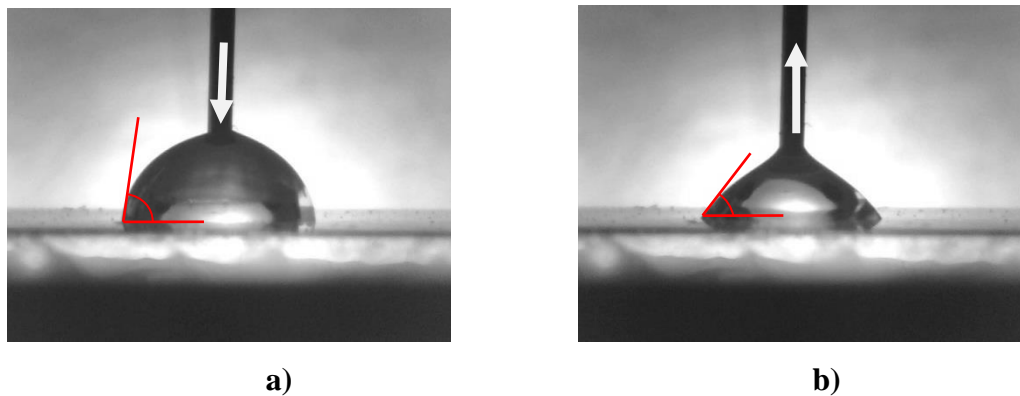


Figure 2.12 Example of a) advancing and b) receding angles of water on PET foils.

In general, for finding the surface energy of an unknown sample, droplets of one or several different liquids with known surface energies are used. Several approaches

exist for determination of surface energy. The basic equation for calculation of surface energy is the Young equation:

$$\gamma_s = \gamma_{sl} + \gamma_l \cos\theta \quad (2.8)$$

where γ_s is the surface energy of a solid, γ_{sl} is the surface energy of a surface –liquid interface, γ_l is the surface energy of liquid and θ is the contact angle of liquid (see **Figure 2.11**).

In order to define γ_{sl} from equation (2.8) additional relations between γ_s , γ_l and γ_{sl} must be stated. Fowkes assumed separation of the surface energy into independent parts that reflect specific interactions [115]:

$$\gamma_s = \gamma_s^p + \gamma_s^d + \gamma_s^h + \gamma_s^i + \gamma_s^{ab} + \gamma_s^o \quad (2.9)$$

where γ_s^p , γ_s^d , γ_s^h , γ_s^i , γ_s^{ab} and γ_s^o are connected with polar force, dispersion force, hydrogen bonding force, induction force, acid/base force and other remaining force components of surface energy, respectively.

For two surface-liquid component systems that assumes both polar and dispersion interactions Owens and Wendt derived following equation [116]:

$$\gamma_{sl} = \gamma_s + \gamma_l - 2\sqrt{(\gamma_s^d \gamma_l^d)} - 2\sqrt{(\gamma_s^p \gamma_l^p)} \quad (2.10)$$

Taking into account the last equation (2.10), Young equation (2.8) and assumptions:

$$\gamma_s = \gamma_s^p + \gamma_s^d \quad (2.11),$$

$$\gamma_l = \gamma_l^p + \gamma_l^d \quad (2.12),$$

the polar and dispersion components of the solid can be found.

In this work two liquids (Sigma–Aldrich) were used for the determination of surface energies. Substituting known values of polar and dispersive parts of water and diiodomethane, which are listed in **Table 2.2**, to (2.8), (2.10), (2.11) and (2.12) equations the polar and dispersive components of tested polymers can be calculated as:

$$\gamma_s^p = \{5.09(1 + \cos\theta_w) - 2.32(1 + \cos\theta_{DM})\}^2 \quad (2.13)$$

$$\gamma_s^d = 12.7(1 + \cos\theta_{DM})^2 \quad (2.14)$$

where θ_w is the water contact angle (WCA) and θ_{DM} is the contact angle of diiodomethane.

Table 2.2 The polar and dispersive surface energies.

Liquid	γ_s^p , mJ·m ⁻²	γ_s^d , mJ·m ⁻²
Water	51	21.8
Diiodomethane	0	50.8

2.3.11 Mass loss measurements

In order to assess the etching rate of the polymeric foils, they were weighted before and after the plasma treatment by means of Mettler Toledo XS205 balances (readability 0.01 mg). All presented values are statistical averages of three independent measurements.

2.4 Protocols of biological tests

2.4.1 Cell growth on polymeric foils

Influence of DBD plasma pretreatment on cell growth on PET foils was investigated in collaboration with Institute of Physiology, Academy of Sciences of the Czech Republic. In these experiments untreated and DBD treated PET foils were sterilized in 70% ethanol for 2 hours. After that they were cut into pieces 1.2 cm × 1.0 cm, inserted into 24-well polystyrene cell culture plates (TPP, Switzerland; internal well diameter 15.4 mm) and seeded either with human umbilical vein endothelial cells (HUVEC, single donor, isolated in EGM-2 media; Lonza, Cat. No. C2517A) suspended in EGM-2 medium (Lonza, Cat.No. CC-3156) or with human osteogenic cells from osteosarcoma (Saos-2; European Collection of Cell Cultures, Salisbury, UK, Cat. No.89050205) suspended in McCoy's medium (Sigma, Cat. No. M4892). EGM-2 medium was supplemented with 2% fetal bovine serum and other supplements (Lonza, Cat. No. CC-4176) and McCoy's medium was supplemented with 15% fetal bovine serum (SebakGmbH, Aidenbach). Both media contained gentamicin. Each well contained 30,000 cells (i.e. approximately 16,000 cells/cm²) and 2 mL of media. The cells were cultured at 37⁰ C in a humidified air atmosphere containing 5% CO₂ up to 7 days. In all tested time intervals, samples were rinsed with PBS, fixed with 70% frozen ethanol (room temperature, 20 min) and stained with Hoechst #33258, which stains the cell nuclei (Sigma–Aldrich, USA; 5 µg/ml of PBS). It has been applied for 2 h at room temperature. The number of cells on the material surface was evaluated on microphotographs taken under an IX 51 microscope, equipped with a DP 70 Digital Camera (both from Olympus, Japan, objective 20x). The quantitative data are presented as mean ± SEM (standard error of mean). Three samples were used for each experimental group and time interval.

2.4.2 Evaluation of sporicidal effect of DBD plasma

The effect of the DBD plasma on bacterial spores was studied using the *B. subtilis* ATCC 6633 spores that are commonly used as a control strain for chemical disinfectants and antiseptic testing. The samples preparation and handling was performed in an aseptic environment in order to avoid their contamination. The spore suspension as well as samples preparation followed the protocol proposed as a standard biological protocol for assessing the biocidal efficacy of gas plasma devices [117], [118]. Following this protocol, vegetative cells of *B. subtilis* were pipetted on Petri dishes containing Sporulation Agar (Himedia, Mumbai, India). Petri dishes were subsequently incubated at 30 °C for three weeks. In order to harvest the spores sterile physiological solution (5 ml) was added to the Petri dishes and agar debris was removed from the suspension by centrifugation. The supernatant was poured away and 10 ml of fresh sterile physiological solution was added followed by shaking in order to re-suspend the spore pellet. The spore suspension contained in a sterile glass bottle was transferred to a water bath at 70 °C for 30 min. Following this protocol prepared spore suspension can be stored for a long period of time, within which spores maintain their viability and reproducibility. The suspension with *B. Subtilis* spores was preserved in the dark inside a refrigerator at 4 °C and was used when necessary.

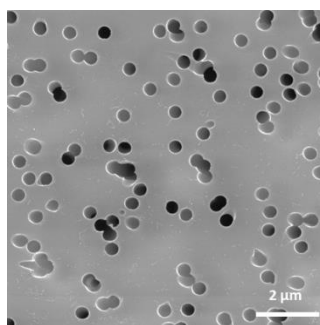


Figure 2.13 SEM image of untreated Polycarbonate membrane using for biological tests.

For the testing of sterilization efficiency of DBD plasma polymeric membranes (Nuclepore Polycarbonate, Whatman, with the diameter of 13 mm and pore size of $0.4\ \mu\text{m}$) seeded with bacterial spores were used. The SEM image of Polycarbonate (PC) membrane is represented in **Figure 2.13**. For inoculation, 1.2 ml of prepared spore solution with concentration of approximately 10^7 colony formit units per ml was spattered through the autoclaved membrane (121 °C for 15 min) inside a filter holder (EMD Millipore Swinnex) using a syringe and a vacuum water pump for 45 s. Such prepared samples were immediately exposed to the DBD plasma.

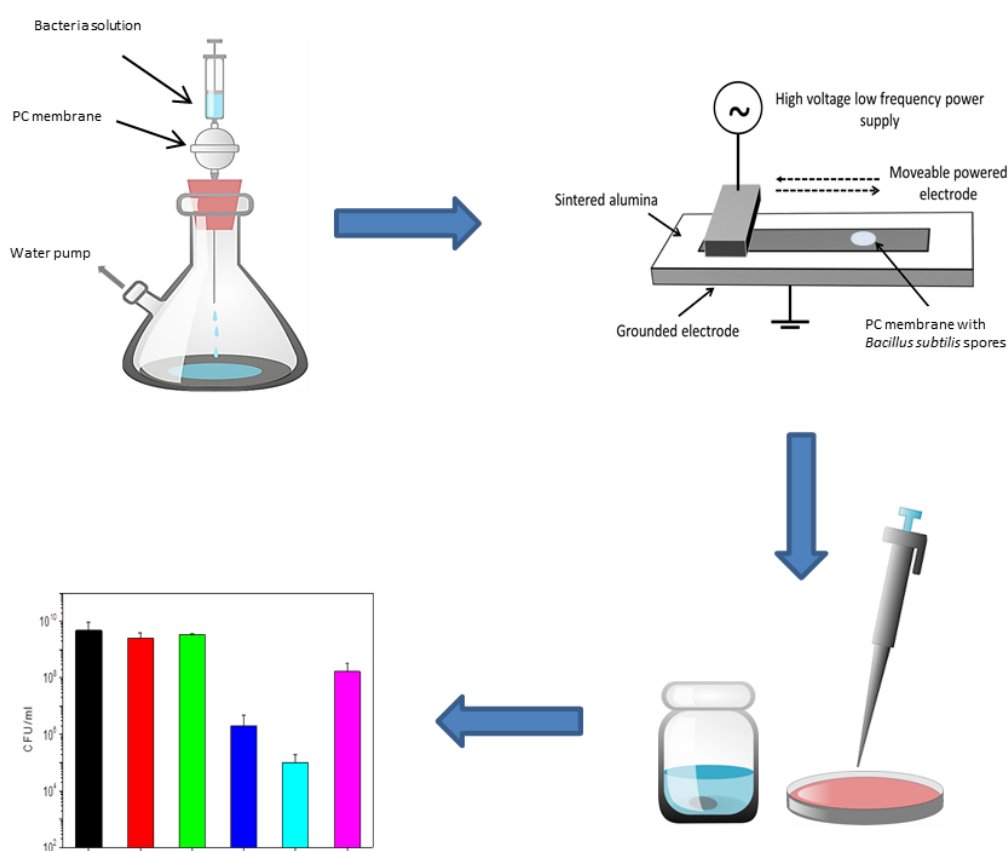


Figure 2.14 Schematic representation of biological experiments with spores *B.subtilis*.

In order to determinate bacterial spore's reduction induced by the DBD plasma treatment standard cultivation method was used. In this method following steps were performed. First, each treated sample was placed inside a sterile bottle with 10 ml of

physiological saline and three glass beads and then it was shaken for 45 s to recover spores to the solution. After the serial dilution, 100 μ l of suspension was inoculated on Petri dishes with tryptic soy agar by a sterile disposable spreader. Plates were subsequently incubated for 24 h at 30 °C in a thermostat and grown colony forming units (CFU) were calculated. The entire procedure is schematically represented in **Figure 2.14**.

All presented data are means of at least three independent experiments. In addition, one set of samples was autoclaved as positive control, where no viable spores were detected.

2.4.3 Antibacterial activity of nanocomposites

Antibacterial efficiency of produced silver-based nanocomposite materials was performed in collaboration with RNDr. Jana Beranová, Ph.D. (Faculty of Science, Charles University). The bactericidal activity was determined by two methods: disc diffusion test and dilution test. In both cases a gram-negative bacterium *Escherichia coli* strain K12 (laboratory stock) was used as a model microorganism. Bacteria were cultivated in Luria-Bertani (LB) agar at 37 °C until mid-exponential phase of growth (optical density at 450 nm ca. 0.5).

In case of disc diffusion tests, the culture was diluted 1:10 in sterile distilled water and 1 ml was placed on the surface of LB agar plate. After all liquid soaked into the agar, a glass disc coated by silver containing nanocomposites (sterilized by UV light for 30 min from each side) was placed onto the inoculated agar surface (the coated side facing down). Glass coated with films of plasma polymerized HMDSO and SiO_x served as negative controls. After overnight incubation at 37°C, the plates were photographed and the inhibition zones (clear zones where bacteria did not grew) around discs were measured.

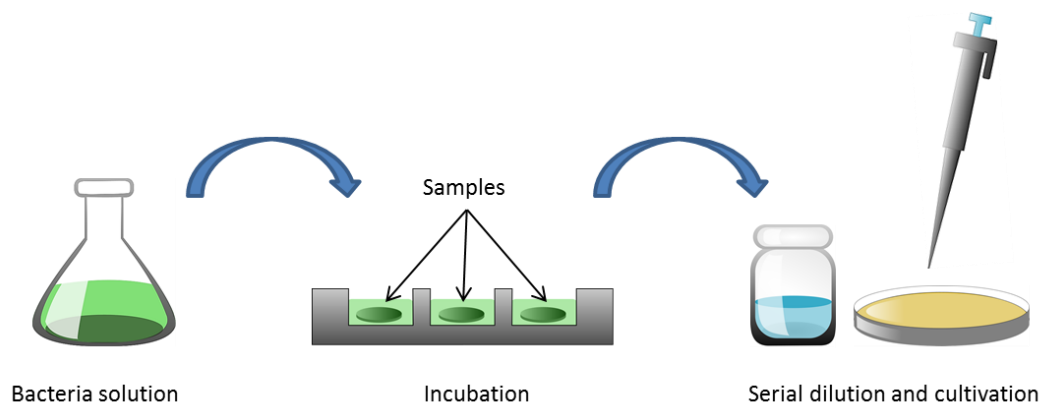


Figure 2.15 Steps of biological test for investigation of antibacterial activity of nanocomposites.

To perform the dilution method, the following steps have been carried out (see **Figure 2.15**). First, bacterial culture was diluted in PBS buffer to gain approximately $10^6 \text{ CFU} \cdot \text{ml}^{-1}$. Samples sterilized before the tests by UV light (30 min from each side) were then placed into the well plates and incubated with 3 ml of bacterial suspension at 37°C with shaking at 150 rpm. The cultivation time was up to 4 hours. Afterwards, aliquots of bacterial suspension were appropriately diluted and plated on Luria-Bertani agar plates. After incubation for 24 h 37°C , bacterial colonies were counted and the $\text{CFU} \cdot \text{ml}^{-1}$ was calculated. Glass discs were served as negative control sample. Each reported value is the average from three replicas.

3 Results and discussion

In this chapter the main results reached during my thesis will be summarized and discussed. The results will be divided into two main thematic parts.

The first one relates to the modification of polymeric materials by means of atmospheric pressure dielectric barrier discharge operated in air. In this part will be presented not only the results describing changes in physico-chemical surface properties of polymers (chemical composition, morphology, wettability and surface energy) induced by plasma treatment, but also some tests focused on the possible applications of treated surfaces. In addition, effect of DBD plasma on bacterial spores will be briefly mentioned as well.

In the second part of this chapter results focused on the development of thin functional coatings will be discussed. Again, possible applications of produced coatings will be presented.

3.1 DBD treatment of polymers

3.1.1 DBD plasma characterization

The first step of this study was characterization of used DBD setup. Typical waveforms of voltage and current are presented in **Figure 3.1a**. It is obvious that the employed discharge operates in multi-filamentary mode, which is characterized by sharp current bursts. Detailed temporal behavior of discharge pulses evolving during both positive and negative half-cycles is presented **Figure 3.1b** and **Figure 3.1c**. It can be seen that during both intervals the current pulses are characterized by similar durations (tens of ns) and amplitudes (hundreds of mA) causing the transient distortion of the high voltage waveform (typical voltage drop during a current pulse ΔU was 200–300 V). Statistical analysis of recorded waveforms revealed that the number of current pulses, which correspond to individual micro-discharges, varies from 7×10^5 micro-discharges per second observed for the applied peak-to-peak voltage 9.6 kV up to 1.5×10^6 micro-discharges per second for the peak-to-peak voltage 10.8 kV.

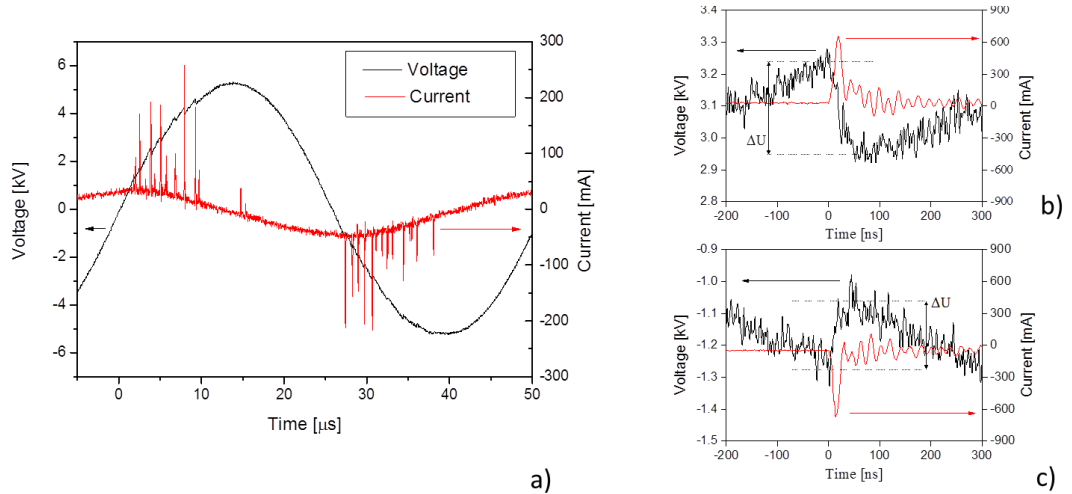


Figure 3.1 a) Current and voltage waveforms recorded for the applied peak-to-peak voltage of 10.4 kV and averaged characteristics of discharge pulses produced during the b) positive and c) negative half-cycle.

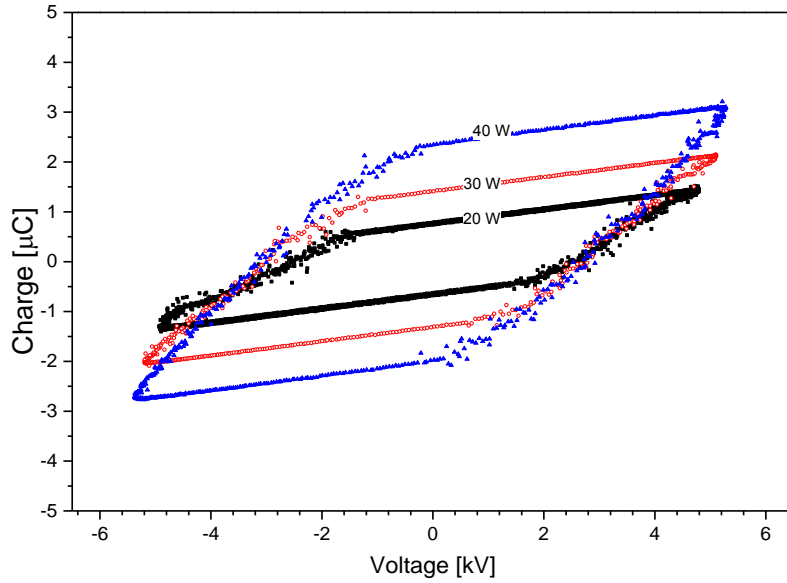


Figure 3.2 Lissajous Q–V figures corresponding to the DBD powers of 20, 30 and 40 W.

The discharge power was determined from so-called Lissajous figures that represent the transferred charge Q flowing into the circuit as a function of the voltage difference between the electrodes [119]. As it is depicted in **Figure 3.2** obtained Lissajous figures have the shape of a parallelogram, which is common for planar DBD configurations [13], [119]. The power consumed may be then calculated from the area of the Lissajous figures. It ranged from 20 W up to 40 W as the peak-to-peak voltage increased from 9.6 kV up to 10.8 kV. Taking into account the area of the powered electrode and the discharge gap, the power density was estimated to be in the order of tens of W per cm^{-3} .

In order to estimate the composition of used DBD plasma, optical emission spectra were recorded in the spectral range from 300 nm to 900 nm. As can be seen in **Figure 3.3** the only detectable spectral emission bands and lines were the ones that correspond either to the first and second positive systems of N_2 (in the wavelength range 500–900 nm and 300–450 nm, respectively), the first negative system of N_2^+ (around 391 nm) and weak emission lines of atomic oxygen. However, the most intense spectral bands that dominated the emission spectra were the ones belonging to the second positive system of N_2 ($\text{C}^3\Pi_u \rightarrow \text{B}^3\Pi_g$). It was observed that the

intensity of spectral bands belonging to this emission system increased with increasing DBD power - the intensity was approximately doubled as the power increased from 20 W to 40 W (see **Figure 3.4**).

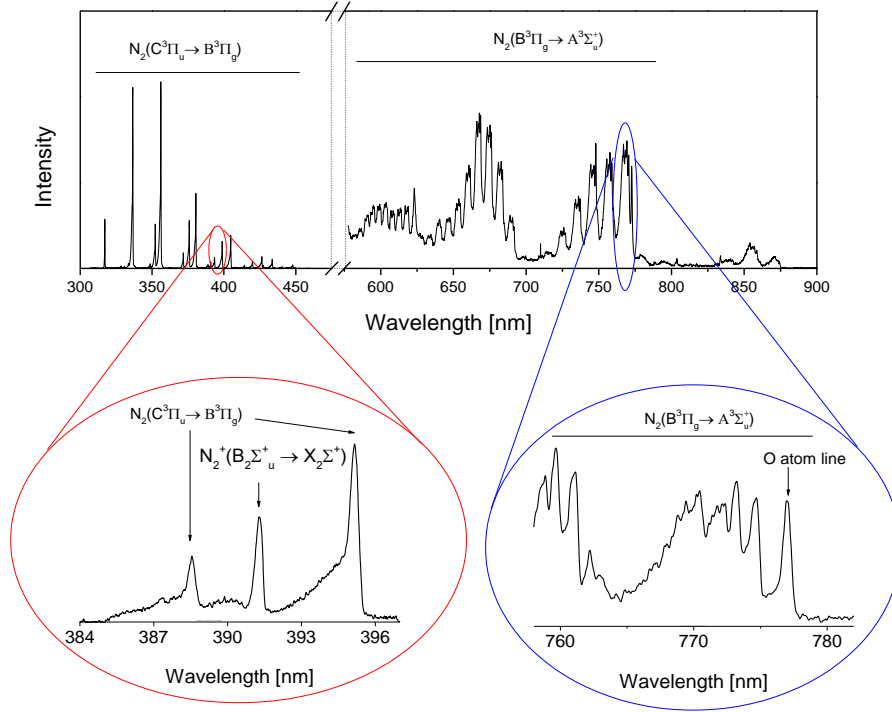


Figure 3.3 Characteristic emission spectra of the volume asymmetric DBD produced in humid air.

However, no significant variations of T_{vib} were observed with increasing the DBD power and the vibrational temperature stayed in between 2710 K and 2860 K independently of the DBD power. Similar values of vibrational temperature measured for different powers suggest that the electron energy distribution function is not significantly affected by the DBD power. Observed increase of intensities of the detected nitrogen spectral bands is mainly due to the increasing density of the discharge filaments with the DBD power.

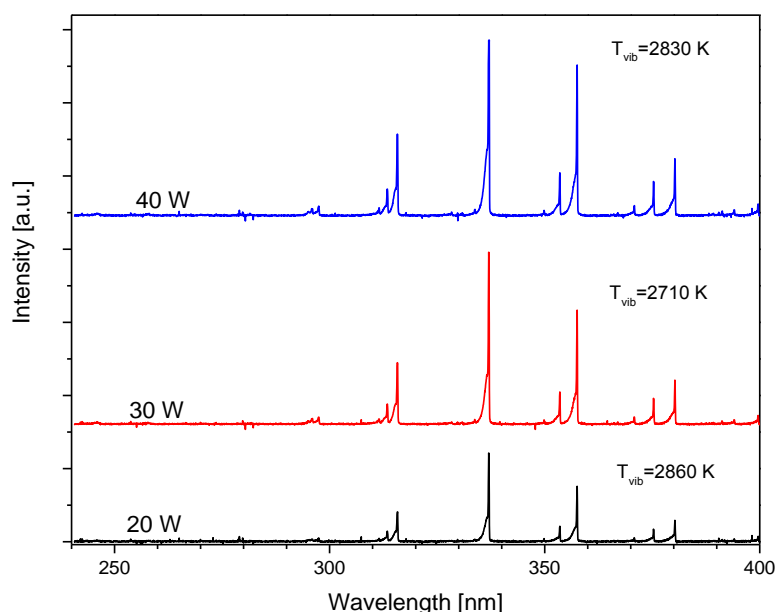


Figure 3.4 Sections of optical emission spectra recorded at different discharge powers.

Another important parameter that is determinative for the possible use of DBD plasma for processing of polymeric materials is temperature. According to the detailed analysis of the first positive and negative systems of nitrogen emission bands the rotational temperature, that reflects local heating of gas in streamer filaments, may reach rather high values exceeding 150°C [120], i.e. temperature that is not compatible with the majority of the polymers. Therefore in order to limit the thermal load on treated samples, the upper electrode was periodically moved above the lower grounded electrode, where the samples were placed. The scanning speed was 4.0 cm.s⁻¹. Taking into account the dimensions of the moveable electrode and the scanning speed each part of the sample was exposed to DBD plasma for 0.5 s during one scan. The pyrometric evaluation of the temperature of surfaces of polymeric foils placed on the bottom electrode proved that scanning mode causes substantial reduction of the thermal load on polymeric samples: the temperature reached after 120 scans (i.e. for total exposure time 1 min) values around 80 °C, 60 °C and less than 40 °C for DBD powers of 40 W, 30 W and 20 W, respectively. This was furthermore confirmed by use of thermo-camera [121].

3.1.2 Influence of DBD plasma treatments at atmospheric pressure on properties of polymeric foils

Next step of this work was evaluation of effect of DBD plasma treatment on common polymers. In contrast to earlier studies of other groups that were dedicated to this topic, in our case higher number of polymeric materials was treated under identical conditions with aim to compare the plasma action on larger set of materials. Taking into account results presented in the previous section all tests were performed in dynamic regime (i.e. upper electrode scanned the surface of treated samples) and applied power of 30 W was selected as a compromise between treatment efficiency and heating of the samples. Finally, it is worth noting that the study of plasma influence on particular property of polymers will be usually divided into two parts. First, results obtained for all foils will be briefly summarized. This will be than followed by more detailed discussion of the results reached for nylon 6,6 and PET foils selected as representative examples of observed phenomena. Analogous experiments were, however, performed also for other polymers, but they are not included here.

3.1.2.1 Chemical composition

First studied property of polymeric foils was their surface chemical composition that was determined by means of XPS before and immediately after the DBD treatment. The surface atomic concentrations of all untreated and treated foils (treatment times 1 sec and 16 sec) are presented in **Table 3.1**. As shown in this table, the fraction of oxygen significantly increased on the surface for all tested polymers already after 1 sec of DBD plasma treatment duration independently of the chemical structure of untreated polymers. This occurred at the expense of the atomic concentration of carbon and for several polymers it was also accompanied either by appearance or slight increase of nitrogen surface concentration. Moreover, it can be seen in **Table 3.1** that prolonged plasma treatment led for most of the polymers only to imperceptibly small additional alterations of their surface chemical composition. Exceptions were nylon 6,6, PP and LDPE, for which additional enhancement of

amount of oxygen was observed as the treatment duration was increased. Such differences are most likely due to the different structure of individual polymers or due to their gradual etching by DBD plasma. The latter hypothesis will be discussed in detail in the *section 3.1.2.5*.

Table 3.1 Chemical composition of untreated and DBD plasma treated polymeric foils measured by XPS.

Polymer	Time of treatment [s]	C [%]	O[%]	N [%]	O/C	N/C
Nylon 6,6	0	76	13	11	0.17	0.14
	1	70	18	12	0.26	0.17
	16	61	26	13	0.43	0.21
PET	0	72	28	0	0.39	0
	1	64.5	35	0.5	0.54	0.01
	16	62	37	1	0.60	0.02
PEN	0	71	27	2	0.38	0.03
	1	63	33.5	3.5	0.53	0.06
	16	63	29	8	0.46	0.13
PP	0	92.5	5.5	2	0.06	0.02
	1	83	16	1	0.20	0.01
	16	67	32	1	0.48	0.01
LDPE	0	100	0	0	0	0
	1	81.5	18	0.5	0.22	0.01
	16	67.5	31.5	1	0.47	0.01
PEEK	0	80	20	0	0.25	0
	1	75	24	1	0.32	0.01
	16	73	26	1	0.36	0.01
PMMA	0	74.5	25.5	0	0.34	0
	1	68	32	0	0.47	0
	16	64	35.5	0.5	0.56	0.01

Alongside with increasing O and N surface concentration, also the abundance of functional groups was varied and new functional groups were formed on surfaces of treated foils after the treatment. This effect is most easily observable for polyethylene foils, for which only C1s peak at 284.8 eV that corresponds to aliphatic C-C/C-H bonds was detected in XPS spectra (see **Figure 3.5, a**). After 1 sec of DBD treatment, C1s peak changed dramatically (see **Figure 3.5, b**) and new components appeared that can be attributed to β -shift of the carbon atom adjacent to a carboxyl group (285.7 eV), C-O groups (286.5 eV), carbonyl groups (C=O, around 288 eV)

and ester and/or carboxyl groups (O-C=O) positioned at 289.3 eV. Presence of C-O and C=O bonds was confirmed also by high resolution XPS spectra of O1s peak (Figure 3.5, c).

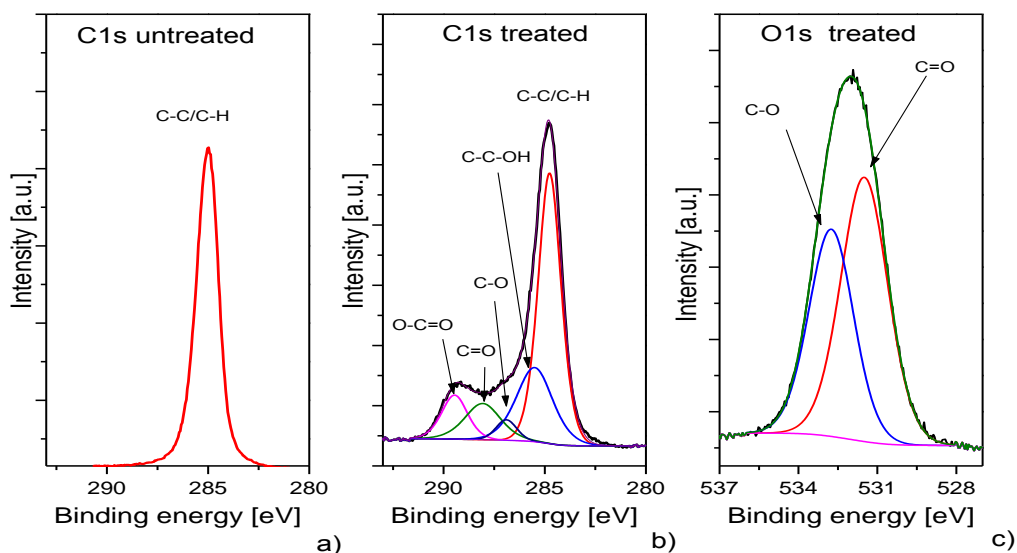


Figure 3.5 High resolution C1s peak of **a)** untreated and **b)** DBD treated LDPE. **c)** High resolution O1s peak of DBD treated LDPE.

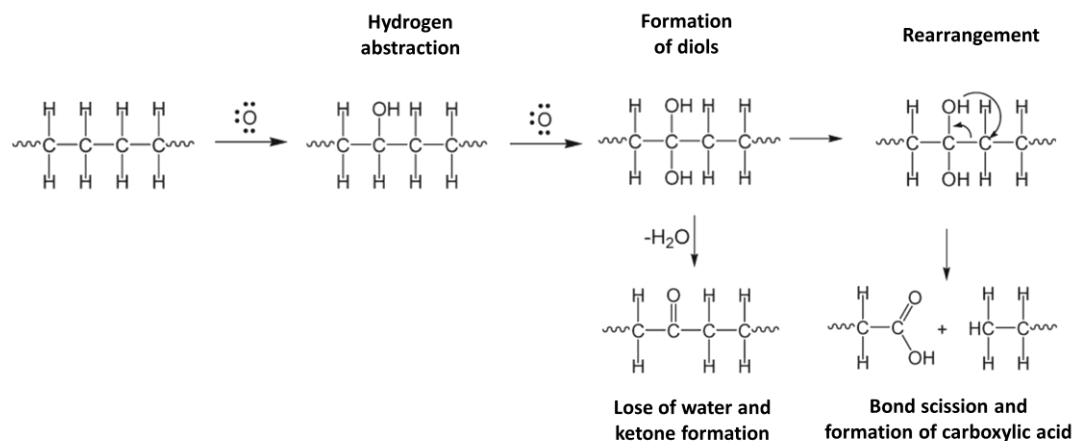


Figure 3.6 Mechanism of modification of polyethylene in DBD plasma.

According to the experiments focused on plasma treatment of polymers in oxygen-containing plasma [122], these results may be interpreted as schematically depicted in **Figure 3.6**. First, atomic oxygen that is produced in DBD plasma interacts with

hydrocarbon chain and forms hydroxyl species that gives rise to C-O component of C1s peak. This is repeated and diols may be formed. Due to the rearrangement, chain scission occurs, which is accompanied by the formation of carboxylic acid -COOH. This may explain both the decrease of C-C/C-H bonds and the rise of amount of O-C=O functional groups. Alternatively, diols may lose water to form a ketone. This results again in a decrease of C-C/C-H bonds and in a formation of carbonyl groups (C=O).

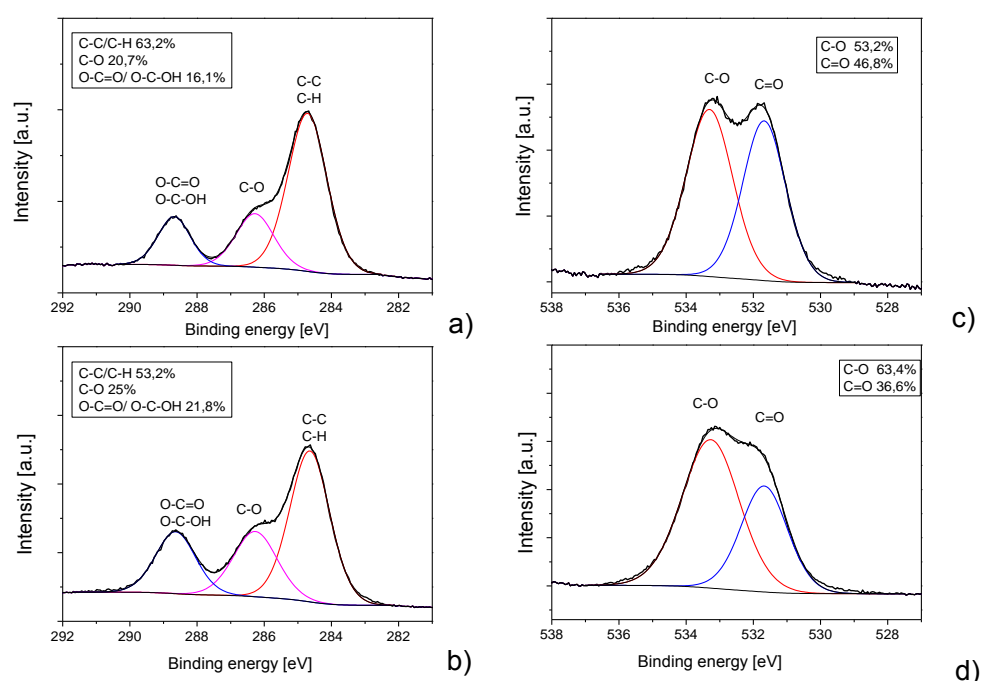


Figure 3.7 High resolution C1s XPS peak of PET **a)** before and **b)** after DBD treatment. High resolution O1s XPS peak of PET **c)** before and **d)** after DBD treatment.

Alteration of surface chemical structure induced by plasma treatment may be documented also on PET foils. Also in this case the plasma treatment resulted in increase of components of C1s peaks that correspond to C-O and O-C=O or O-C-OH, respectively (compare **Figure 3.7, a** and **Figure 3.7, b**). Moreover, as PET contains oxygen in its native structure, effect of DBD on bonding state of oxygen may be demonstrated as well. In the case of O1s peak observed changes suggest decrease of amount of C=O functional groups (binding energy 531.7 eV) that is

counterbalanced by relative increase of abundance of C-O groups at binding energy of 533.3 eV (see **Figure 3.7, c** and **Figure 3.7, d**). These changes, i.e. increasing ratio of C-O/C=O bonds after the plasma treatment, which are in agreement with results presented and in detail discussed for plasma treatment of PET foils with Diffuse Coplanar Surface Barrier Discharge [123], were observed also for other oxygen-containing polymeric foils studied in the frame of this work.

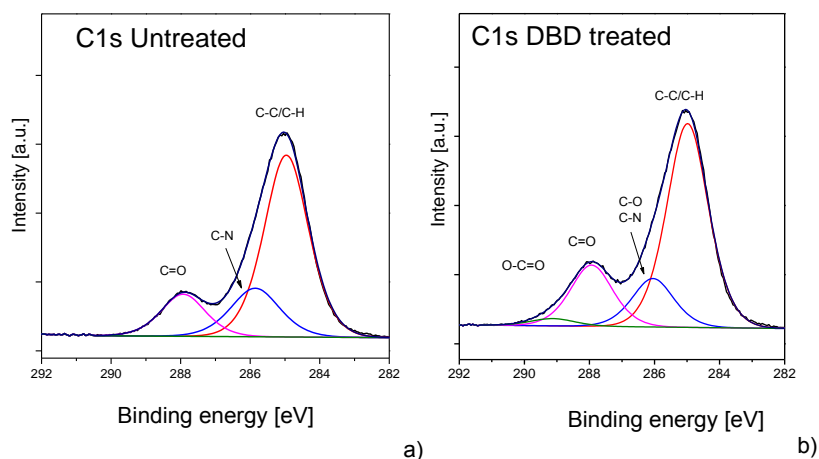


Figure 3.8 High resolution XPS spectra of C1s peak of nylon 6,6 **a)** before and **b)** after DBD treatment.

Final example is nylon 6,6 as this polymer is the only one from the tested polymers that contains nitrogen. The C1s XPS peak measured on untreated nylon foil was fitted by three components as shown in **Figure 3.8, a**. The component at the binding energy of 285 eV was attributed to C-C/C-H bonds, the component at the binding energy of 285.9 eV was assigned to the carbon atoms bonded to the -NH- group in nylon 6,6, and the component at the binding energy of 288 eV is characteristic for carbon atoms of amide carbonyl groups (CO-NH) [124]. After the DBD treatments in air following changes in C1s peak were observed (**Figure 3.8, b**): besides decrease of C-C/C-H component and increase of C=O new component appeared in C1s XPS spectra after the plasma treatment at the binding energy around 289 eV. In agreement with other studies [34], this component indicates again formation of O-C=O functional group.

In analogy to above-discussed XPS spectra of PET, plasma treatment leads to enhancement of C-O bonds that happens on expense of C=O bonds (see **Figure 3.9**).

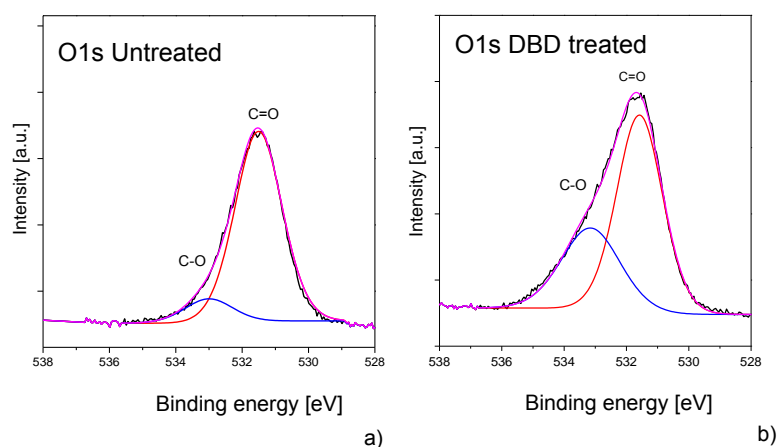


Figure 3.9 High resolution XPS spectra of O1s peak of nylon **a)** before and **b)** after DBD treatment.

Finally, plasma treatment influenced also N1s XPS peak, which is demonstrated in **Figure 3.10**. For untreated nylon foils N1s peak may be fitted by one component at the binding energy of 399.9 eV, which is typical for amides.

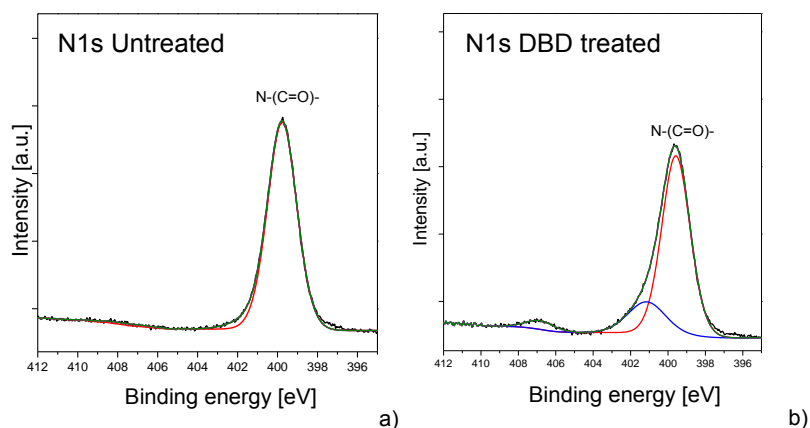


Figure 3.10 High resolution XPS spectra of N1s peak of nylon 6,6 **a)** before and **b)** after DBD treatment.

After the DBD plasma treatment two new components were observed at binding energies around 401.5 eV and 407 eV. Whereas the peak at 407 eV may be identified as nitrate nitrogen [124], the peak at 401.5 eV suggests either nitrogen bonded to

highly oxidized carbon (e.g. hydroxyimide structure) or the presence of hydrogen bonded to amide nitrogen. In the latter case the chemical shift of the binding energy may be assigned to an increase in the positive charge of the nitrogen atom produced by hydrogen bonding [125].

3.1.2.2 Surface morphology

The second investigated surface characteristic was morphology of polymeric foils. Although the initial morphology of studied polymeric foils differs significantly (some foils were smooth with randomly distributed ridges originated from the manufacturing process, some exhibited rather rough granular- or star-like structure) plasma treatment in general caused an increase of their roughness (see **Table 3.2**).

Table 3.2 RMS roughness of untreated and DBD treated polymeric foils.

Polymer	RMS [nm]			
	Time of treatment [s]			
	0	1	8	16
Nylon 6,6	14.5±1.2	15.2±0.8	14.6±0.8	17.9±2.4
PET	1.1±0.1	3.2±0.2	6.2±0.2	8.1±1.1
PEN	6.4±0.6	7.9±1.0	12±1.8	17.5±3
PP	20.7±5.3	23.9±8.2	42±0.8	68.8±3.5
LDPE	14.8±2.3	15.6±1.2	17.5±1.3	22.9±1.0
PEEK	1.6±0.1	3.8±0.4	3.4±0.2	4.6±0.3
PMMA	9.4±0.3	10.9±0.1	10.6±1.9	11.9±0.8
PLA	4.6±0.2	5.3±0.1	13.2±0.2	13.4±0.3

Closer look on acquired AFM images allows us to divide tested polymers into two groups in dependence on the plasma action. The first group, into which fall PET, PEN, PEEK and PMMA, exhibited appearance of small almost circular “bumps” after the plasma treatment (see **Figure 3.11**). The size of these bumps gradually increased with DBD treatment time, but the overall character of the surface morphology was not changed. According to literature such structures may be result of differences in the etching rates of amorphous and crystalline regions of polymers (e.g. [37], [126]).

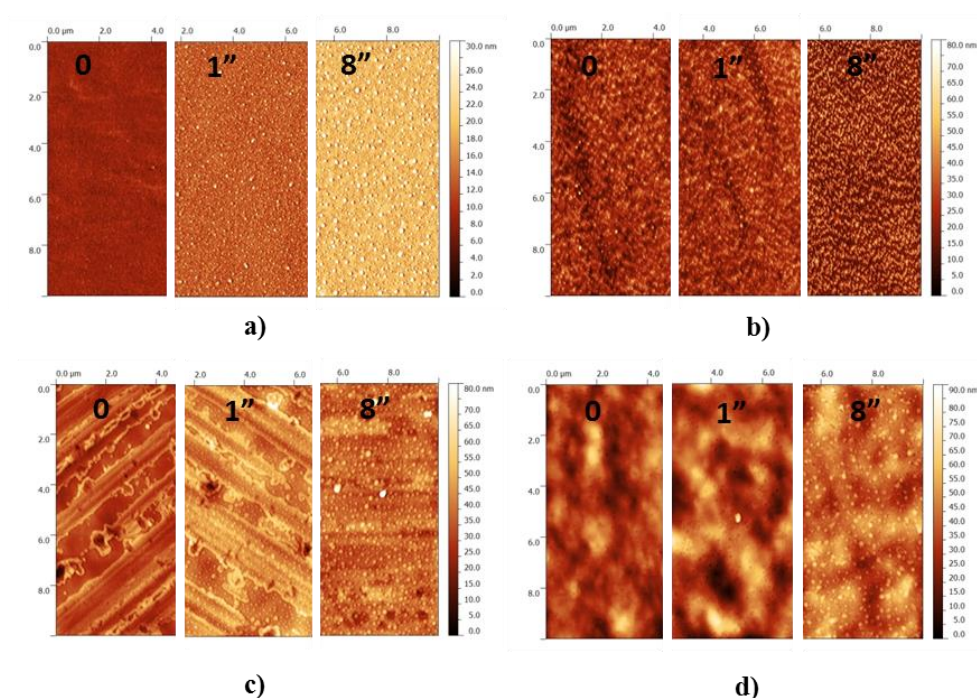


Figure 3.11 Sections of AFM images of **a) PET**, **b) PEN**, **c) PEEK** and **d) PMMA** of untreated (left) and DBD treated for 1 sec (middle) and 8 sec (right) foils

The second group, into which belong PP, LDE, nylon 6,6 and PLA, showed different behavior – in addition to small “bumps” observed also for the first group, considerable larger and in some cases rather irregular structures were formed on their surfaces after the plasma treatment. This can be seen in **Figure 3.12**. Possible explanation of the origin of the bigger structures is the local heating of foils surfaces at locations, where the foil was hit by the plasma channel. This hypothesis is supported by the fact that all the polymers in the first group pose much higher thermal stability as compared to all polymers in the second group.

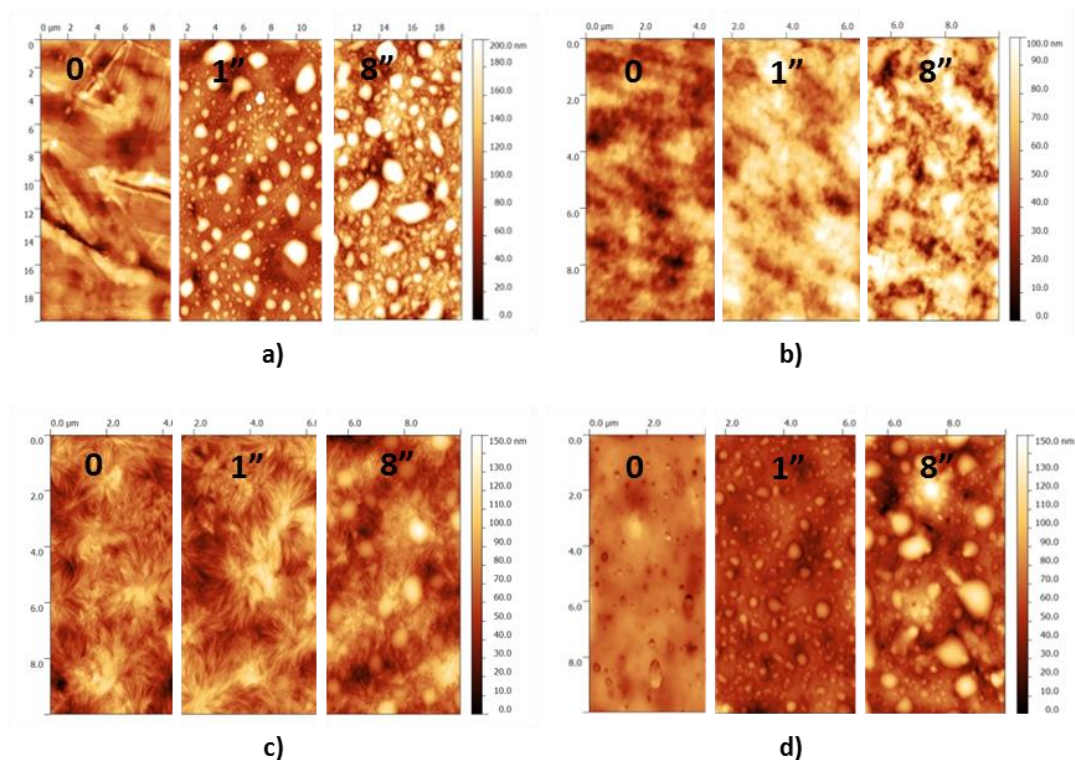


Figure 3.12 Sections of AFM images of **a)** PP, **b)** LDPE, **c)** nylon 6,6 and **d)** PLA of untreated (left) and DBD treated for 1 sec (middle) and 8 sec (right).

In order to test the hypothesis that larger structures are connected with local heating of foils additional experiments were done. Nylon 6,6 was used for these experiments. As it was mentioned above, the temperature of plasma treated surfaces reached 60 °C after 1 minute of treatment at 30W. Nylon foils were therefore exposed to hot air at 80°C for 2 min and AFM image of such treated foil was compared with AFM image of untreated foil. As can be seen in **Figure 3.13**, no differences in morphology between heated and non-heated samples were observed. This suggests that the changes observed after the DBD treatment are not due to the homogeneous heating of polymeric foil and must be connected with plasma action itself.

In the second set of experiments the plasma treatment was divided into 8 treatments for 4 seconds separated by 10 min cooling period, i.e. time sufficient for the foil to come back to the room temperature. This procedure limited thermal load on the treated foil. Another sample was then treated in continuous mode for 32 seconds. The total time of plasma exposure for both samples was the same. As can be seen in

Figure 3.14, their morphologies are very similar in both cases. As the thermal load on both samples was dramatically different, this result confirms that observed changes in the morphology of nylon 6,6 are indeed connected with the plasma treatment (or “plasma dose”) – most likely resulting in substantial local heating. However, it is important to stress that further experiments are still needed to confirm this hypothesis.

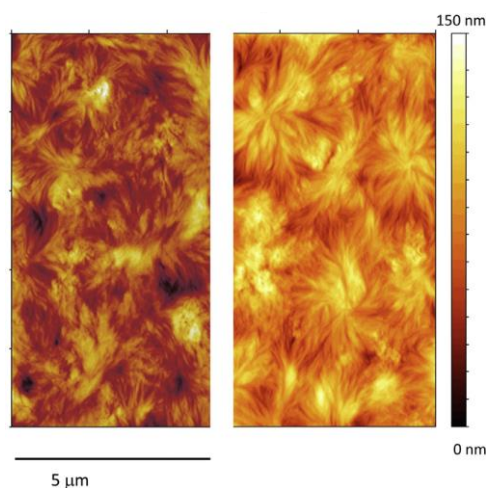


Figure 3.13 AFM images of untreated nylon 6,6 (left) and nylon 6,6 exposed to hot air for 2 min (right)

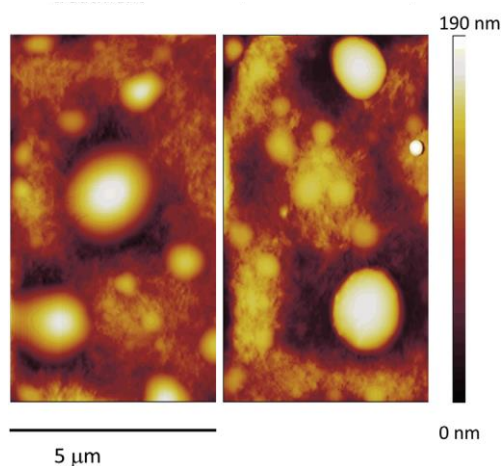


Figure 3.14 Comparison of 10 x 5 μm AFM scans of nylon foil after 32 s of DBD treatment performed at once (left) and in 8 steps (right)

3.1.2.3 Wettability and surface energy

Next step was evaluation of wettability and surface free energy of polymer's surfaces after the DBD plasma treatment. Each of the polymeric foils was in this set of experiments exposed to the DBD plasma for 1 sec, 8 sec and 16 sec. In agreement with other studies the decrease of water contact angles was observed for all tested polymeric foils as can be seen in **Table 3.3**, where values of static, advancing and receding water contact angles are summarized.

It can be seen that already 1 sec of plasma treatment led to significant increase of wettability. After prolonged plasma exposure the values of water contact angles slowly decreased but not as dramatically as during the first seconds of the treatment. In order to highlight observed changes, static water contact angles measured before and after 16 sec plasma treatment are graphically presented in **Figure 3.15**.

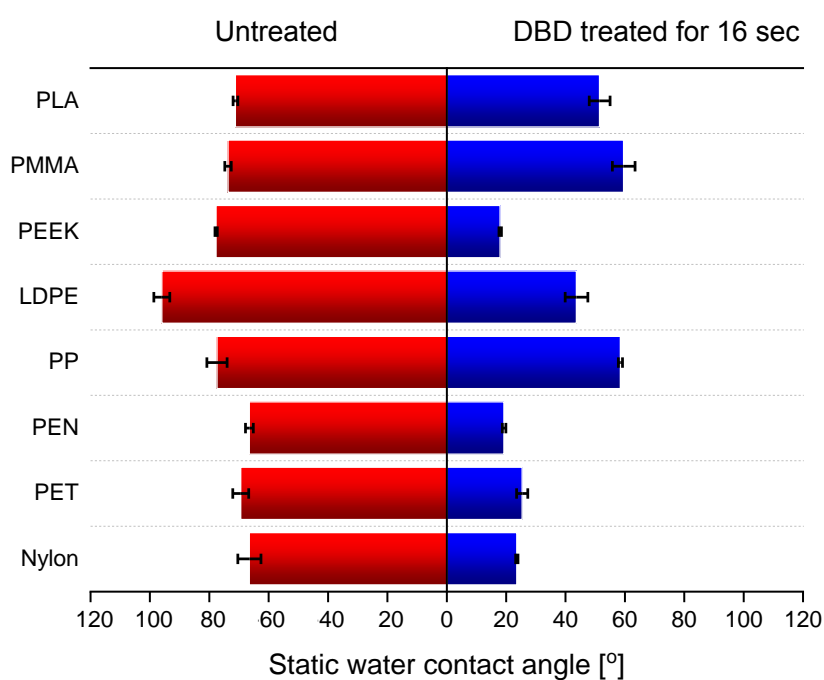


Figure 3.15 Static water contact angles measured on different polymeric foils before and after 16 sec DBD plasma treatment.

Table 3.3 WCA of untreated and DBD plasma treated polymeric foils.

Polymeric foil	Treatment time [s]	Static Contact Angle [°]	Advancing Contact Angle [°]	Receding Contact Angle [°]
Nylon 6,6	0	66.5 ±3.9	70.4 ±4.4	40.7 ±5.7
	1	29.8 ±2.1	32.5 ±0.2	9.4 ±0.9
	8	25.7 ±0.9	26.7 ±0.3	9.6 ±1.0
	16	23.6 ±0.4	24.6 ±0.5	9.5 ±0.4
PET	0	69.4 ±2.7	81.7 ±2.5	52.0 ±1.0
	1	38.8 ±2.1	46.5 ±2.3	9.7 ±1.0
	8	27.4 ±1.5	31.9 ±2.2	6.6 ±0.6
	16	25.4 ±1.9	28.5 ±1.1	6.7 ±0.6
PEN	0	66.5 ±1.3	75.6 ±1.7	52.3 ±3.1
	1	50.0 ±1.9	60.3 ±1.6	17.9 ±3.4
	8	24.6 ±3.7	30.2 ±0.3	11.7 ±0.3
	16	19.3 ±0.6	22.9 ±2.9	5.8 ±1.0
PP	0	77.4 ±3.4	88.7 ±1.9	52.0 ±5.4
	1	61.4 ±0.8	64.7 ±1.6	34.1 ±3.3
	8	60.1 ±0.7	60.9 ±1.6	33.0 ±4.8
	16	58.5 ±0.7	58.3 ±3.6	25.8 ±3.6
LDPE	0	96.0 ±2.7	99.2 ±2.8	78.0 ±3.0
	1	54.4 ±2.5	62.2 ±0.9	27.3 ±1.4
	8	41.8 ±2.9	54.3 ±2.2	22.5 ±1.4
	16	43.7 ±3.8	54.4 ±1.6	17.4 ±1.7
PEEK	0	77.7 ±0.4	80.5 ±1.0	26.9 ±6.0
	1	27.8 ±1.1	32.4 ±1.0	11.5 ±1.6
	8	21.2 ±1.8	24.9 ±2.3	6.9 ±1.0
	16	18.0 ±0.4	22.7 ±0.5	6.9 ±0.8
PMMA	0	73.7 ±1.1	88.6 ±0.4	57.5 ±2.9
	1	58.3 ±1.8	70.7 ±1.8	28.9 ±1.0
	8	56.4 ±4.1	70.0 ±1.1	23.4 ±2.8
	16	59.6 ±3.8	69.8 ±0.4	17.4 ±2.0
PLA	0	71.2 ±0.8	76.1 ±0.3	66.6 ±1.3
	1	56.0 ±1.0	63.9 ±1.2	39.4 ±1.4
	8	54.3 ±1.9	58.7 ±0.8	27.9 ±1.2
	16	51.5 ±3.5	57.5 ±1.8	20.8 ±2.5

The changes in wettability are due to the rapid change of surface energy. It has been found that plasma treatment for all tested materials caused predominantly the rise of polar component of surface energy, whereas its dispersive part was almost unchanged (see **Figure 3.16**). This is in agreement with the results of XPS that indicated increase or formation of oxygen or nitrogen containing functional groups on plasma treated polymers (see *section 3.1.2.1*). Furthermore, the strong correlation between wettability and surface energy was confirmed experimentally, which is evident from **Figure 3.17, a**, where is plotted the dependence of water contact angle on total surface energy for both untreated and DBD treated polymeric foils.

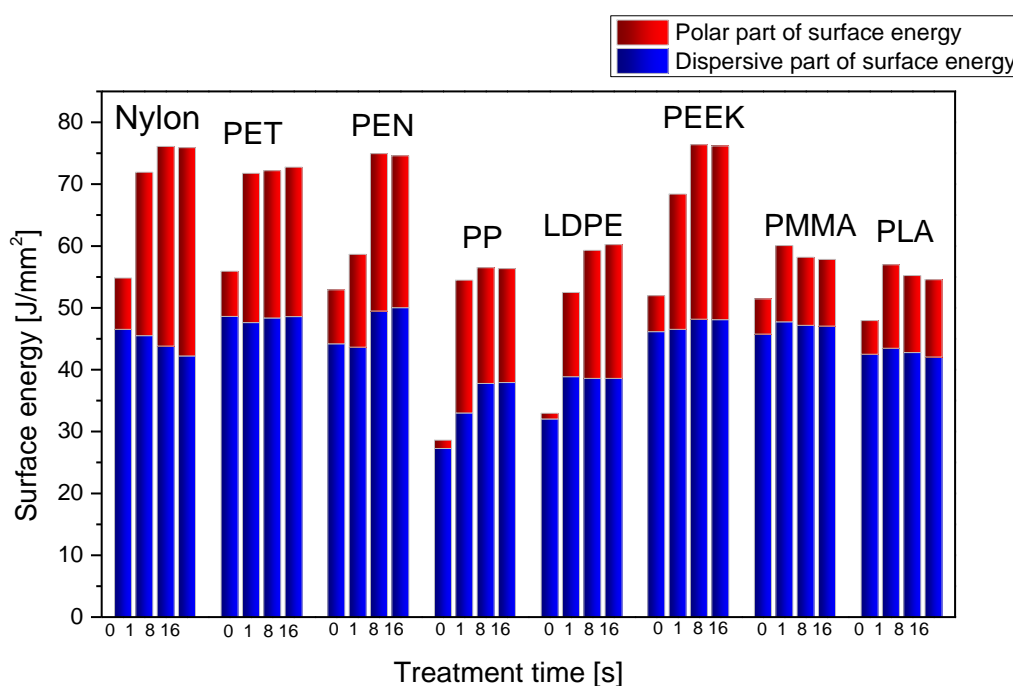


Figure 3.16 Evolution of polar and dispersive components of surface energy with DBD treatment for different polymeric foils.

Although it is quite difficult to make direct link between the wettability and surface chemical composition derived from XPS spectra, general trend that correlates these two quantities was observed. As can be seen in **Figure 3.17, b**, the values of water contact angles follow for all tested samples the same trend – they decrease as the fraction of oxygen and nitrogen at surface increases.

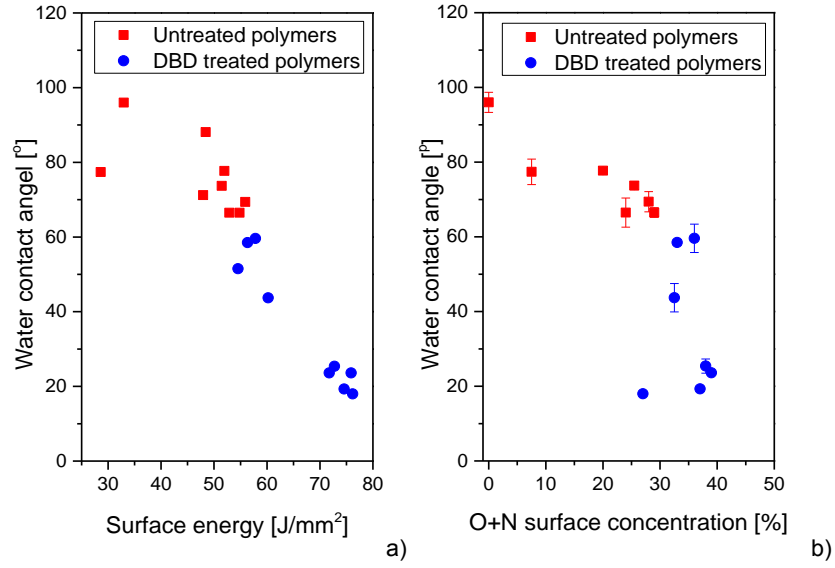


Figure 3.17 a) Dependence of measured values of water contact angles on total surface energy. **b)** Dependence of water contact angle on O+N surface concentration.

However, the wettability was not stable and gradual increase of water contact angles with storage time was observed for all polymers. For examples of nylon 6,6 foils and PET foils refer to **Figure 3.18**. This effect, that is sometimes termed ageing or hydrophobic recovery, is explained either by reorientation of polar functional groups on a polymeric surface, outward-diffusion of low-weight oligomers or additives and/or by accumulation of air-born impurities [35], [36], [127]. In order to quantify the ageing process, the time dependence of the static water contact angle on the storage time was fitted by empirical formula [128]:

$$\theta(t) = \theta_{sat} - A \cdot e^{-\frac{t}{\tau}} \quad (3.1)$$

where θ_{sat} corresponds to the saturation contact angle, A is the fitting parameter and τ represents the characteristic restoration time of the contact angle. According to the fitting procedure of measured data the characteristic time τ was determined to be 1 and 7 days for nylon 6,6 and PET, respectively.

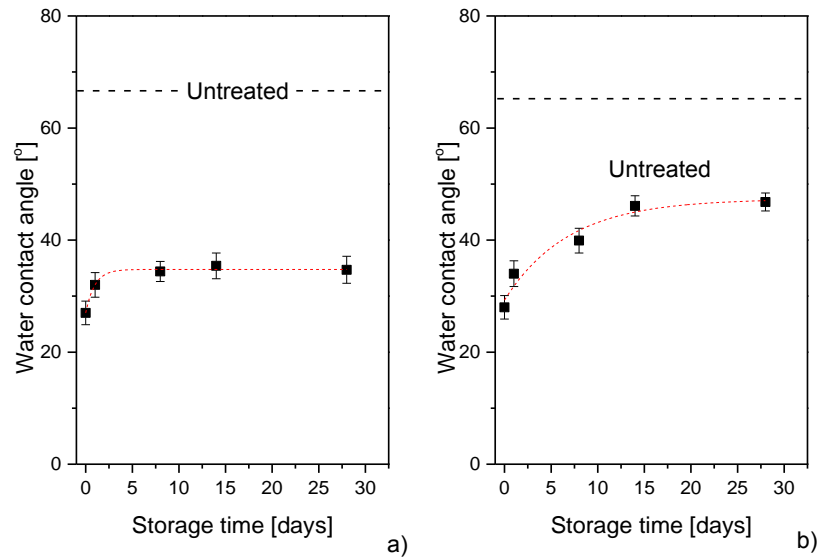


Figure 3.18 Dependence of water angle of DBD treated for 8 sec a) nylon 6,6 and b) PET foils on storage time.

Finally, it has to be noted that even after prolonged storage time the values of water contact angles were in all case still considerably lower as compared to the ones measured on untreated samples.

3.1.2.4 Mechanical properties of Nylon and PET foils

Within a project preliminary tests focused on the investigation of the influence of DBD treatment on mechanical properties of polymeric foils were performed. It was decided to choose nylon 6.6 and PET foils as test materials for these experiments and their mechanical properties before and after the plasma treatment were evaluated by means of nanoindentation method.

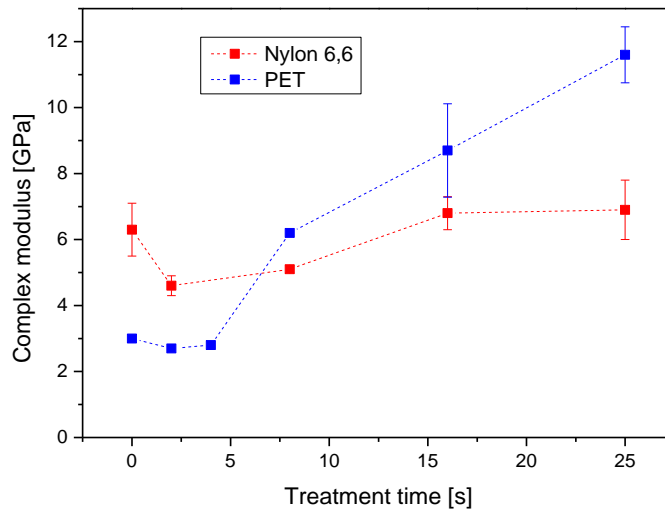


Figure 3.19 Variation of complex modulus with DBD treatment time for nylon 6,6 and PET foils.

The results are summarized in **Figure 3.19**. It can be seen that different behavior was observed for these two polymers: whereas the value of complex modulus was not significantly modified when nylon foils were treated by the DBD plasma up to 25 s (complex modulus stayed in the range 4.6-6.9 GPa), DBD treatment caused considerable increase of complex modulus in the case of PET (from 3 GPa up to 11 GPa). The latter may be possibly explained by enhanced crosslinking of the surface layer of PET foils induced by plasma treatment. Although performed measurements proved that nanoindentation may be used to study changes of mechanical properties of plasma treated polymeric foils, more detailed and systematic studies are needed to allow drawing relevant conclusions.

3.1.2.5 Plasma etching of conventional polymers

The action of atmospheric pressure air DBD plasma on polymers was also investigated with focus given on the etching rates of these materials, i.e. phenomenon usually overlooked in literature related to atmospheric pressure DBD treatment of

polymers. The etching rates were measured for all polymers at DBD power of 30 W gravimetrically, i.e. by weighting the foils before and after the plasma treatment. In all cases the decrease of the mass of treated polymers was linearly dependent on the treatment time, i.e. the etching rates were temporally stable, at least for the treatment times used in this study. Measured values of etching rates calculated from the mass loss, known area of treated foils and under assumption that the density of polymeric foils is not influenced by the plasma treatment were found to be several nm per minute. This value is comparable with the results of DBD etching of photoresist (~ 3 nm/min [129]).

However, the measured rates of the mass losses were found to significantly vary in dependence on the chemical structure of treated polymer as demonstrated in **Figure 3.20**. The slowest etching effect was observed for hydrocarbon polymers (LDPE and PP) and the highest one was reached for PLA. These results are in qualitative agreement with the results reported for the low-pressure plasma treatment in oxygen containing atmosphere that showed that the presence of oxygen in the polymeric structure enhances, at otherwise identical treatment conditions, the etching rates of polymers (e.g. [130]). In order to highlight this effect, the mass loss rates were plotted as a function of O/C ratio in untreated polymers (**Figure 3.20, b**). It can be seen that etching rate substantially increases with increasing O/C ratio. This suggests that the key parameter that influences the removal rates of polymers by air DBD plasma is indeed presence of oxygen in their structures.

Furthermore, the etching, i.e. gradual volatilization of treated polymers, may be behind the dependence of the surface chemical structure on the treatment time discussed in *section 3.1.2.1*. Non-negligible etching of the top most layer causes continual removal of plasma modified layer and thus non-modified (“fresh”) polymer is exposed to the plasma. Removal and surface modifications should at some point reach the steady-state at which the chemical changes and removal is in equilibrium. The moment at which the steady-state is reached naturally depends on the rates of both processes. As pointed out, the slowest etching was observed for polymers that have no oxygen in their native structure, i.e. for LDPE and PP. Following the proposed scheme and assuming that the rates of chemical changes are the same or at

least comparable for all tested polymers this means that the stabilization should take for these two polymers longer time. This is in agreement with XPS data.

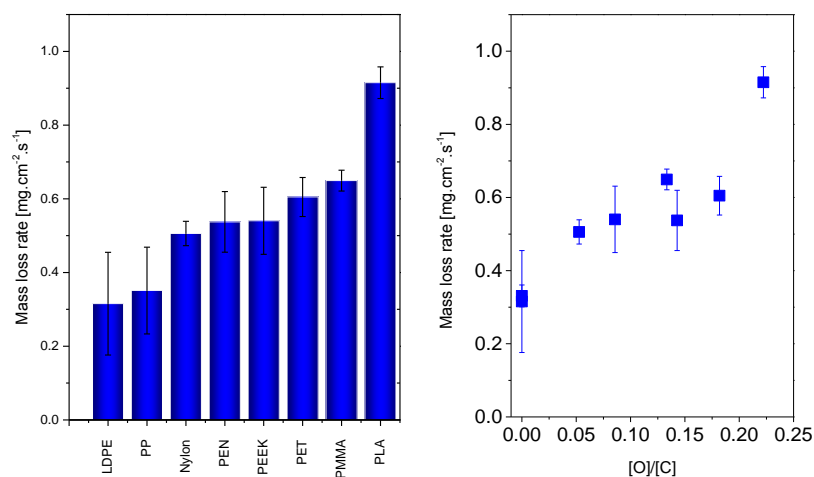


Figure 3.20 a) Mass loss rates of polymers exposed to 30 W DBD plasma and b) mass loss rates plotted as a function of [O]/[C] ratio.

3.1.3 Application of DBD plasma

3.1.3.1 Influence of DBD plasma on cell growth

One of possible applications, where plasma modification of polymers by atmospheric pressure plasma is expected to play significant role, is enhancement of biocompatibility of common polymers. In this work experiments were performed in collaboration with Institute of Physiology, Academy of Sciences of the Czech Republic with aim to evaluate the growth of two different types of cells on untreated and DBD pretreated PET foils. For this study Saos-2 osteoblasts like cells and Human Umbilical Vein Endothelial Cells (HUVEC) cells were selected. Times of DBD plasma exposure were 1 sec and 8 sec.

Table 3.4 Number of Saos-2 and HUVEC cells on untreated and DBD plasma treated PET foils.

Day after seeding	SAOS cells [$\times 10^3$]			HUVEC cells [$\times 10^3$]		
	Untreated	1" DBD	8" DBD	Untreated	1" DBD	8" DBD
1	15.5 \pm 0.8	17 \pm 1	17 \pm 1	0.51 \pm 0.4	8.6 \pm 0.6	8.8 \pm 0.5
3	30 \pm 3	39 \pm 3	36 \pm 3	7.7 \pm 0.8	29 \pm 2	35 \pm 1
7	180 \pm 8	278 \pm 14	227 \pm 7	74 \pm 4	100 \pm 3	99 \pm 2

Results reached for both Saos-2 and HUVEC cells are summarized in **Table 3.4**. As can be seen, slight enhancement of the growth of Saos-2 osteoblast-like cells on DBD treated PET foils was observed. The highest increase in the number of Saos-2 cells was approximately 50% on day 7 after seeding. The maximum cell number was obtained on foils treated with plasma for 1 s, and it slightly decreased on foils treated for 8 s. This effect is in line with previous studies with low-pressure Ar plasma modification of polymers that showed that shorter plasma exposure times were often more appropriate for increasing number of vascular smooth muscle cells than longer exposure times [131]. However, in the other time intervals (days 1 and 3), the Saos-2 cell numbers were similar on PET foils treated with plasma for 1 and 8 s and untreated PET. This is evident also from acquired pictures of Saos-2 cells on these three surfaces after 3 days of seeding (**Figure 3.21, a, b and c**).

In contrast to Saos-2 cells, plasma pretreatment of PET foils resulted in much more pronounced increase of number of attached endothelial cells especially on day 1 (approximately 17x) and on day 3 that (approximately 4x) after seeding as compared to untreated PET (**Figure 3.21, d, e and f**). Although on day 3 the increase in cell number was more apparent on foils treated for 8 sec than for 1 sec (approximately by 20%), in the other time intervals (days 1 and 7) the cell numbers were similar on foils treated for both times. Thus, the dependence of cell number on the plasma exposure time was not systematic and was rather accidental. In other words, no straight correlation between the cell number and plasma treatment duration was observed. Taking into account increasing surface roughness of PET foils with increasing treatment time (see **Table 3.2**) and almost stable surface chemical composition and

wettability irrespective of the treatment time (see **Table 3.1** and **Table 3.3**) this suggests that the key factor that positively influences attachment and growth of HUVEC cells on plasma treated PET foils is surface activation and not changes in morphology induced by DBD plasma treatment. This can be explained by improving of wettability, as hydrophilic surfaces are considered as more favored for cell attachment and growth than hydrophobic ones [131].

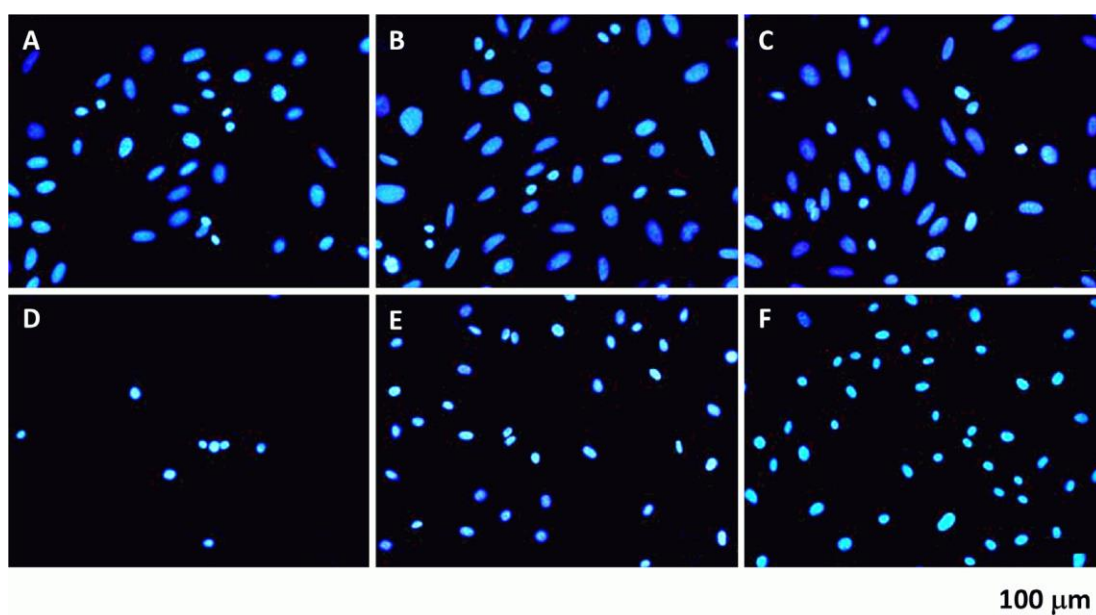


Figure 3.21 Saos-2 (A, B, C) and HUVEC (D, E, F) in 3-day-old cultures on the untreated PET samples (A, D), PET foil treated by DBD for 1 s (B, E) PET foil treated by DBD for 8 s (C,F); the cells were fixed with 70% frozen ethanol and stained with Hoechst #33258 (blue fluorescence)

However, not only higher wettability, but also oxygen content, that is in our case more abundant on PET foils treated by DBD plasma, has an impact to cell behavior. It is known that oxygen groups on the surface can promote cell attachment and proliferation. In previous studies it was observed that Saos-2 cells proliferated better on O-terminated nanocrystalline diamond films, produced more extracellular matrix and deposited higher amount of calcium than the cells on H-terminated films [132]. Results published in [133] showed better growth of vascular smooth muscle cells on

O⁺-implanted polymers, which contained more oxygen than C⁺-implanted samples, although the surface wettability of both types of samples was generally similar.

However, presented results also clearly show that an important role plays also the kind of cells. This can be explained by different sensitivity of Saos-2 and HUVEC cells to different stimuli – whereas Saos-2 are less sensitive because they are maintained in artificial (i.e. *in vitro*) conditions for a long time, freshly isolated endothelial cells easily answer to stimuli. This finding is of high importance, since it clearly shows that it is not possible to generalize results obtained for one particular cell type on another cell types and thus each cell type has to be considered separately.

3.1.3.2 Effect of DBD plasma on bacterial spores of *B. Subtilis*

As it was shown in **section 3.1.2.5** DBD plasma is capable to etch polymeric materials. This is highly interesting finding in view of possible use of DBD plasma for removal of organic pathogens from surfaces, i.e. for plasma sterilization. In order to test the possibility to etch more complex biological samples by DBD plasma operated in air, impact of DBD plasma on *B. subtilis* spores was evaluated. It has been found, that the DBD plasma can be indeed used also as an effective plasma source for spores etching. This is demonstrated in **Figure 3.22**, where SEM images of untreated as well as plasma treated spores are presented. It can be seen that DBD plasma had dramatic impact on the spores: whereas untreated *B. subtilis* spores are ellipsoidal with smooth and undamaged external membrane (**Figure 3.22, a**), SEM images of *B. subtilis* spores after 1 minute of DBD treatment (**Figure 3.22, b**) revealed decrease of their size as well as substantial damages of their shells. Clearly visible defects in the spores shells, that were previously reported for low-pressure plasma treatments in oxygen containing gases (e.g. [134]) as well as for spores exposed to Ar microwave plasma sustained at atmospheric pressure [135], indicate erosion of spores by the DBD plasma. Within this treatment time period the mean length and width of spores slightly decreased from $(1.31 \pm 0.1) \mu\text{m}$ and $(0.70 \pm 0.07) \mu\text{m}$ down to $(1.23 \pm 0.13) \mu\text{m}$ and $(0.67 \pm 0.07) \mu\text{m}$ as determined from the analysis of

SEM images. This corresponds to an etching rate close to 0.1 nm.s^{-1} . Moreover, after prolonged plasma exposure most of the spores were almost completely etched and only their residues were detectable on the surface after 3 minutes of DBD plasma duration (**Figure 3.22, c**).

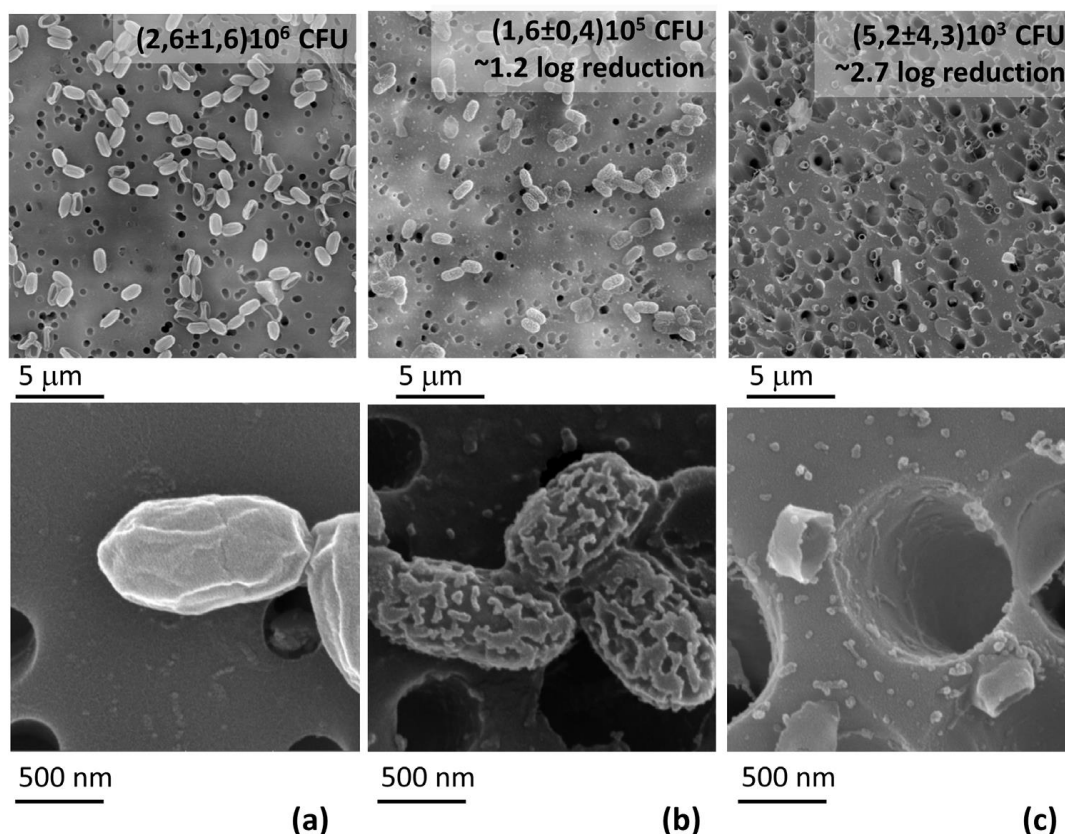


Figure 3.22 SEM images of *B. subtilis* spores **a)** before DBD plasma treatment, **b)** after 1 minute of DBD treatment and **c)** after 3 minutes of DBD treatment.

Taking into account the initial width of spores, their almost complete etching within 180 second of plasma treatment yields etching rate of approximately 5 nm/s , which is value comparable with the etching rates of polymeric foils discussed in **section 3.1.2.5**. The difference in the values of etching rates for the initial and the later phases of plasma treatment is most likely due to the differences in the composition of the outer coat of spores and their inner parts. Presented data thus suggest that the outer coat is much more resistant towards plasma etching.

In addition to morphological changes, also the viability of spores was determined by means of biological tests to assure sterilization effect of DBD plasma. The measured values of the CFU of untreated samples are together with values obtained for samples exposed for different treatment durations to the DBD plasma presented in **Table 3.5**. As can be seen, the DBD treatment causes the exponential decay of the number of survived spores with *D* value equal to $(60 \pm 10 \text{ s})$. This value is competitive with the values reported for other kinds of atmospheric pressure systems [136]–[141].

Table 3.5 Number of survived bacterial spores and corresponding log reduction in dependence on the treatment time.

Treatment time [sec]	Number of bacteria [CFU/ml]	Log reduction
0	$(2.6 \pm 1.6) \cdot 10^6$	
30	$(1.1 \pm 0.3) \cdot 10^6$	0.4
60	$(1.6 \pm 0.4) \cdot 10^5$	1.2
120	$(3.0 \pm 1.9) \cdot 10^4$	1.9
150	$(1.4 \pm 0.9) \cdot 10^4$	2.3
180	$(5.2 \pm 4.3) \cdot 10^3$	2.7

Taking into account the results of biological tests (exponential decay of the number of surviving spores with treatment time) and the results of the SEM study (slower spores etching in the initial phase) it can be finally concluded that there is no direct correlation between the etching/erosion of spores and the bactericidal effect of the DBD plasma that is thus presumably due to the produced reactive species that can penetrate into the spores and cause their irreversible and lethal damage. However, the etching of spores by the DBD assures their complete removal from the surface and thus reduces possible adverse bio-relevant effects connected with the presence of dead spores on a surface.

3.2 Preparation of functional thin films

As mentioned in the introduction, second possible strategy to modify surfaces of polymeric materials is their coating by thin films with desired properties. In this part the main attention will be devoted to the investigation of SiO_x and plasma polymerized HMDSO coatings as well as their nanocomposites with silver (or C:H) NPs. The selection of these materials was done based on their valuable properties that make them applicable in wide range of applications, e.g. as antibacterial or barrier coatings or as coatings with tailorable wettability. Reached results will be summarized in following subchapters.

3.2.1 SiO_x and plasma polymerized HMDSO

The first step in the study of SiO_2 and plasma polymerized HMDSO thin films was the characterization of deposition process and evaluation of physico-chemical properties of coatings produced using different oxygen/HMDSO mixtures.

Regarding the deposition process the plasma properties were monitored by means of optical emission spectroscopy in the wavelength range from 250-800 nm. Examples of emission spectra recorder for different gas mixture compositions are presented in **Figure 3.23**. As can be seen only spectral lines of atomic hydrogen and weak CH molecular system were present in the emission spectra of plasma operated in pure HMDSO. Absence of oxygen lines or bands belonging to oxygen containing species (such as CO and OH) in the emission spectra suggests very low level of fragmentation of HMDSO molecule in the plasma bulk, which is in agreement with previous studies (e.g. [142]). Addition of oxygen to HMDSO resulted in significant alteration of recorded emission spectra. These changes may be summarized as follows. First, CH molecular band rapidly disappears from the emission spectra after addition of small amount of oxygen that is accompanied by appearance of bands belonging to CO, OH a CO_2^+ molecules or molecular ions and spectral lines of atomic oxygen. These changes may be explained by interaction of oxygen either with HMDSO molecule or its fragments produced in the plasma. Further increase of

oxygen fraction in the working gas mixture caused gradual decrease of intensities of spectral bands of CO, OH and CO_2^+ . Possible explanation of diminishing of these spectral systems is formation of oxygen containing species (e.g. CO_2 , SiO_2) difficult to be detected by optical emission spectroscopy.

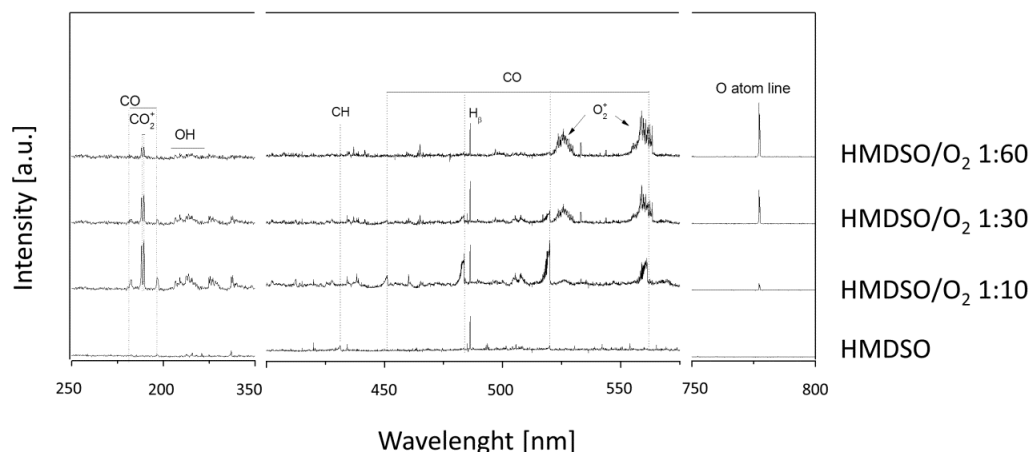


Figure 3.23 Sections of optical emission spectra of discharges sustained in different working gas mixtures.

Above described changes in the plasma composition in turn resulted in significant alterations of chemical composition of coatings prepared using different working gas mixtures as witnessed by XPS measurements (see **Figure 3.24**).

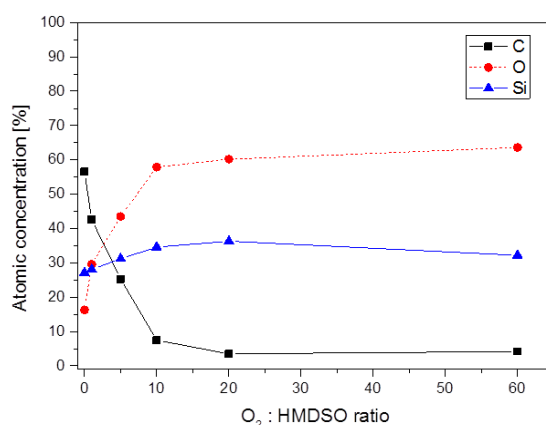


Figure 3.24 Dependence of chemical composition on the O_2 :HMDSO ratio.

It was found, that thin films, which were deposited using only pure HMDSO have a high amount of carbon (57%) and relatively low atomic concentration of oxygen (16%) and silicon (27%). This corresponds to the structure typical for plasma polymerized films with high fraction of “organic” component. In the case of presence of oxygen in the working gas mixture the chemical composition of deposited coating dramatically changed. As can be seen in **Figure 3.24**, atomic concentration of carbon decreased at the expense of increasing of oxygen atomic concentration with increasing of O₂:HMDSO ratio up to 20. Further increase of oxygen fraction in the working gas mixture had then no significant impact on the chemical composition of deposited coatings that exhibited glass-like structure with negligible carbon content and Si to O₂ ratio close to 0.5, i.e. structure close to stoichiometric SiO₂. These findings are in qualitative agreement with previous studies using mixture of HMDSO and oxygen [143], [64].

As the surface free energy and with it connected wettability of deposited coatings strongly depends on their chemical composition, significant changes in these characteristics were observed in dependence on the used working gas mixture. The **Figure 3.25** represents the results of water contact angle and surface energy measurements in dependence on O₂:HMDSO ratio.

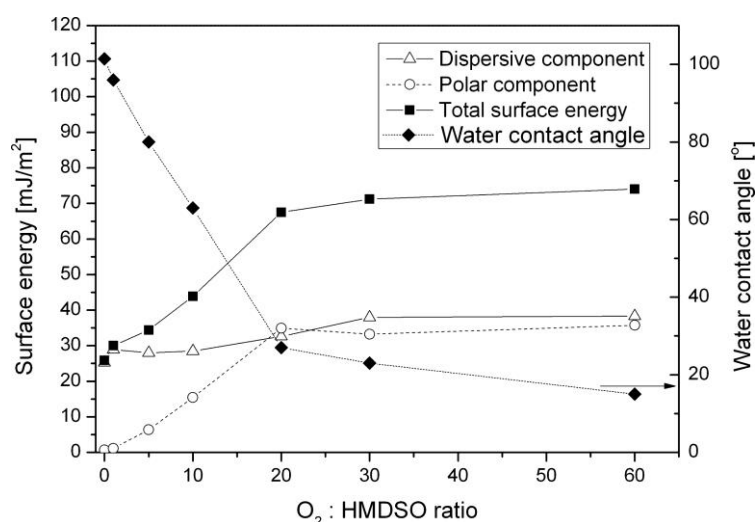


Figure 3.25 Surface energy and water contact angles of coatings prepared at different O₂:HMDSO ratio.

The wettability as well as the surface energy grows up with increasing of fraction of oxygen in the working gas mixture. Namely the water contact angle decreased from 101.4° observed for coatings produced in pure HMDSO vapors down to 15° for the films deposited using O_2 :HMDSO ratio 60:1 (see **Figure 3.26**). This behavior is consistent with decrease of hydrocarbon (non-polar) content in the coatings and increasing their silica-like character with increasing amount of oxygen in the working gas mixture.

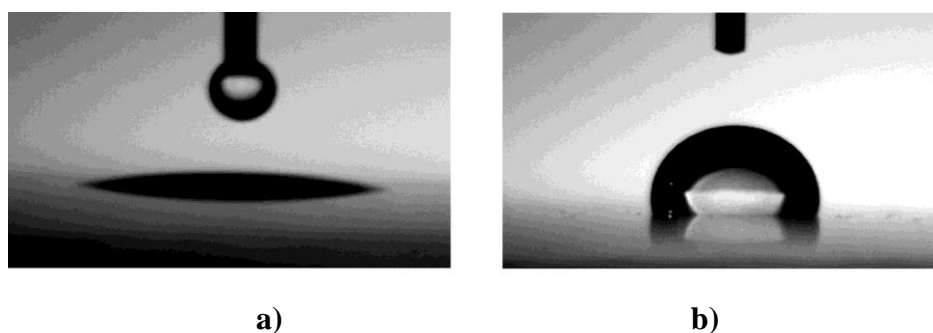


Figure 3.26 Water droplets deposited of coatings deposited in **a)** O_2 :HMDSO 60:1 and **b)** pure HMDSO working gas mixture.

Taking into account the obtained data, discharge mixture with ratios of 0:1 and 60:1 of O_2 :HMDSO, i.e. mixtures that correspond to the production of hydrophobic plasma polymerized HMDSO (further in the text just pHMDSO) and hydrophilic silicon oxide-like (further in the text just SiO_x) films, were chosen for further studies. Mechanical properties of pHMDSO and SiO_x coatings were investigated by nanoindentation method. For these measurements, the thickness of prepared coatings was fixed at value of 200 nm in order to limit possible influence of substrate material on the measurements. The laboratory soda-lime glass was chosen as a reference material. As can be seen in **Figure 3.27**, where values of complex modulus of laboratory glass, SiO_x and pHMDSO films are presented, complex modulus of produced SiO_x coatings is approximately two times higher than the value measured for pHMDSO, but it is still lower as compared to the value measured for conventional laboratory glass. Thus, besides of chemical composition and wettability

the mechanical properties of deposited coatings can also be controlled by choosing of appropriate working gas mixture during the deposition process.

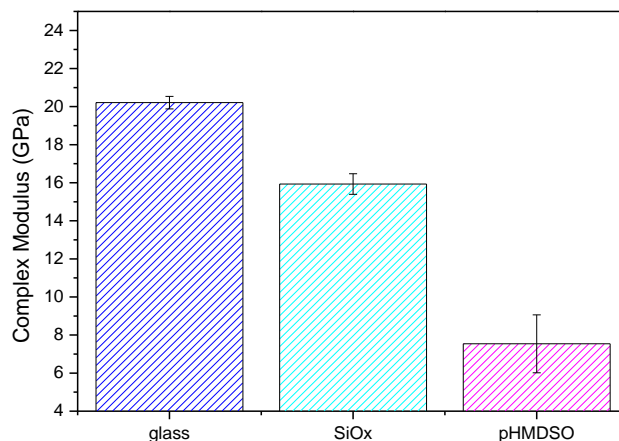


Figure 3.27 Complex modulus of laboratory glass, SiOx and pHMDSO films.

To conclude this part it was shown that it is possible to tailor chemical structure (from the one common for plasma polymers to inorganic silicon oxide-like), wettability (from hydrophobic to super-hydrophilic character), or mechanical properties (complex modulus ranging from 7 to 16 GPa) of produced coatings by changing the amount of oxygen in the working gas mixture. This, as it is going to be demonstrated in the following text, is beneficial in terms of production of novel functional coatings with tailorable antibacterial behavior, wettability and barrier properties.

3.2.2 Antibacterial nanocomposites

The first possible application of pHMDSO and SiO_x films that is going to be discussed in this work is their use for the fabrication of antibacterial nanocomposites based on Ag nanoparticles. Ag/pHMDSO and Ag/ SiO_x nanocomposites will be examined not only from the point of view of their antibacterial behavior, but also their morphology, chemical composition and stability in water will be investigated. Considerable attention will be paid to the ability of nanocomposites to release silver ions that is directly related to the aptitude of Ag containing nanocomposites to destroy and inhibit the growth of bacteria.

3.2.2.1 Characterization of silver nanoparticles

First of all, before fabrication and investigation of silver containing nanocomposites, it is necessary to characterize pure Ag nanoparticles. These were fabricated by means of a gas aggregation source (GAS) of own construction that was in more details described in previous work [87].

The first method employed for the characterization of Ag NPs films was UV-Vis spectrophotometry. Examples of UV-Vis spectra of Ag NPs produced by GAS and deposited onto pHMDSO or SiO_x substrates at different deposition times are shown in **Figure 3.28**. As can be seen, clear absorption peak connected with localized surface plasmon resonance (LSPR) of silver NPs was detected in the UV-Vis spectra. The intensity of this LSPR peak increased with deposition time of Ag NPs, which corresponds to increase of their amount on a substrate. In addition, LSPR position and shape were found to be independent of the deposition time, which indicate that the size of Ag NPs is not influenced by the time of deposition. As highlighted in [144] this represents one of the key features of NPs deposition by GAS systems that differentiate this deposition strategy from more commonly used technique for NPs production - magnetron sputtering – for which the size of produced NPs is strongly linked with the deposition time.

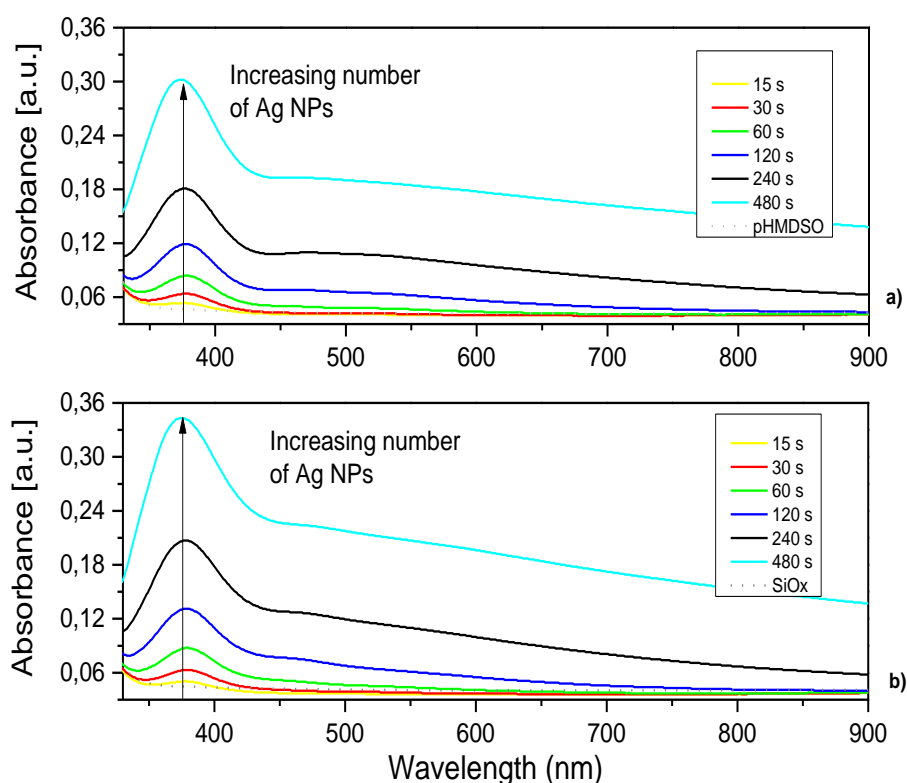


Figure 3.28 UV-Vis spectra of Ag NPs deposited at different deposition time on **a)** pHMDSO and **b)** SiO_x substrate. Ag NPs were produced by GAS.

The independence of size of NPs of the deposition time was also confirmed by SEM images, which are presented in **Figure 3.29**. The amount of Ag nanoparticles increased with time of deposition, while the average diameter of Ag NPs stayed constant. More detail statistical analysis of the SEM images is summarized in **Figure 3.30**, which represents the dependence of number of Ag NPs and their diameter on the deposition time. According to this data processing the deposition rate was found to be $225 \pm 15 \text{ NPs} \cdot \mu\text{m}^{-2} \cdot \text{min}^{-1}$ and the mean size of NPs was $14 \pm 5 \text{ nm}$. Such width of size distribution of produced NPs as well as occasional appearance of higher- size NPs visible in **Figure 3.30** is common for gas aggregation sources operated without utilization of mass or size filtration of produced NPs. Nevertheless, despite this the relative fraction of NPs with diameters higher than 25 nm was lower than 3%.

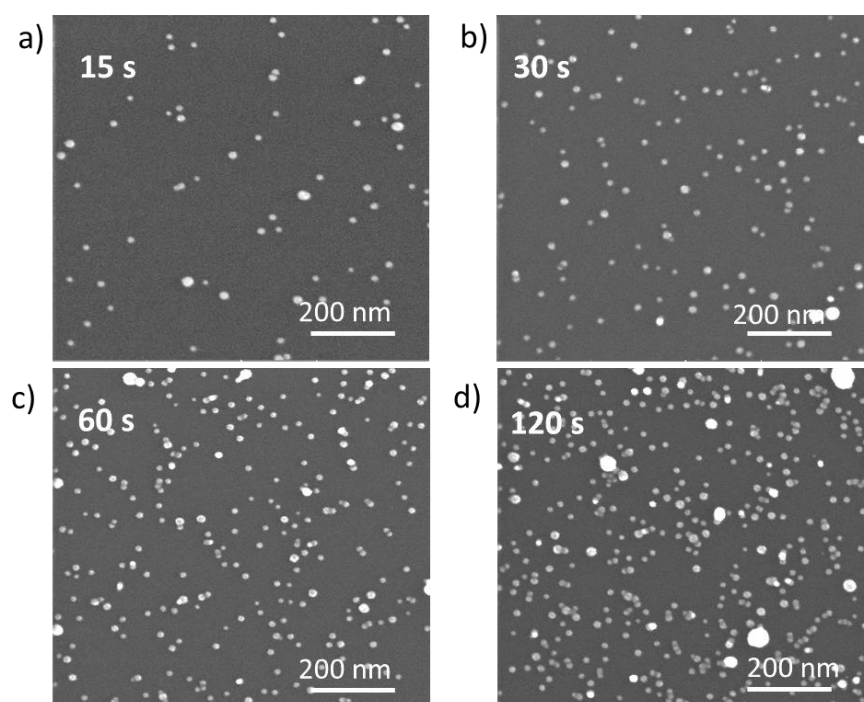


Figure 3.29 SEM images of Ag nanoparticles deposited for different deposition times: **a)** 15s, **b)** 30s, **c)** 60s, **d)** 120s.

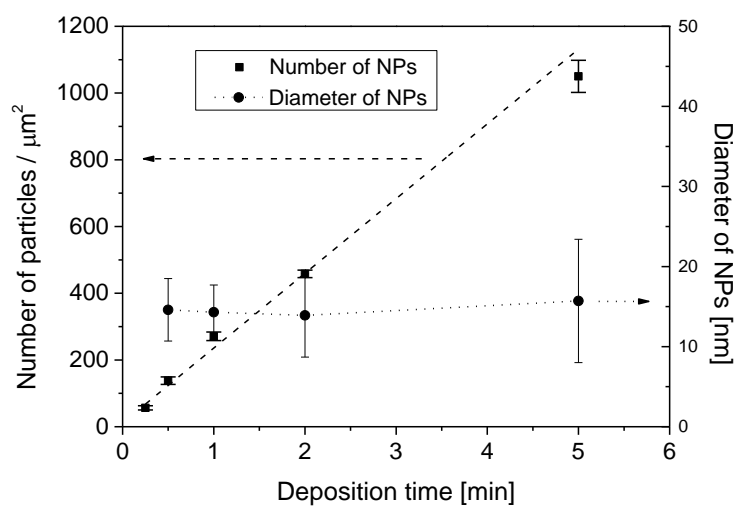


Figure 3.30 Dependence of the number of deposited NPs and their sizes on the deposition time.

3.2.2.2 Characterization of Ag/pHMDSO and Ag/SiO_x nanocomposites

Nanocomposites containing Ag NPs were subsequently fabricated by sequential deposition of pHMDSO or SiO_x layers and Ag NPs (see schematic illustration in **Figure 2.4**). Such Ag/pHMDSO and Ag/SiO_x nanocomposites were analyzed concerning their optical properties first. As can be seen in **Figure 3.31** increasing the number of interlayers of Ag nanoparticles resulted in enhancement of the intensity of LSPR peak of silver, which confirmed increasing amount of NPs in the coating. The difference in appearance of UV-Vis spectra recorder for Ag/pHMDSO and Ag/SiO_x nanocomposites may be ascribed to differences in the dielectric constants of pHMDSO and SiO_x that influences the position of maxima of LSPR peak as well as to possible partial oxidation of Ag NPs when oxygen rich working gas mixture is used.

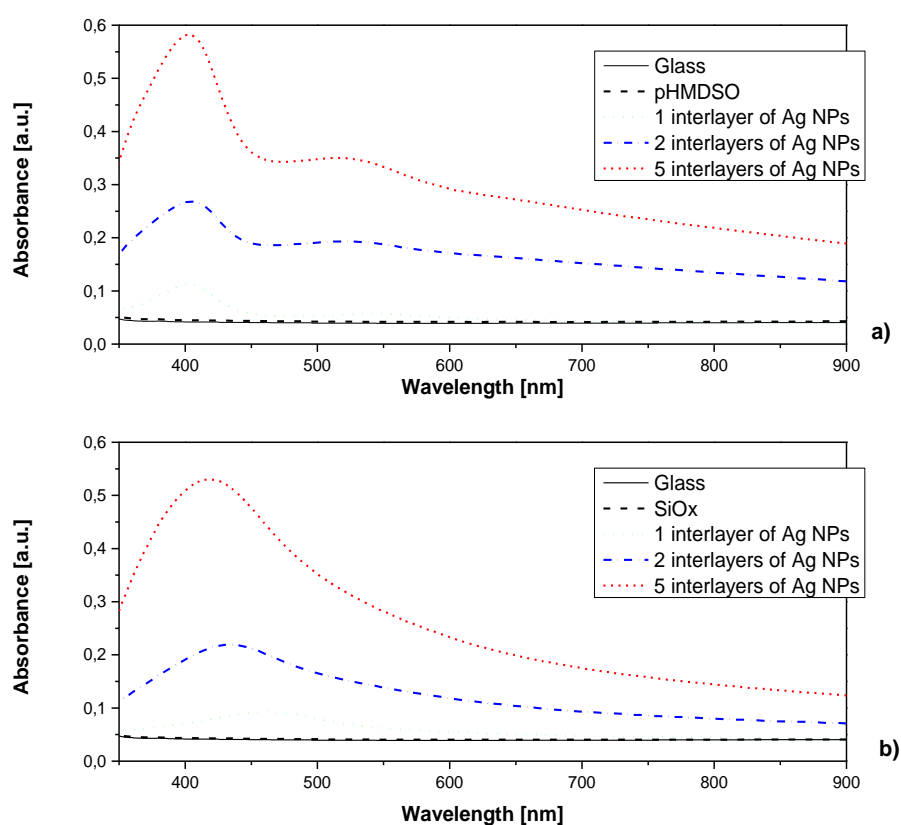


Figure 3.31 UV-Vis spectra as dependence on interlayer numbers of Ag NPs in **a)** pHMDSO and **b)** SiO_x matrixes. For comparison is presented also UV-Vis spectrum of uncoated glass.

Chemical composition of nanocomposite coatings with one interlayer of Ag NPs sandwiched in between two layers of either pHMDSO or SiO_x matrix is presented in **Table 3.6**. In both cases the surface elemental composition that was determined by XPS was found to be similar to the one observed for coatings without Ag NPs except appearance of small peak of silver in the XPS spectra (corresponding to atomic concentration of silver 1-1.5%). It is important to stress that such small atomic percentage of detected silver does not reflect the fraction of silver in the coatings, which is due to the fact that the overcoat thickness of 10 nm used in these experiments is commensurable with the analysis depth of XPS. However, based on XPS data it is possible to conclude that the presence of Ag NPs does not markedly influence the chemical composition of pHMDSO and SiO_x overlayers.

Table 3.6 Chemical composition of nanocomposites based on silver nanoparticles inside pHMDSO and SiO_x matrixes. Thickness of overcoat was 10 nm.

Nanocomposite	O [%]	C [%]	Si [%]	Ag [%]
pHMDSO/Ag/pHMDSO	24	52	23	1
SiO_x/Ag/SiO_x	58	10.5	30	1.5

Subsequently, stability of silver containing nanocomposites based on both pHMDSO and SiO_x matrixes was studied. The results of UV-Vis measurements of the samples before and after their immersion in water are presented in **Figure 3.32 a)** for 10 and **b)** 20 nm of thickness of the top layers. As can be seen in **Figure 3.32, a)**, only a slight red shift of Ag LSPR peak (up to 4 nm) was observed for pHMDSO/Ag/pHMDSO nanocomposites within 7 days of water immersion for 10 nm thick overcoat layer, while in the case of SiO_x/Ag/SiO_x for the same time of immersion the LSPR maxima exhibited much more pronounced shift to the lower wavelengths (up to 30 nm). Intensity of LSPR peaks decreased both for pHMDSO/Ag/pHMDSO and SiO_x/Ag/SiO_x nanocomposites with 10 nm top layers. Since the position and shape of LSPR peak of silver is very sensitive to size, density of Ag nanoparticles in nanocomposites and their interactions with matrices, observed

changes may be interpreted as follows. Red shift in the case of pHMDSO/Ag/pHMDSO nanocomposites and blue shift in the case of $\text{SiO}_x/\text{Ag}/\text{SiO}_x$ nanocomposites are connected with specific Ag NPs and pHMDSO or SiO_x matrix interactions [145].

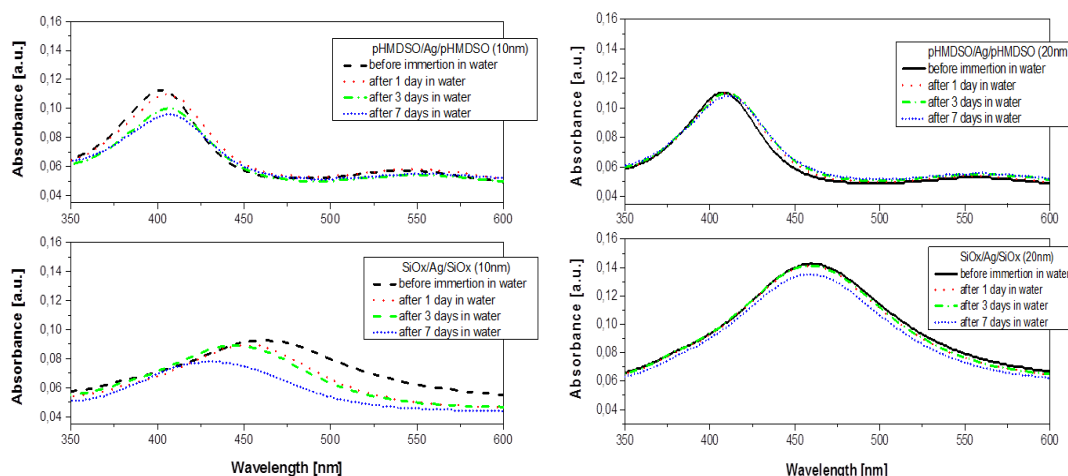


Figure 3.32 UV-VIS spectra of pHMDSO/Ag/pHMDSO and $\text{SiO}_x/\text{Ag}/\text{SiO}_x$ nanocomposite before and after immersion in water.

Decrease of absorption maxima of $\text{SiO}_x/\text{Ag}/\text{SiO}_x$ and pHMDSO/Ag/pHMDSO nanocomposites is probably due to the decrease of the mean size of Ag nanoparticles. This is most likely connected with oxidation of Ag nanoparticles by oxygen dissolved in water, which leads to release of Ag^+ ions and consequently to partial dissolution of Ag nanoparticles. Reduction of mean size of Ag NPs inside SiO_x films was also proved by SEM images, which are depicted in **Figure 3.33**. Amount of smaller Ag NPs inside the SiO_x matrix increased after water immersion for 2 days and the mean size of Ag NPs decreased from 26.9 ± 6.1 nm down to 23.3 ± 6.7 nm. In contrast, mean size of Ag NPs inside pHMDSO matrix stayed constant at value of 17.2 ± 5.5 nm after 2 days in water (**Figure 3.34**). The difference between this value and value reported in **Figure 3.29** is due to the presence of overcoat layer that leads to apparent increase of size of NPs. In addition, for different overcoats their growth on Ag NPs may differ and thus the appearance of samples with Ag NPs overcoated with SiO_x and pHMDSO may vary.

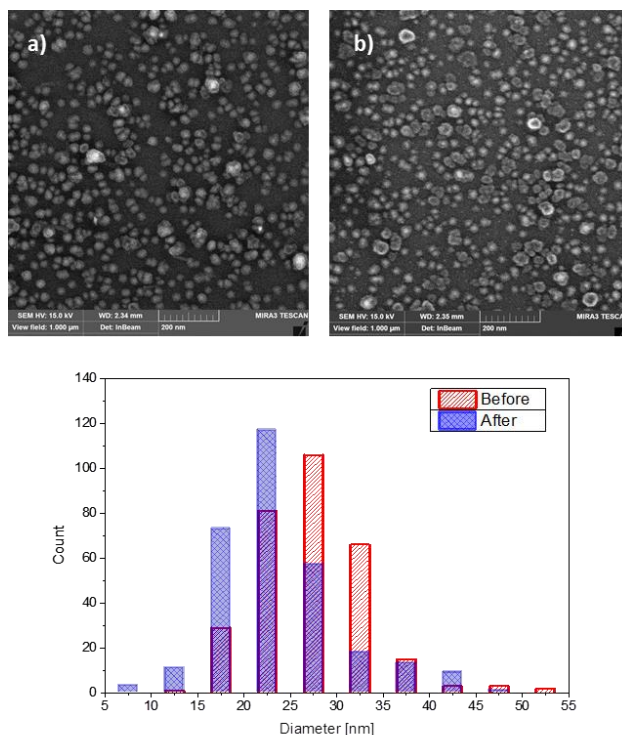


Figure 3.33 SEM images of SiOx/Ag/SiOx nanocomposite **a)** before and **b)** after 2 days immersion in water. Thickness of overcoat layer of SiOx is 10 nm.

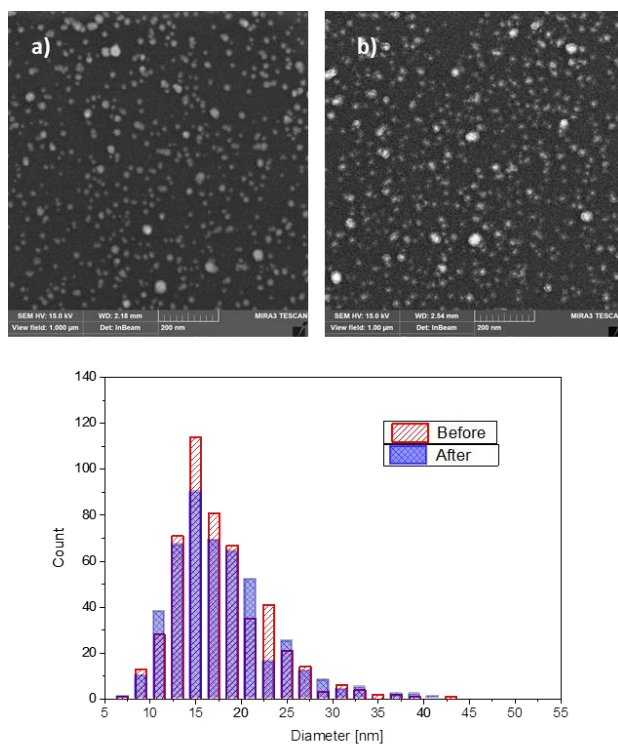


Figure 3.34 SEM images of pHMDSO/Ag/pHMDSO nanocomposite **a)** before and **b)** after 2 days immersion in water. Thickness of pHMDSO overcoat is 10 nm.

In contrast to the situation when 10 nm overlayers were used, no significant changes in UV-Vis spectra were detected for nanocomposites with 20 nm of overcoat thickness of SiO_x or pHMDSO (see **Figure 3.32, b**). This indicates that at larger thicknesses the top layer acts as a barrier, which prevents the penetration of water into the nanocomposite and hence disables the release of silver ions. Because silver dissolution that is connected with silver ion release is crucial for assurance of antibacterial behavior of silver containing nanocomposites thickness of top and inter layers was chosen as 10 nm for further studies.

3.2.2.3 Ion release from Ag/pHMDSO and Ag/SiO_x nanocomposites

As mentioned above, the antibacterial nature of Ag-based nanocomposites is connected with their ability to release Ag⁺ ions. Because of this it is necessary to evaluate the quantity of released silver ions and kinetics of this process that was done during my scientific mission at Kiel University (Germany). In order to evaluate the effect of SiO_x or pHMDSO overlayer on the ability of prepared nanocomposites to release silver ions, the first experiments were done with Ag NPs deposited for 2 min (approximately 500 NPs/μm²) onto SiO_x or pHMDSO films and with samples that contained the same amount of Ag NPs, but overcoated with either SiO_x or pHMDSO films with thicknesses 10 nm.

As expected, the fastest initial release of silver ions was observed for uncoated Ag NPs, i.e. NPs that were in direct contact with water, independently of the underlying material. Moreover, as can be seen in **Figure 3.35**, after 1 day in water the amount of released silver for bare silver nanoparticles reached the value around 1.25 μg·cm⁻². Taking into account SEM images of samples immersed for 1 day in water that revealed the presence of NPs on the substrate (**Figure 3.36**) the NPs were not fully dissolved in water. Observed saturation is thus due to the passivation of metallic Ag NPs (e.g. by thin oxide layer or impurities) that prevents further Ag⁺ ion release.

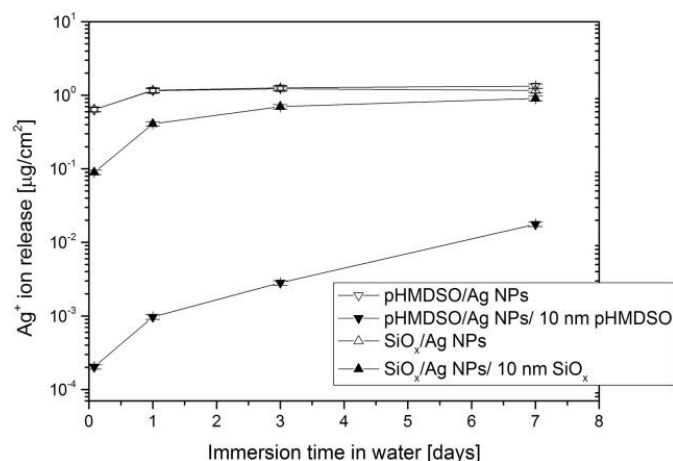


Figure 3.35 Silver ion release from films of Ag NPs deposited onto pHMDSO or SiO_x and AgNPs overcoated with 10 nm thick film of either pHMDSO or SiO_x. Deposition time of Ag NPs was 2 min (500 NPs/µm²).

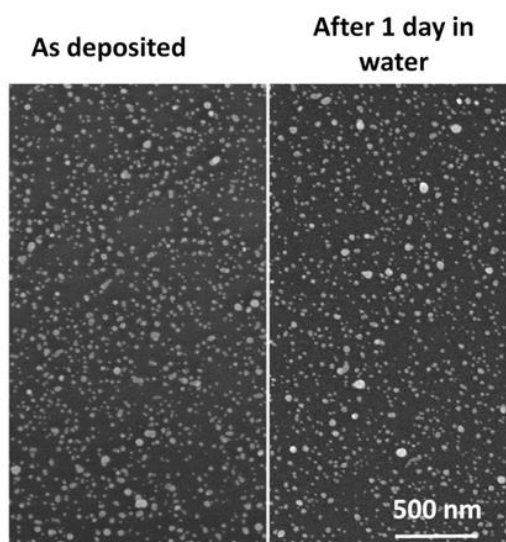


Figure 3.36 SEM images of bare Ag NPs after 1 day in water.

Another important finding that is visible in **Figure 3.35** is markedly different kinetics of Ag⁺ ion release from pHMDSO/Ag/pHMDSO and SiO_x/Ag/SiO_x sandwiches: as can be seen much higher amount of released silver ions was observed for SiO_x-based nanocomposites as compared to Ag NPs overcoated by pHMDSO. This finding is in qualitative agreement with previous study performed with sputtered silver overcoated

with pHMDSO and SiO_x-like thin films [113]. In the case of SiO_x/Ag/SiO_x nanocomposites, the silver ion release rate gradually decreased with immersion time in water from about 1.1 μg·cm⁻²·day⁻¹ observed for 2 h immersion down to approximately 0.05 μg·cm⁻²·day⁻¹ observed between 3 and 7 days of immersion in water. These values are comparable with the results reported for Ag/amino-hydrocarbon nanocomposites prepared by Ag co-sputtering [80] and indicate so-called burst release of silver that lasts few hours for samples that are in contact with water. On the other hand, much lower, but temporally stable release of silver ions was observed for pHMDSO/Ag/pHMDSO coatings. The value of Ag⁺ release rate was in this case close to 0.002 μg·cm⁻²·day⁻¹. However, it is important to stress that the silver nanoparticles remained in both cases in the nanocomposite and were not “washed” away (see **Figure 3.33** and **Figure 3.34**) and thus do not enter into the surrounding aqueous media. This is important mainly with respect to possible use of such nanocomposites, since it prevents undesirable release of Ag NPs in to the environment.

Observed differences in behavior of silver ion release kinetics from pHMDSO/Ag/pHMDSO and SiO_x/Ag/SiO_x coatings indicate different rate of water permeation into these two kinds of coatings that may be ascribed to their different wettability as suggested by Alissawi et al. [113]. In addition, the faster Ag⁺ release from SiO_x/Ag/SiO_x films as compared to pHMDSO/Ag/pHMDSO nanocomposites is consistent with recent experiments that were performed by Blanchard et al. [146]. These authors studied the water uptake ability of pHMDSO and SiO_x films by means of neutron reflectometry and infrared spectroscopy and proved faster permeation of water into SiO_x films as compared with pHMDSO ones. Such behavior is due to the reaction diffusion mechanism, in which silanol groups are formed along the siloxane network upon reaction with water. Highly hydrophilic silanol groups that are more readily formed in SiO_x coatings consequently promote water penetration into the coatings that in turn facilitates the silver ion release.

Other possibility, how to tailor the silver ion release is to vary the amount of Ag NPs in the nanocomposites. In order to evaluate the dependence of the Ag⁺ release on the amount of Ag NPs two different strategies were followed.

The first option tested in this study was based on the variation of the deposition time of NPs. Three sets of samples were produced with 500, 1000 and 2500 NPs/ μm^2 and thickness of the overcoat material (either SiO_x or pHMDSO) 10 nm. The amount of released Ag^+ increases almost linearly with the amount of NPs presented in the coatings as it is depicted in **Figure 3.37**. This confirms assumption that for the silver ion release is crucial number of available Ag NPs.

In the second strategy, the number of silver NPs was adjusted by sequential deposition of Ag NPs and matrix inter-layers. The deposition time of Ag NPs was 2 min and the thicknesses of individual pHMDSO and SiO_x inter-layers were kept constant and equal to 10 nm. Here it is important to stress that since the thickness of pHMDSO and SiO_x inter-layers is lower than the mean lateral distance of NPs deposited in a single step with duration 120 seconds (see **Figure 3.29**), the coatings may be still considered as nanocomposites with randomly dispersed Ag NPs rather than multi-layered sandwich structures.

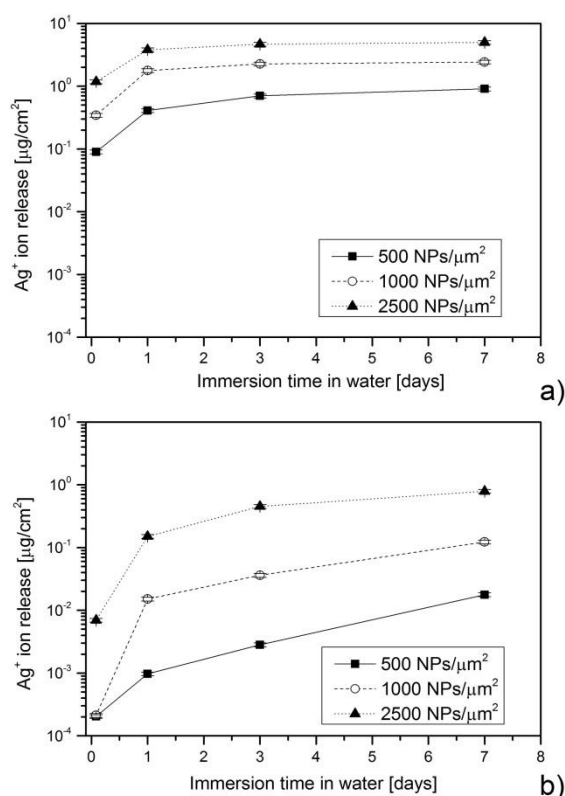


Figure 3.37 Ag^+ ion release from a) $\text{SiO}_x/\text{Ag NPs}/\text{SiO}_x$ and b) pHMDSO/Ag NPs/pHMDSO nanocomposites with different amounts of deposited Ag NPs.

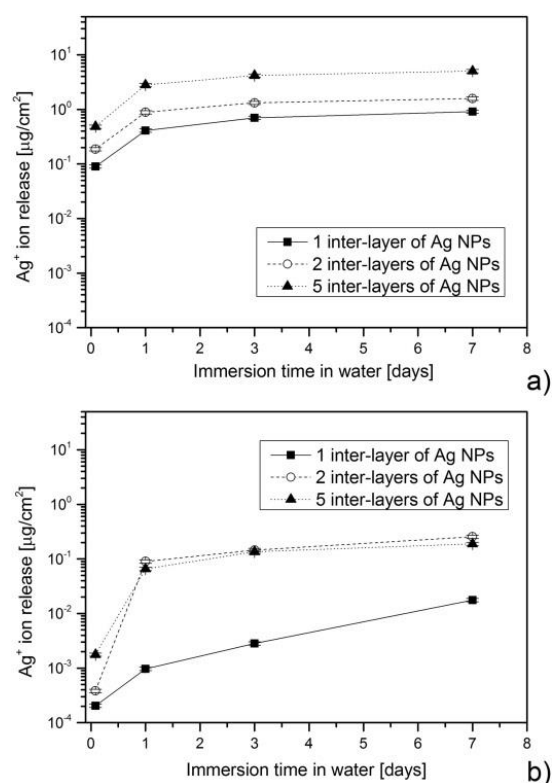


Figure 3.38 Ag⁺ ion release from a) SiO_x/Ag NPs/SiO_x and b) pHMDSO/Ag NPs/pHMDSO nanocomposites with different number of inter-layers of Ag NPs.

According to the results presented in **Figure 3.38**, different dependence of the silver ion release on the number of Ag NPs inter-layers was observed for Ag/SiO_x and Ag/pHMDSO nanocomposites. In the case of Ag/SiO_x coatings the amount of released Ag⁺ increased almost linearly with the number of Ag NPs inter-layers (and thus with the total number of Ag NPs in the coatings). This increase of amount of released silver ions with increasing number of Ag NPs inter-layers that was observed for all immersion times represents clear evidence that all Ag NPs including the ones in the lowest layers are accessible by water. In contrast, no significant difference between samples that have 2 and 5 inter-layers of Ag NPs was observed when Ag/pHMDSO coatings were tested. This result indicates that pHMDSO protects Ag NPs in the lower laying layers from the interaction with water. In other words, lower laying Ag NPs are not accessible for water and thus do not contribute to the Ag⁺ release. Here again the explanation of the difference between SiO_x and pHMDSO is based on the differences of water penetration into these two materials. As shown by Blanchard et al. [146] in a given time scale water can penetrate much deeper into

SiO_x as compared to pHMDSO films. In addition, the presence of NPs in the coatings and their increasing number causes substantial increase of surface roughness, which in the case of hydrophobic pHMDSO causes further rise of value of water contact angle (this phenomena will be in more details discussed in subsequent section). For instance the water contact angle measured on Ag/pHMDSO coatings with 5 inter-layers of Ag NPs was $137\pm4^\circ$, which is almost by 40° higher as compared with smooth pHMDSO films. Highly hydrophobic character of such coatings further limits water permeation into the nanocomposite and thus reduces the ion release. This is an important finding with respect to the optimization of the thickness of Ag/pHMDSO since it shows that the increase of the thickness of such nanocomposites above certain limit does not lead to the enhancement of the ion release rate and with it connected antibacterial performance of deposited coatings.

3.2.2.4 Antibacterial activity of Ag/pHMDSO and Ag/SiO_x nanocomposites

Final step was evaluation of antibacterial activity of produced Ag containing nanocomposites that was done in co-operation with Dr. J. Beranová (Faculty of Science, Charles University). Since the antibacterial efficiency of silver containing nanocomposites is commonly related to the Ag⁺ silver release, antibacterial tests were performed only on selected samples that differed significantly in the level of released silver.

The first method that was used for the determination of antibacterial potency of produced coatings was disc diffusion test, i.e. test in which glass discs coated with nanocomposites were placed onto the agar surface inoculated with bacteria (the coated side facing down) and incubated overnight at 37°C. The antibacterial activity may be then deduced from the size of the inhibition zones (clear zones where bacteria did not grow) formed around discs. **Figure 3.39** shows representative photographs of glass discs coated with Ag/SiO_x and Ag/pHMDSO and placed on agar surface inoculated with *E. coli* bacteria after overnight incubation. It is clear that

whereas for samples without any Ag NPs no inhibition zone was observed, i.e. samples do not exhibit any antibacterial activity, and inhibition zones were formed in the case of samples that contained Ag NPs. However, the size of the inhibition zones was considerably bigger for Ag/SiO_x coatings as compared to Ag/pHMDSO samples and their size increased with increasing number of Ag inter-layers. These results are in good agreement with the results of Ag ion release measurements.

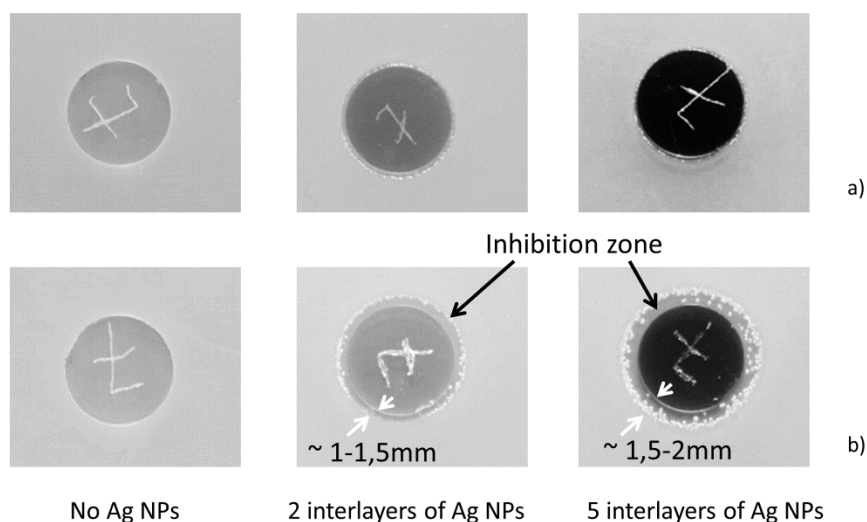


Figure 3.39 Photographs of glass discs placed on the Luria broth agar surface inoculated with *E. coli*, after overnight incubation. a) discs coated with pHMDSO and Ag/pHMDSO nanocomposites and b) discs coated with SiO_x and Ag/SiO_x nanocomposites. The diameter of discs was 12 mm.

In spite of clear confirmation of antibacterial nature of Ag based nanocomposites, the application of disc diffusion test does not allow intelligible and quantitative analysis of bacteria reduction [147]. Because of this for further tests dilution method that enables to count number of bacteria in the solution after incubation with tested samples was used.

As can be seen in **Figure 3.40** no reduction in *E. coli* bacteria counts were observed after 150 min of incubation with glass slides or with glass slides coated only with SiO_x or pHMDSO films. On the other hand, the presence of Ag NPs in the coatings

caused substantial decrease of bacteria counts. As expected from the silver ion release experiments, the antibacterial effect was found to be strongly dependent on the amount of Ag NPs as well as on the matrix material.

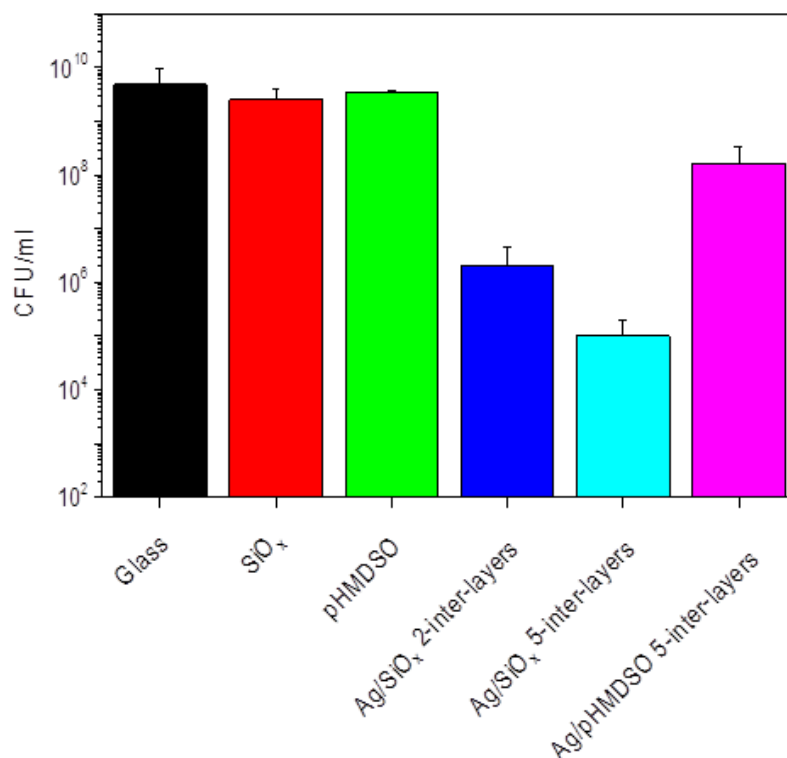


Figure 3.40 Bacterial survival after 150min incubation with different samples.

From the comparison of results obtained for Ag/SiO_x coatings with 2 or 5 inter-layers of Ag NPs, it may be concluded that increasing number of Ag NPs leads to the enhancement of the antibacterial potential of the coatings: whereas for samples with 2 inter-layers of Ag NPs 3-log reduction of bacteria number was observed, 4-log reduction was found for samples with 5 inter-layers of Ag NPs. This finding is in agreement with the higher amount of released Ag⁺ ions observed for samples with higher number of embedded Ag NPs (**Figure 3.40**). In addition performed antibacterial tests confirmed also the role of matrix material as the Ag/SiO_x coatings with 5 inter-layers of Ag NPs exhibited much higher antibacterial effect as compared to Ag/pHMDSO coatings with the same number of Ag inter-layers (4-log and 1-log reduction, respectively).

3.2.2.5 Final remarks and preliminary results related to the role of Ag nanoparticles oxidation

In the previous section it was demonstrated that silver containing nanocomposites fabricated by combination of plasma enhanced chemical vapor deposition of matrix and deposition of Ag NPs by means of gas aggregation source may be used as antibacterial coatings. Furthermore it was shown that this approach makes it possible to tune the kinetics of silver ion release that is responsible for antibacterial character of such materials either by the thickness of the top layer deposited over Ag NPs or by the matrix material. These results are highly promising from the point of view of preparation of coatings with well-defined and controllable antibacterial action. However, it has to be emphasized that Ag/SiO_x and Ag/pHMDSO nanocomposites are not the only ones that may exhibit antibacterial nature. In the frame of this study also other materials were successfully tested, namely composites based on the magnetron sputtering of polytetrafluoroethylene (PTFE) with embedded Ag or Cu NPs or Ag NPs embedded into Al_xO_y matrix deposited by RF magnetron sputtering in Ar atmosphere from Al₂O₃ target. Some of these experiments that I was involved in were already published [148] and presented at international conferences [149]–[151], or were introduced in the PhD. thesis of M. Petr [152] and therefore are not included in this thesis. Some of the main findings are briefly summarized as follows. First, it was proven in agreement with the results reached with Ag/SiO_x and Ag/pHMDSO nanocomposites that the antibacterial activity of Ag/PTFE or Cu/PTFE nanocomposites may be tuned either by the amount of metallic NPs or by the thickness of the top layer deposited over them NPs. This allowed the production of coatings that were either antibacterial or bacteriostatic (i.e. coatings that did not cause either increase or decrease of bacteria). Moreover, experiments with magnetron sputtered PTFE used as overcoat showed that the wettability of the surface of produced samples is not the only parameter that plays roles – strong antibacterial activity was observed on such samples in spite of almost super-hydrophobic character of Ag/PTFE nanocomposites [148].

In addition to these experiments, preliminary tests were performed focused on the evaluation of the role of Ag NPs oxidation on the Ag⁺ release. These experiments were motivated by following consideration: since the release of Ag ions, which in turn define the antiseptic effect of Ag nanoparticles, depends strongly on the presence of oxygen in the aqueous solution, the oxidation of Ag nanoparticles may enhance Ag ion release. Thus oxidized particles may be more suitable for the situations when higher and faster silver ion release is required. To test this hypothesis, i.e. to compare Ag⁺ ion release from metallic and oxidized Ag NPs, following experiments were done in which Ag NPs were after their deposition on the substrate material oxidized by an auxiliary RF plasma sustained in oxygen and overcoated with thin film of magnetron sputtered PTFE. Magnetron sputtered PTFE coatings were selected because of their hydrophobic character and absence of oxygen in their chemical structure. The latter is important as it enables to avoid possible oxidation of Ag NPs during the deposition of the overcoat layer, which may happen when HMDSO that contains oxygen in its structure or oxygen-HMDSO is used. For comparison in all experiments the amount of Ag and oxidized Ag NPs was the same. SEM images of Ag NPs before and after O₂ plasma treatment are depicted in **Figure 3.41**. As can be seen, the morphology of Ag NPs slightly changed after oxygen plasma treatment: NPs edges acquired an uneven and not smooth structure. Oxidation of Ag NPs after oxygen plasma exposure was subsequently proved by XPS analysis. As shown in **Table 3.7**, atomic concentration of oxygen increased after the oxygen treatment of Ag nanoparticles in comparison with untreated Ag NPs.

Table 3.7 Chemical composition of Ag nanoparticle before and after O₂ treatment. Nanoparticles were deposited on gold substrate.

Nanocomposite	C [%]	O[%]	Au[%]	Ag[%]
Ag nanoparticles	42	12	5	41
Ag NPs treated by O2 plasma	39	23	4	34

Oxidation was visible also in the high resolution XPS spectra of Ag3d and O1s peaks that are presented in **Figure 3.42**. The shift of Ag3d peak to lower binding energies from 368.2 eV (for Ag NPs) to 367.8 eV (for O₂ plasma treated Ag NPs) and increase of a peak at 531 eV in O1 s spectra indicates the presence of silver oxide [153].

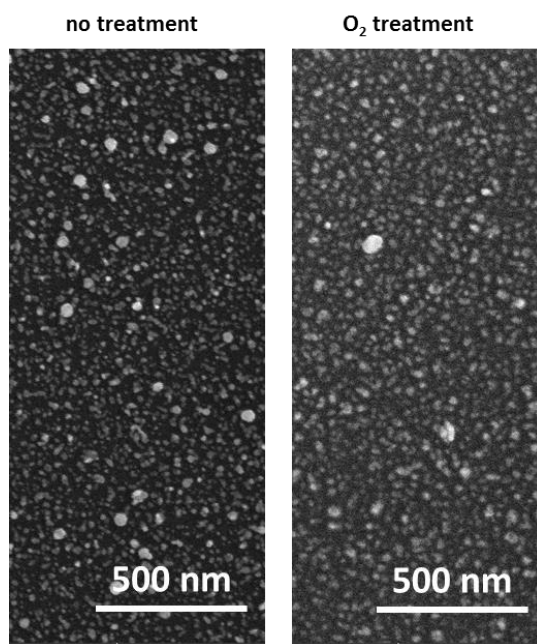


Figure 3.41 SEM images of Ag NPs and Ag NPs treated by oxygen plasma.

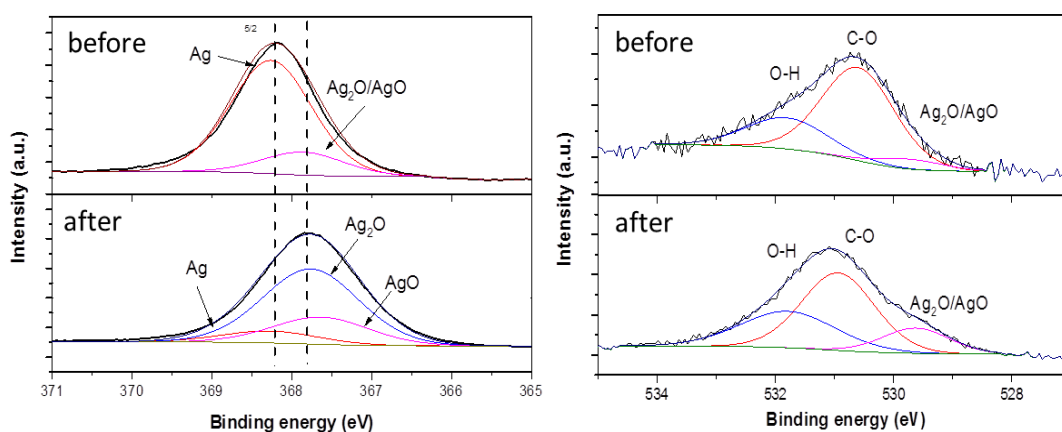


Figure 3.42 High resolution spectra of a) Ag 3d peaks and b) O1s peaks of Ag nanoparticles before and after oxygen treatment.

Finally, in order to evaluate the influence of oxygen treatment of Ag nanoparticles on antibacterial properties, the measurement of release of Ag^+ ions was performed. It was found that much higher silver ion release was observed in the case of oxidized Ag nanoparticles (approximately two orders of magnitude) in comparison with untreated ones as can be seen in **Figure 3.43**. O_2 treated Ag NPs had rapid ion release within one day of the immersion time in water and no significant difference was observed for samples that contained different amount of Ag NPs (deposition times of Ag NPs were 1, 2 and 4 min). In addition, prolonged immersion in water (6 days) caused only slight increase of released silver ions when Ag NPs were oxidized, while for metallic NPs amount of released silver increased with prolongation of the immersion time. Such different release kinetics is consistent with hypothesis of more effective silver ion release from oxidized silver: all the silver that may be released is released within the first day in this case. In contrast, the process of silver ions release is much slower in the case of metallic silver as it requires interaction of Ag NPs with oxygen dissolved in water.

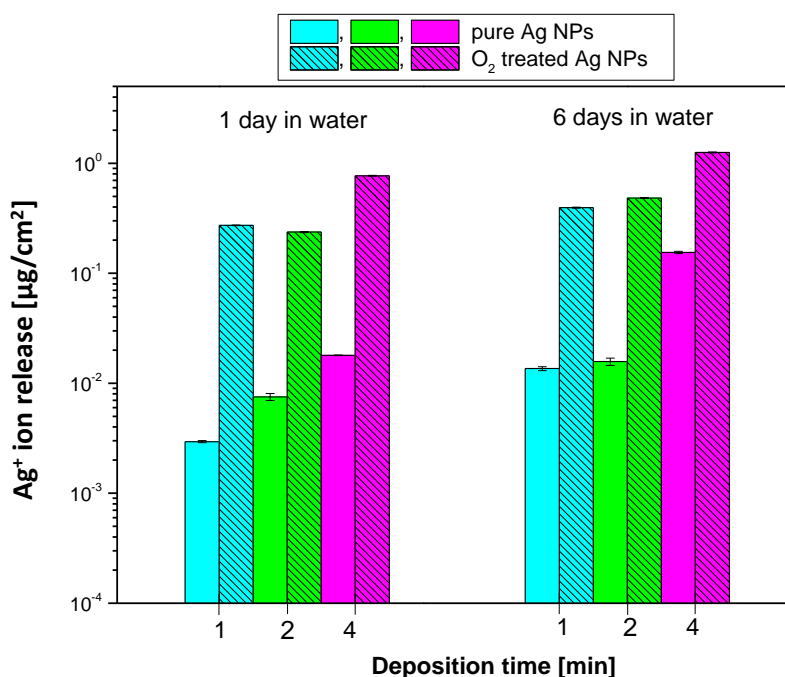


Figure 3.43 Dependence of silver ion release of Ag NPs and oxygen treated Ag NPs deposited on PET foils and covered by PTFE film (10 nm) on the immersion time in water and deposition time of Ag NPs.

3.2.3 Coatings with tailorable wettability

As it was reported in the **section 3.2.1**, selection of working gas mixture during the plasma polymerization of HMDSO enables production of coatings with wetting angles that range from 101.4° down to 15°, i.e. surfaces that cover the range from slightly hydrophobic to highly hydrophilic. However, for some applications it is desirable to extend the range of achievable water contact angles (WCA). This cannot be reached by variation of chemical composition of the coatings and thus the films have to be nanostructured. This strategy is based on a well-known phenomenon described by Wenzel [154], who found the relation between water contact angle of ideally smooth surface θ , ratio of real surface and projected surface areas r and water contact angle of roughened surface θ_a :

$$\theta_a = r * \cos(\theta) \quad (3.2)$$

From this equation it is clear that for hydrophobic surfaces with water contact angle θ higher than 90° increasing roughness causes increase of WCA and for surfaces with water contact angle θ lower than 90° increasing roughness leads to increase of their wettability.

Although there are numerous methods that may be used for surface roughening, in this study, approach based on nanoparticles subsequently overcoated by pHMDSO or SiO_x films was used. The main advantage of this strategy, which was firstly reported in [155], is possibility to tune independently the surface chemical composition of produced films that is given solely by the chemical structure of the overcoat material and the surface roughness that is influenced by the number and size of NPs in the base layer.

Two sets of experiments were performed. In the first one C:H NPs (110 nm in diameter) produced by the gas aggregation source and deposited on smooth Si wafers (RMS roughness < 0.5 nm) were overcoated with hydrophobic pHMDSO or hydrophilic SiO_x films. C:H NPS were fabricated by colleague P. Solar in the frame

of his work (details may be found in [97]). The thickness of pHMDSO and SiO_x layers was 100 nm in order to fix and fully cover the C:H NPs. As it is clear from **Figure 3.44**, where examples of AFM images of acquired for samples with different amount of C:H NPs in the base layer and overcoated with pHMDSO are presented, coatings with markedly different morphologies and roughness were obtained. According to analysis of AFM images the root-mean-square roughness increased with the amount of C:H NPs from 33 nm up to 180 nm. This substantial change in the surface roughness in turn resulted in different surface wettability of produced coatings. In the case of plasma polymerized HMDSO overcoat the water contact angle increases with increasing surface roughness. This is furthermore accompanied for RMS roughness higher than 110 nm by a rapid decrease of water contact hysteresis, i.e. difference between advancing and receding water contact angles. Such behavior indicates transition between a homogeneous wetting state (surface is fully wetted by a droplet) and heterogeneous wetting (a droplet sits on the surface protrusions and thus does not wet the entire surface [156]). As consequence of this, the surface becomes slippery and water droplets roll-off. In contrast, when hydrophilic SiO_x film was used instead of hydrophobic pHMDSO layer, the wettability of produced coatings was enhanced and the coatings become super-hydrophilic (see **Figure 3.45**).

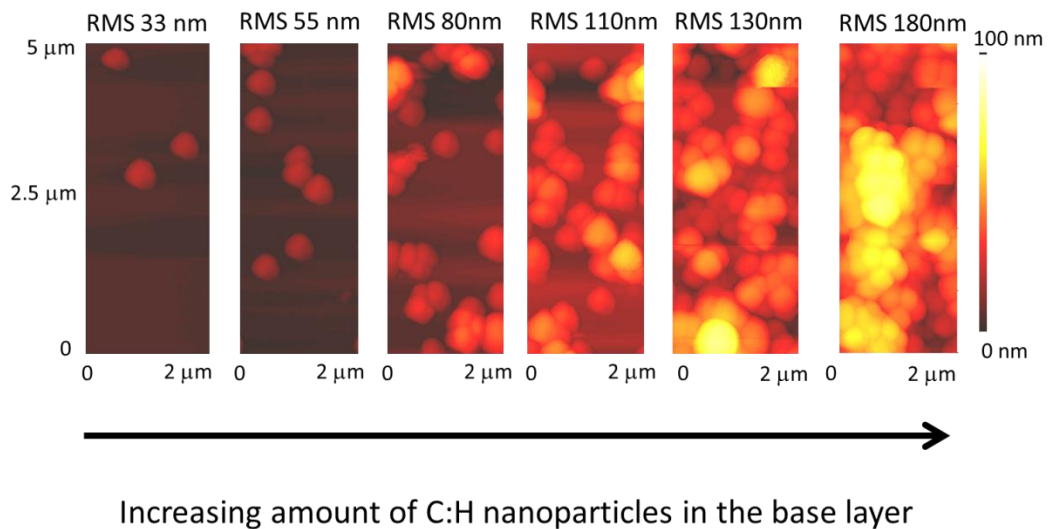


Figure 3.44 Sections of AFM scans on samples with different amount of C:H nanoparticles that form the base layer.

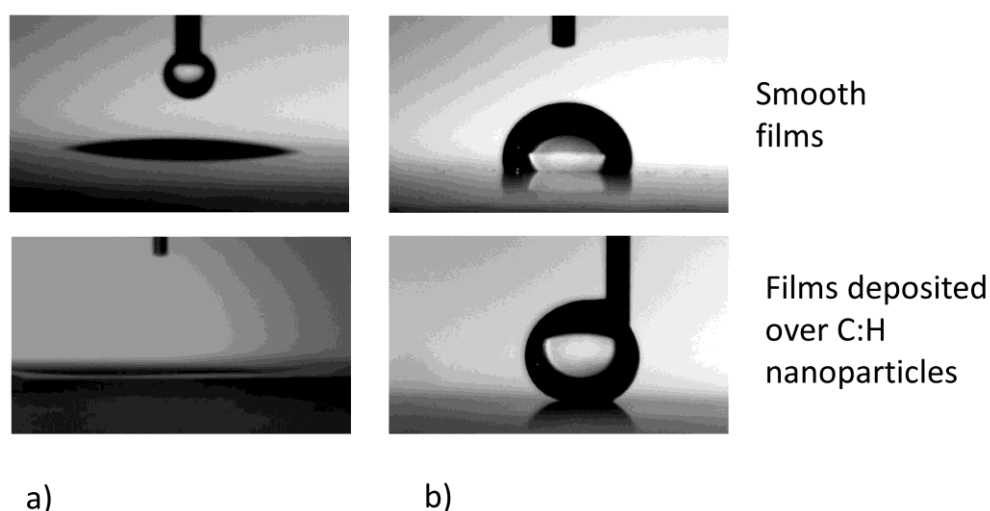


Figure 3.45 Water droplets on smooth (upper row) and roughened (bottom row) coatings deposited in **a)** O₂:HMDSO 60:1 mixture and **b)** pure HMDSO. The deposition time of C:H particles used for surface roughening was 20 min.

More detailed investigation of super-hydrophilic surfaces was performed in the second set of experiments, in which the substrates were PMMA and PEN polymeric foils and Ag NPs were used instead of C:H NPs. Also in this case rapid increase of surface roughness with deposition time of NPs (i.e. with increasing of the amount of deposited Ag NPs) was confirmed by AFM measurements for both PMMA and PEN samples (see **Figure 3.46**). Furthermore as can be seen in **Figure 3.47, a** all the fabricated surfaces were super-hydrophilic with water contact angles lower than 10°. Here it is important to make two comments. First the lower WCA than the one measured when SiO_x was deposited onto smooth Si wafer even for coatings without any NPs in the base layer is due to the intrinsic roughness of polymeric foils. Second, the values of WCA below 10° are difficultly measurable and are thus not very precise that is due to the fact that it is not easy to determine the triple point.

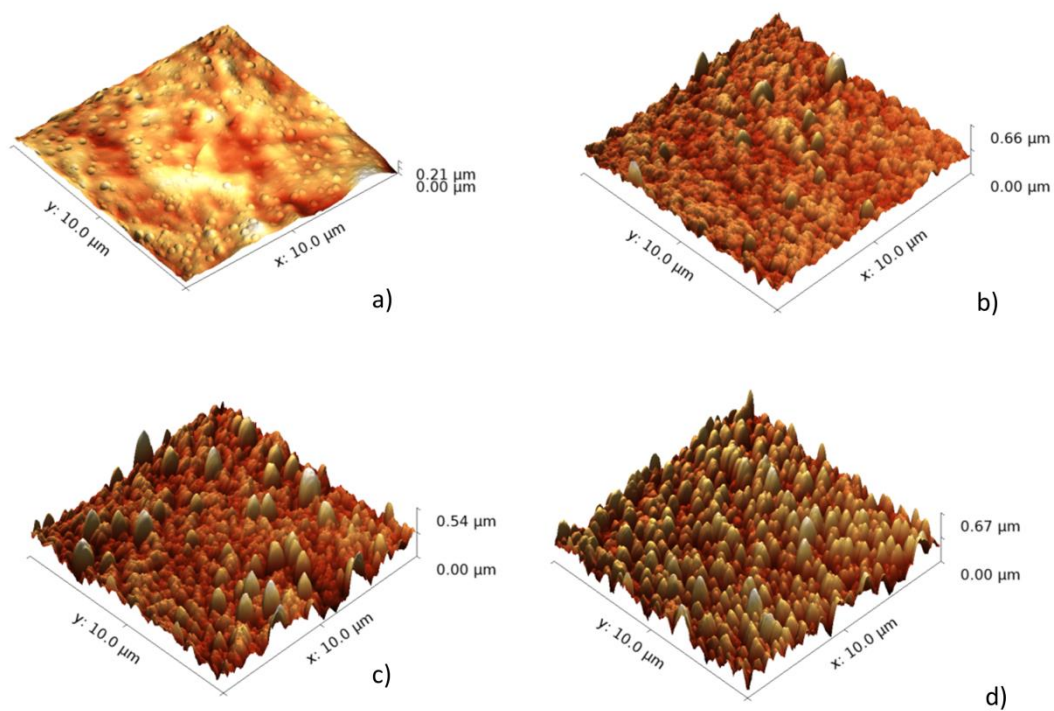


Figure 3.46 AFM images of **a)** PMMA foils coated with SiO_x film and **b)-d)** PMMA coated with Ag NPs and overcoated with SiO_x film. Deposition time of Ag NPs was **b)** 30 sec, **c)** 1 min and **d)** 2 min

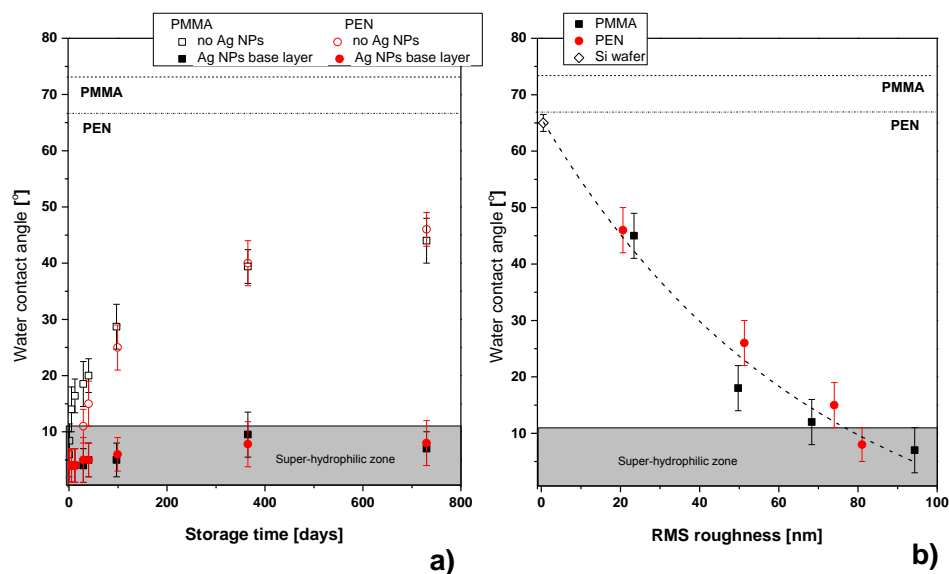


Figure 3.47 Dependence of water contact angle **a)** on storage time (deposition time of Ag NPs was 2min) and **b)** on surface roughness measured 2 years after deposition.

In spite of similarity of measured WCA on all samples independently of the presence, absence or amount of Ag NPs in the base layer, significant differences were observed with increasing storage time: whereas the WCA gradually increased with storage time (WCA close to 45° was observed for SiO_x coatings after 2 years), the ageing process was dramatically reduced for samples with the base layer of AgNPs (**Figure 3.47, a**). Related to later the ageing effect was found to be linked with the surface roughness of produced coatings. This is demonstrated in **Figure 3.47, b** where values of water contact angles measured on samples that were stored 2 years on open air are plotted in dependence on their RMS roughness. As can be seen, the surfaces remained super-hydrophilic after 2 years. Only for the samples with lower number of NPs in the base layer gradual increase of the WCA value was found. Such behavior may be explained in the following way. First, the surface of SiO_x films degrades with time or is contaminated by airborne carbonaceous contamination. This leads to lose of super-hydrophilic nature and WCA of SiO_x films increases. However, according to **equation 3.2** this effect may be substantially diminished by increasing the surface roughness. For instance for the surface with r parameter equal to 1.37, i.e. the value that was measured for the samples with the highest amount of NPs in the base layer, the WCA stays below 10° even when the WCA on smooth surface is 44° . This effect, i.e. lowering of WCA due to the surface roughness, is naturally more important for coatings with higher level of roughness, which is consistent with measured dependence of WCA on the roughness.

3.2.4 Investigation of barrier properties

The barrier properties of produced coatings in terms of water vapor permeation were investigated for SiO_x films deposited on PET foils with different thicknesses from 10 up to 70 nm. The results of performed measurements are depicted in **Figure 3.48**. It was found that water vapor permeability coefficient decreases (i.e. barrier efficiency increases) with increasing thickness of deposited SiO_x . The maximum improvement of barrier properties of PET foils was observed for overcoat thickness of 35 ± 5 nm, for which one order of magnitude of permeability enchantment was reached. Further increase of overcoat thickness subsequently led to dramatic

deterioration of barrier properties (for thicknesses of ~50 nm and higher). Such behavior of permeability coefficient can be explained by formation of micro-cracks in SiO_x films due to the increasing intrinsic stress. The appearance of micro-cracks was furthermore confirmed by AFM (see AFM image presented in **Figure 3.49**), where the uniformly distributed cracks are clearly visible for 200 nm thick SiO_x film. The presence of such surface defects obviously leads to a rupture of the integral structure of the films and consequently lower their barrier properties to water vapor.

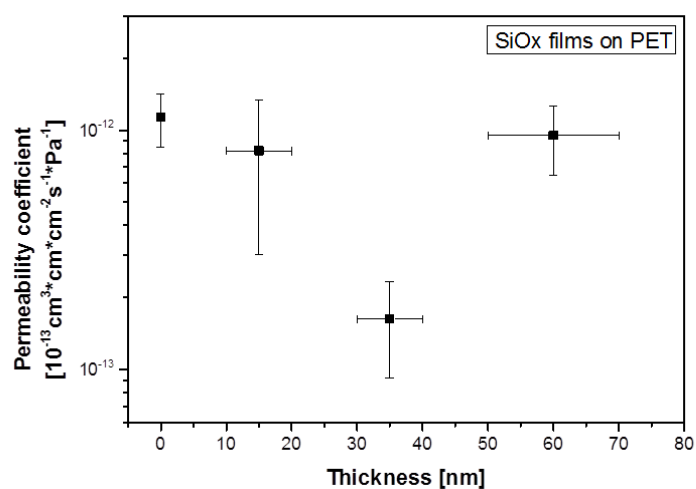


Figure 3.48 Water vapor permeability coefficient of non-coated PET foils and PET foils coated by SiO_x films as dependent on barrier thickness.

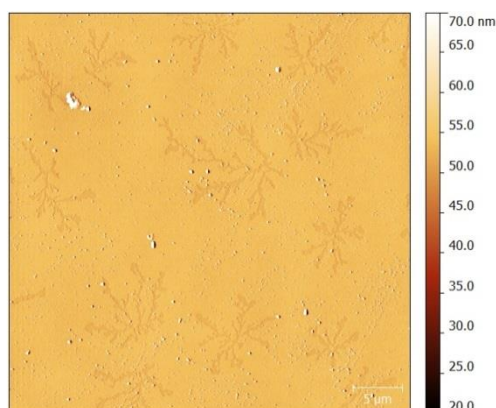


Figure 3.49 The AFM image of SiO_x coating with 200 nm of thickness.

Significant lowering of barrier properties of various coatings with their increasing thickness due to the occurrence of microcracks is common problem (e.g. [157],[158]). One possible strategy to limit this undesirable effect was introduced by Schwarzer [159], who proposed optimal coating structure with nonhomogeneous depth profile of mechanical properties that may protect the coating from deformation and avoid the film cracking. It was found that the bottom and top layer of film should have lower Young's modulus than the inner layer. In this work, such scheme has been adopted using the step by step deposition of polymerized HMDSO with lower Young's modulus, followed by deposition of hard SiO_x film that was finally coated again with pHMDSO. The schematic illustration of the structure of prepared coatings is shown in **Figure 3.50, a**. As can be seen in **Figure 3.51** prepared multilayered coatings with total thickness of approximately 80 nm showed much better barrier behavior to water vapor than pure SiO_x films with 35 nm of thickness.

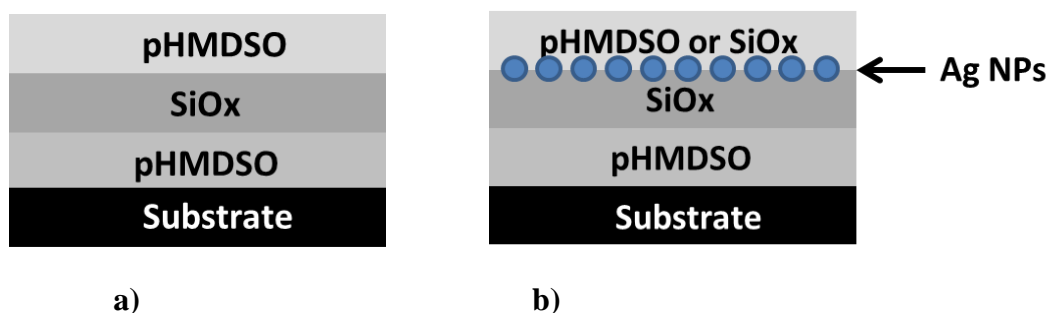


Figure 3.50 Schematic illustration of multilayer coatings **a)** without and **b)** with Ag NPs

In order to use these multilayered coatings not only as barrier but as antibacterial coatings, where for example silver nanoparticle (see *chapter 3.2.2*) can be utilized as antibacterial agent, the nanocomposites with incorporated Ag nanoparticles were also prepared. The scheme of nanocomposite structure is depicted in **Figure 3.50, b**. Values of permeability to water vapor did not significantly change in the case of the presence of Ag NPs inside the nanocomposite in comparison with nanocomposites without of silver NPs ($\text{pHMDSO/SiO}_x/\text{pHMDSO}$), only slightly higher value of

permeability coefficient was for SiO_x top layer (**Figure 3.51**). Thus, nanoparticle containing nanocomposites can be used as barrier coatings.

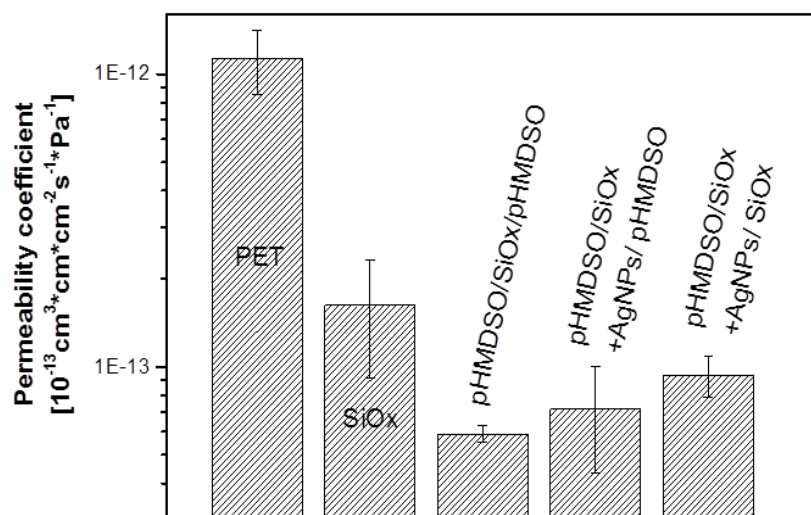


Figure 3.51 Water vapor permeability coefficient of PET foil, SiO_x and nanocomposite coatings deposited on PET foils. Total thickness of SiO_x films was 35 nm, pHMDSO/SiO_x/pHMDSO(or SiO_x) coatings without or with Ag NPs was approximately 80nm.

4 Conclusions

In the first part of this study, influence of atmospheric pressure DBD plasma treatment on the surface properties was investigated for the wide range of polymeric foils: nylon 6,6, PET, PEN, PP, LDPE, PEEK, PMMA and PLA. All investigations were made using the same DBD experimental setup at identical conditions. In the frames of this work, additional experiments were carried out that were focused on applications of this kind of plasma, namely the effect of DBD plasma pretreatment on growth of two types of cell as well as the ability of this kind of plasma to kill bacteria were examined. The results of this part of thesis were partly published in **4 peer-reviewed articles** and were continuously presented on international workshops and conferences. The main conclusions may be summarized as follows:

1. Surface chemical composition was measured and analyzed for all represented polymers. Surface oxidation was the main result of DBD plasma treatment. This was accompanied by the formation or increase of surface fraction of polar functional groups, which resulted in substantial increase of wettability and surface free energy of treated polymers. However, these changes were not temporally stable and so-called ageing effect was reported.
2. The surface RMS roughness increases as a result of DBD plasma treatment. The factor of growth of RMS depends on type of polymer.
3. The etching rates of different polymers were measured. It was demonstrated that DBD plasma operated in air at atmospheric pressure is capable to etch all tested polymers. However, it has been found that etching rates depend on the presence of oxygen in the untreated polymers: higher values of the etching rates were observed for polymers with higher O/C ratios.
4. DBD pretreatment of PET foils revealed promising effect on growth of endothelial cells. In the case of osteoblast like cells no significant changes for treated and untreated PET was observed.

5. It was found out that DBD plasma can etch and hence inactivate high resistively spores of *B. subtilis*. 3 minutes of DBD plasma exposure led to complete etching of spores from the substrate surface and only their residues were detected. This suggests that DBD plasma could be used as an effective plasma source for biofilm removal in biomedicine.

In the second part, different functional films with bactericidal, superhydrophilic or superhydrophobic and barrier properties were prepared and analyzed. The main attention was devoted to SiO_x and pHMDSO surfaces as well as to Ag/SiO_x and Ag/pHMDSO nanocomposites that were prepared by sequential deposition of matrix and Ag NPs. All samples were characterized not only in terms of their chemical composition, wettability, morphology and mechanical properties but also in terms of their antibacterial activity as well as barrier characteristics. Ag NPs were produced by relatively innovative method namely by means of gas aggregation source. Fabricated NPs were analyzed concerning their deposition rate, size distribution, stability in water for both nanoparticles themselves and inside nanocomposites. In the case of antibacterial coatings the main focus was devoted to silver ion release as the direct indicator of bactericidal behavior of Ag containing nanocomposites. In addition, nanostructured surfaces with tailorable wettability based on C:H nanoparticles were performed. The results related to the fabrication of functional coatings were partly published in **6 peer-reviewed articles** and were continuously presented on international workshops and conferences. The main conclusions of this part are:

1. Incorporation of Ag NPs into pHMDSO or SiO_x makes it possible to produce coatings with antibacterial, barrier and tailor-made wettability properties.
2. It was demonstrated that the release of Ag⁺ ions and thus also antibacterial performance of produced coatings may be adjusted by the amount of Ag NPs embedded into the matrix material as well as by the matrix material itself. The Ag⁺ ion release was found to range from 0.002 µg·cm⁻²·day⁻¹ measured for low amount of Ag NPs embedded into pHMDSO matrix up to more than 10 µg·cm⁻²·day⁻¹ in case of Ag/SiO_x nanocomposites that contained high amount of Ag NPs. Thus, possibility of tuning silver ion release was demonstrated.

3. Based on the results of performed biological tests it is possible to reduce number of *E. coli* bacteria incubated with Ag/SiO_x nanocomposites by 4 orders of magnitude within 150 min of incubation time. In addition, biological tests were in good agreements with the results of measurements of Ag⁺ release.
4. It was found out that oxygen treated silver nanoparticles have rapid and more intensive Ag⁺ release in comparison with untreated Ag NPs.
5. The proper design of nanocomposites (e.g. matrix material or number of NPs) is highly important with respect to fabrication of antibacterial materials with well-defined and controlled antibacterial behavior needed for biomedical application, for example, novel implant materials.
6. Use of substrates pre-seeded with NPs and overcoated with pHMDSO or SiO_x enabled production of super-hydrophobic or super-hydrophilic surfaces. Furthermore, excellent temporal stability of super-hydrophilic coatings was demonstrated for surfaces with sufficiently high roughness.
7. It was found out that the optimal thickness of SiO_x coatings in order to reach enhanced barrier properties was 35±5 nm.
8. Employed multilayered nanocomposite with different Young's modulus was found as the most appropriate barrier coatings. The permeability coefficient of water vapor through pHMDSO/SiO_x/pHMDSO nanocomposite 20 times less than through the pure PET foil and 2 times less than through the PET with 35 nm thick SiO_x coating. Moreover, it was found that presence of Ag nanoparticles inside such nanocomposites did not influence permeability coefficient that makes it possible to use them both as barrier and bactericidal surfaces.

Within the PhD. thesis I have participated in several grant projects. The DBD treatment of polymers was performed in the frame of COST Action MP1101 supported by the grant LD 12066 financed by the Ministry of Education, Youth and Sports of the Czech Republic. Development and investigation of antibacterial

nanocomposites was subject of my GAUK project (GAUK 277915 “Deposition and investigation of properties of antibacterial metal/plasma polymer nanocomposites”). Investigation of nanocomposite materials and their characterization was covered by grants GACR 13-09853S and GACR 16-14024S both from the Grant Agency of the Czech Republic.

Bibliography

- [1] Plastics Europe, “Plastics - the facts 2015. An analysis of European plastics production, demand and waste data,” *Plast. 2015*, pp. 1–30, 2015.
- [2] A. L. Andrady and M. A. Neal, “Applications and societal benefits of plastics,” *Philos. Trans. R. Soc. B Biol. Sci.*, vol. 364, no. 1526, pp. 1977–1984, 2009.
- [3] R. O. Ebewele, “Chapter 1: Introduction,” *Polym. Sci. Technol.*, pp. 1–23, 2000.
- [4] L. H. Baekeland, “Original papers: The synthesis, constitution, and uses of bakelite,” *Ind. Eng. Chem.*, vol. 1, no. 3, pp. 149–161, 1909.
- [5] J. M. G. Cowie and V. Arrighi, “Polymers: chemistry and physics of modern materials,” *CRC Press*, 2007.
- [6] W. Amass, A. Amass, and B. Tighe, “A review of biodegradable polymers: uses, current developments in the synthesis and characterization of biodegradable polyesters, blends of biodegradable polymers and recent advances in biodegradation studies,” *Polym. Int.*, vol. 47, no. 2, pp. 89–144, 1998.
- [7] K. Van De Velde and P. Kiekens, “Biopolymers: Overview of several properties and consequences on their applications,” *Polym. Test.*, vol. 21, no. 4, pp. 433–442, 2002.
- [8] P. Fabbri and M. Messori, *Surface Modification of Polymers: Chemical, Physical, and Biological Routes*. Elsevier Inc., 2016.
- [9] R. Foest, E. Kindel, A. Ohl, M. Stieber, and K.-D. Weltmann, “Non-thermal atmospheric pressure discharges for surface modification,” *Plasma Phys. Control. Fusion*, vol. 47, no. 12B, pp. B525–B536, 2005.
- [10] S. Yoshida, K. Hagiwara, T. Hasebe, and A. Hotta, “Surface modification of polymers by plasma treatments for the enhancement of biocompatibility and controlled drug release,” *Surf. Coatings Technol.*, vol. 233, pp. 99–107, 2013.
- [11] M. A. Lieberman and A. J. Lichtenberg, *Principles of Plasma Discharges and Materials Processing: Second Edition*. 2005.
- [12] J. R. Roth, “Application to Nonthermal Plasma Processing,” *J. Plasma Phys.*, vol. 2, no. 3, pp. 237–240, 2002.

- [13] U. Kogelschatz, "Dielectric-barrier Discharges : Their History, Discharge Physics, and Industrial Applications," *Plasma Chem. Plasma Process.*, vol. 23, no. 1, pp. 1–46, 2003.
- [14] H.-H. Kim, "Nonthermal Plasma Processing for Air-Pollution Control: A Historical Review, Current Issues, and Future Prospects," *Plasma Process. Polym.*, vol. 1, no. 2, pp. 91–110, 2004.
- [15] X. Xu, "Dielectric barrier discharge - Properties and applications," *Thin Solid Films*, vol. 390, no. 1–2, pp. 237–242, 2001.
- [16] U. Kogelschatz, "Atmospheric-pressure plasma technology," *Plasma Phys. Control. Fusion*, vol. 46, no. 12 B, 2004.
- [17] G. Fridman, G. Friedman, A. Gutsol, A. B. Shekhter, V. N. Vasilets, and A. Fridman, "Applied plasma medicine," *Plasma Process. Polym.*, vol. 5, no. 6, pp. 503–533, 2008.
- [18] U. Kogelschatz, B. Eliasson, W. Egli, P. I. V France, and E. Abb, "Dielectric-Barrier Discharges. Principle and Applications," *J. Phys. IV Fr. 7 Colloq. C4, supplément au J. Phys. III*, vol. 7, no. 1 997, pp. C4-47-66, 1997.
- [19] A. Mizuno, "Industrial applications of atmospheric non-thermal plasma in environmental remediation," *Plasma Phys. Control. Fusion*, vol. 49, no. 5 A, 2007.
- [20] E. E. Kunhardt, "Generation of large-volume, atmospheric-pressure, nonequilibrium plasmas," *IEEE Trans. Plasma Sci.*, vol. 28, no. 1, pp. 189–200, 2000.
- [21] J. M. Grace and L. J. Gerenser, *Plasma Treatment of Polymers*, vol. 24, no. 3–4, 2003.
- [22] O. J. Kwon, S. W. Myung, C. S. Lee, and H. S. Choi, "Comparison of the surface characteristics of polypropylene films treated by Ar and mixed gas (Ar/O₂) atmospheric pressure plasma," *J. Colloid Interface Sci.*, vol. 295, no. 2, pp. 409–416, 2006.
- [23] N.-Y. Cui and N. M. D. Brown, "Modification of the surface properties of a polypropylene (PP) film using an air dielectric barrier discharge plasma," *Appl. Surf. Sci.*, vol. 189, no. 1–2, pp. 31–38, 2002.

- [24] P. Esena, C. Riccardi, S. Zanini, M. Tontini, G. Poletti, and F. Orsini, "Surface modification of PET film by a DBD device at atmospheric pressure," *Surf. Coatings Technol.*, vol. 200, no. 1–4 SPEC. ISS., pp. 664–667, 2005.
- [25] K. G. Kostov, A. L. R. dos Santos, R. Y. Honda, P. A. P. Nascente, M. E. Kayama, M. A. Algatti, and R. P. Mota, "Treatment of PET and PU polymers by atmospheric pressure plasma generated in dielectric barrier discharge in air," *Surf. Coatings Technol.*, vol. 204, no. 18–19, pp. 3064–3068, 2010.
- [26] Z. Fang, L. Hao, H. Yang, X. Xie, Y. Qiu, and K. Edmund, "Polytetrafluoroethylene surface modification by filamentary and homogeneous dielectric barrier discharges in air," *Appl. Surf. Sci.*, vol. 255, no. 16, pp. 7279–7285, 2009.
- [27] T. Shao, C. Zhang, K. Long, D. Zhang, J. Wang, P. Yan, and Y. Zhou, "Surface modification of polyimide films using unipolar nanosecond-pulse DBD in atmospheric air," *Appl. Surf. Sci.*, vol. 256, no. 12, pp. 3888–3894, 2010.
- [28] C. S. Ren, K. Wang, Q. Y. Nie, D. Z. Wang, and S. H. Guo, "Surface modification of PE film by DBD plasma in air," *Appl. Surf. Sci.*, vol. 255, no. 5 PART 2, pp. 3421–3425, 2008.
- [29] G. Borcia, C. A. Anderson, and N. M. D. Brown, "The surface oxidation of selected polymers using an atmospheric pressure air dielectric barrier discharge. Part I," *Appl. Surf. Sci.*, vol. 221, no. 1–4, pp. 203–214, 2004.
- [30] M. Kormunda, T. Homola, J. Matousek, D. Kovacik, M. Cernak, and J. Pavlik, "Surface analysis of poly(ethylene naphthalate) (PEN) films treated at atmospheric pressure using diffuse coplanar surface barrier discharge in air and in nitrogen," *Polym. Degrad. Stab.*, vol. 97, no. 4, pp. 547–553, 2012.
- [31] T. Homola, J. Matoušek, B. Hergelová, M. Kormunda, L. Y. L. Wu, and M. Černák, "Activation of poly(methyl methacrylate) surfaces by atmospheric pressure plasma," *Polym. Degrad. Stab.*, vol. 97, no. 6, pp. 886–892, 2012.
- [32] N.-Y. Cui, D. J. Upadhyay, C. a. Anderson, and N. M. D. Brown, "Study of the surface modification of a Nylon-6,6 film processed in an atmospheric pressure air dielectric barrier discharge," *Surf. Coatings Technol.*, vol. 192, no. 1, pp. 94–100, 2005.

- [33] G. Borcia, C. . Anderson, and N. M. . Brown, "The surface oxidation of selected polymers using an atmospheric pressure air dielectric barrier discharge. Part II," *Appl. Surf. Sci.*, vol. 225, no. 1–4, pp. 186–197, 2004.
- [34] D. J. Upadhyay, N.-Y. Cui, C. a. Anderson, and N. M. D. Brown, "A comparative study of the surface activation of polyamides using an air dielectric barrier discharge," *Colloids Surfaces A Physicochem. Eng. Asp.*, vol. 248, no. 1–3, pp. 47–56, 2004.
- [35] J. Kim, M. K. Chaudhury, M. J. Owen, and T. Orbeck, "The mechanisms of hydrophobic recovery of polydimethylsiloxane elastomers exposed to partial electrical discharges," *J. Colloid Interface Sci.*, vol. 244, no. 1, pp. 200–207, 2001.
- [36] M. Pascual, R. Balart, L. Sánchez, O. Fenollar, and O. Calvo, "Study of the aging process of corona discharge plasma effects on low density polyethylene film surface," *J. Mater. Sci.*, vol. 43, no. 14, pp. 4901–4909, 2008.
- [37] T. Jacobs, N. De Geyter, R. Morent, S. Van Vlierberghe, P. Dubruel, and C. Leys, "Plasma modification of PET foils with different crystallinity," *Surf. Coatings Technol.*, vol. 205, no. SUPPL. 2, pp. S511–S515, 2011.
- [38] F. Rossi, O. Kylián, H. Rauscher, M. Hasiwa, and D. Gilliland, "Low pressure plasma discharges for the sterilization and decontamination of surfaces," *New J. Phys.*, vol. 11, no. June 2014, 2009.
- [39] D. Dobrynin, G. Fridman, G. Friedman, and A. Fridman, "Physical and biological mechanisms of direct plasma interaction with living tissue," *New J. Phys.*, vol. 11, 2009.
- [40] M. Hähnel, T. Von Woedtke, and K. D. Weltmann, "Influence of the air humidity on the reduction of Bacillus spores in a defined environment at atmospheric pressure using a dielectric barrier surface discharge," *Plasma Process. Polym.*, vol. 7, pp. 244–249, 2010.
- [41] N. De Geyter and R. Morent, "Nonthermal Plasma Sterilization of Living and Nonliving Surfaces," *Annu. Rev. Biomed. Eng.*, vol. 14, no. 1, pp. 255–274, 2012.

- [42] A. G. Erlat, B. M. Henry, J. J. Ingram, D. B. Mountain, A. McGuigan, R. P. Howson, C. R. M. Grovenor, G. A. D. Briggs, and Y. Tsukahara, "Characterisation of aluminium oxynitride gas barrier films," *Thin Solid Films*, vol. 388, no. 1–2, pp. 78–86, 2001.
- [43] K. Ozeki, I. Nagashima, Y. Ohgoe, K. K. Hirakuri, H. Mukaibayashi, and T. Masuzawa, "Gas barrier properties of diamond-like carbon films coated on PTFE," *Appl. Surf. Sci.*, vol. 255, no. 16, pp. 7286–7290, 2009.
- [44] J. Fahlteich, M. Fahland, W. Schönberger, and N. Schiller, "Permeation barrier properties of thin oxide films on flexible polymer substrates," *Thin Solid Films*, vol. 517, no. 10, pp. 3075–3080, 2009.
- [45] O. Polonskyi, O. Kylián, M. Petr, A. Choukourov, J. Hanuš, and H. Biederman, "Gas barrier properties of hydrogenated amorphous carbon films coated on polyethylene terephthalate by plasma polymerization in argon/n-hexane gas mixture," *Thin Solid Films*, vol. 540, pp. 65–68, 2013.
- [46] P. Favia, "Plasma deposited coatings for biomedical materials and devices: Fluorocarbon and PEO-like coatings," *Surf. Coatings Technol.*, vol. 211, pp. 50–56, 2012.
- [47] S. G. Wise, A. Waterhouse, A. Kondyurin, M. M. Bilek, and A. S. Weiss, "Plasma-based biofunctionalization of vascular implants," *Nanomedicine*, vol. 7, no. 12, pp. 1907–16, 2012.
- [48] S. Bhatt, J. Pulpytel, and F. Arefi-Khonsari, "Low and atmospheric plasma polymerisation of nanocoatings for bio-applications," *Surf. Innov.*, vol. 3, no. 2, pp. 63–83, 2015.
- [49] A. Choukouro, I. Gordeev, O. Polonskyi, A. Artemenko, L. Hanyková, I. Krakovský, O. Kylián, D. Slavínská, and H. Biederman, "Polyethylene (ethylene oxide)-like plasma polymers produced by plasma-assisted vacuum evaporation," *Plasma Process. Polym.*, vol. 7, no. 6, pp. 445–458, 2010.
- [50] J. Berndt, H. Acid, E. Kovacevic, C. Cachoncinlle, T. Strunskus, and L. Boufendi, "Deposition and tuning of nanostructured hydrocarbon deposits: From superhydrophobic to superhydrophilic and back," *J. Appl. Phys.*, vol. 113, no. 6, 2013.

- [51] A. Milella, R. Di Mundo, F. Palumbo, P. Favia, F. Fracassi, and R. d'Agostino, "Plasma nanostructuring of polymers: Different routes to superhydrophobicity," *Plasma Process. Polym.*, vol. 6, no. 6–7, pp. 460–466, 2009.
- [52] L. M. Lacroix, M. Lejeune, L. Ceriotti, M. Kormunda, T. Meziani, P. Colpo, and F. Rossi, "Tuneable rough surfaces: A new approach for elaboration of superhydrophobic films," *Surf. Sci.*, vol. 592, no. 1–3, pp. 182–188, 2005.
- [53] V. Zaporojtchenko, R. Podschun, U. Schürmann, A. Kulkarni, and F. Faupel, "Physico-chemical and antimicrobial properties of co-sputtered Ag-Au/PTFE nanocomposite coatings," *Nanotechnology*, vol. 17, no. 19, pp. 4904–4908, 2006.
- [54] K. Vasilev, S. S. Griesser, and H. J. Griesser, "Antibacterial surfaces and coatings produced by plasma techniques," *Plasma Process. Polym.*, vol. 8, no. 11, pp. 1010–1023, 2011.
- [55] J. Hasan, R. J. Crawford, and E. P. Ivanova, "Antibacterial surfaces: The quest for a new generation of biomaterials," *Trends Biotechnol.*, vol. 31, no. 5, pp. 295–304, 2013.
- [56] H. Yasuda, *Plasma Polymerization*. 1985.
- [57] R. D'Agostino, P. Favia, Y. Kawai, H. Ikegami, N. Sato, and F. Arefi-Khonsari, "Advanced Plasma Technology," *Adv. Plasma Technol.*, pp. 1–457, 2008.
- [58] D. K. Lam, R. F. Baddour, and A. F. Stancell, "A Mechanisms and Kinetics Study of Polymeric Thin-Film Deposition in Glow Discharge," *J. Macromol. Sci. Part A - Chem.*, vol. 10, no. 3, pp. 421–450, 1976.
- [59] H. U. Poll, M. Arzt, and K. H. Wickleder, "Reaction kinetics in the polymerization of thin films on the electrodes of a glow-discharge gap," *Eur. Polym. J.*, vol. 12, no. 8, pp. 505–512, 1976.
- [60] D. Thiry, S. Konstantinidis, J. Cornil, and R. Snyders, "Plasma diagnostics for the low-pressure plasma polymerization process: A critical review," *Thin Solid Films*, vol. 606, pp. 19–44, 2016.
- [61] H. Biederman and D. Slavínská, "Plasma polymer films and their future prospects," *Surf. Coatings Technol.*, vol. 125, no. 1–3, pp. 371–376, 2000.
- [62] H. Biederman, "Plasma polymer films," p. 386, 2004.

- [63] D. Magni, C. Deschenaux, C. Hollenstein, A. Creatore, and P. Fayet, "Oxygen diluted hexamethyldisiloxane plasmas investigated by means of in situ infrared absorption spectroscopy and mass spectrometry," *J. Phys. D. Appl. Phys.*, vol. 34, no. 1, pp. 87–94, 2001.
- [64] L. Zajíčková, V. Buršíková, V. Peřina, A. Macková, D. Subedi, J. Janča, and S. Smirnov, "Plasma modification of polycarbonates," *Surf. Coatings Technol.*, vol. 142–144, pp. 449–454, 2001.
- [65] M. Deilmann, M. Grabowski, S. Theiß, N. Bibinov, and P. Awakowicz, "Permeation mechanisms of pulsed microwave plasma deposited silicon oxide films for food packaging applications," *J. Phys. D. Appl. Phys.*, vol. 41, no. 13, p. 135207, 2008.
- [66] J. Schneider, M. I. Akbar, J. Dutroncy, D. Kiesler, M. Leins, A. Schulz, M. Walker, U. Schumacher, and U. Stroth, "Silicon oxide barrier coatings deposited on polymer materials for applications in food packaging industry," *Plasma Process. Polym.*, vol. 6, no. SUPPL. 1, pp. 700–704, 2009.
- [67] E. Schmachtenberg, F. R. Costa, and S. Göbel, "Microwave assisted HMDSO/oxygen plasma coated polyethylene terephthalate films: Effects of process parameters and uniaxial strain on gas barrier properties, surface morphology, and chemical composition," *J. Appl. Polym. Sci.*, vol. 99, no. 4, pp. 1485–1495, 2006.
- [68] A. Grüniger, A. Bieder, A. Sonnenfeld, P. R. von Rohr, U. Müller, and R. Hauert, "Influence of film structure and composition on diffusion barrier performance of SiO_x thin films deposited by PECVD," *Surf. Coatings Technol.*, vol. 200, no. 14–15, pp. 4564–4571, 2006.
- [69] D. G. Howells, B. M. Henry, J. Madocks, and H. E. Assender, "High quality plasma enhanced chemical vapour deposited silicon oxide gas barrier coatings on polyester films," *Thin Solid Films*, vol. 516, no. 10, pp. 3081–3088, 2008.
- [70] D. Hegemann, H. Brunner, and C. Oehr, "Deposition rate and three-dimensional uniformity of RF plasma deposited SiO_x films," *Surf. Coatings Technol.*, vol. 142–144, pp. 849–855, 2001.

- [71] F. Faupel, V. Zaporojtchenko, T. Strunskus, H. Greve, U. Schürmann, H. Takele, C. Hanisch, V. S. K. Chakravadhanula, N. Ni, A. Gerber, E. Quandt, and R. Podschun, "Functional polymer nanocomposites," *Polym. Polym. Compos.*, vol. 16, no. 8, pp. 471–481, 2008.
- [72] M. Rai, A. Yadav, and A. Gade, "Silver nanoparticles as a new generation of antimicrobials," *Biotechnol. Adv.*, vol. 27, no. 1, pp. 76–83, 2009.
- [73] J. R. Morones-ramirez, J. R. Morones, J. L. Elechiguerra, A. Camacho, K. Holt, J. B. Kouri, J. T. Ram, and M. J. Yacaman, "The Bactericidal Effect of Silver Nanoparticles The bactericidal effect of silver nanoparticles," no. February 2014, 2005.
- [74] C. Marambio-Jones and E. M. V. Hoek, "A review of the antibacterial effects of silver nanomaterials and potential implications for human health and the environment," *J. Nanoparticle Res.*, vol. 12, no. 5, pp. 1531–1551, 2010.
- [75] S. Eckhardt, P. S. Brunetto, J. Gagnon, M. Priebe, B. Giese, and K. M. Fromm, "Nanobio silver: Its interactions with peptides and bacteria, and its uses in medicine," *Chem. Rev.*, vol. 113, no. 7, pp. 4708–4754, 2013.
- [76] E. Sardella, P. Favia, R. Gristina, M. Nardulli, and R. d'Agostino, "Plasma-aided micro- and nanopatterning processes for biomedical applications," *Plasma Process. Polym.*, vol. 3, no. 6–7, pp. 456–469, 2006.
- [77] E. Korner, M. H. Aguirre, G. Fortunato, A. Ritter, J. Ruhe, and D. Hegemann, "Formation and distribution of silver nanoparticles in a functional plasma polymer matrix and related Ag⁺ release properties," *Plasma Process. Polym.*, vol. 7, no. 7, pp. 619–625, 2010.
- [78] S. Lischer, E. Korner, D. J. Balazs, D. Shen, P. Wick, K. Grieder, D. Haas, M. Heuberger, and D. Hegemann, "Antibacterial burst-release from minimal Ag-containing plasma polymer coatings," *J. R. Soc. Interface*, vol. 8, no. 60, pp. 1019–1030, 2011.
- [79] C. Saulou, B. Despax, P. Raynaud, S. Zanna, A. Seyeux, P. Marcus, J. N. Audinot, and M. Mercier-Bonin, "Plasma-mediated nanosilver-organosilicon composite films deposited on stainless steel: Synthesis, surface characterization, and evaluation of anti-adhesive and anti-microbial properties on the model yeast *saccharomyces cerevisiae*," *Plasma Process. Polym.*, vol. 9, no. 3, pp. 324–338, 2012.

- [80] J. Y. Liu and R. H. Hurt, "Ion release kinetics and particle persistence in aqueous nano-silver colloids," *Environ. Sci. Technol.*, vol. 44, pp. 2169–2175, 2010.
- [81] I. H. E.-S. and M. A. E.-S. Prashant K. Jain, Xiaohua Huang, "Noble Metals on the Nanoscale: Optical and Photothermal Properties and Some Applications in Imaging, Sensing, Biology, and Medicine," *Acc. Chem. Res.*, vol. 41, no. 12, pp. 1578–1586, 2008.
- [82] H. Haberland, M. Karrais, M. Mall, and Y. Thurner, "Thin films from energetic cluster impact: A feasibility study," *J. Vac. Sci. Technol. A Vacuum, Surfaces, Film.*, vol. 10, no. 5, pp. 3266–3271, 1992.
- [83] H. Haberland, "Filling of micron-sized contact holes with copper by energetic cluster impact," *J. Vac. Sci. Technol. A Vacuum, Surfaces, Film.*, vol. 12, no. 5, p. 2925, 1994.
- [84] C. Bréchnac, P. Cahuzac, F. Carlier, M. de Frutos, and A. Masson, C. Mory, C. Colliex, and B. Yoon, "Size effects in nucleation and growth processes from preformed soft-landed clusters," *Phys. Rev. B*, vol. 57, no. 4, pp. R2084–R2087, 1998.
- [85] F. Frank, W. Schulze, B. Tesche, J. Urban, and B. Winter, "Formation of metal clusters and molecules by means of the gas aggregation technique and characterisation of size distribution," *Surf. Sci.*, vol. 156, no. PART 1, pp. 90–99, 1985.
- [86] K. Sattler, J. Mühlbach, and E. Recknagel, "Generation of metal clusters containing from 2 to 500 atoms," *Phys. Rev. Lett.*, vol. 45, no. 10, pp. 821–824, 1980.
- [87] O. Polonskyi, P. Solař, O. Kylián, M. Drábik, A. Artemenko, J. Kousal, J. Hanuš, J. Pešička, I. Matolínová, E. Kolíbalová, D. Slavínská, and H. Biederman, "Nanocomposite metal/plasma polymer films prepared by means of gas aggregation cluster source," *Thin Solid Films*, vol. 520, no. 12, pp. 4155–4162, 2012.
- [88] O. Kylián, J. Prokeš, O. Polonskyi, J. Čechvala, J. Kousal, J. Pešička, J. Hanuš, and H. Biederman, "Deposition and characterization of Pt nanocluster films by means of gas aggregation cluster source," *Thin Solid Films*, vol. 571, no. P1, pp. 13–17, 2014.

- [89] M. Drabik, A. Choukourov, A. Artemenko, O. Polonskyi, O. Kylian, J. Kousal, L. Nichtova, V. Cimrova, D. Slavinska, and H. Biederman, "Structure and composition of titanium nanocluster films prepared by a gas aggregation cluster source," *J. Phys. Chem. C*, vol. 115, no. 43, pp. 20937–20944, 2011.
- [90] O. Kylián, J. Kratochvíl, J. Hanuš, O. Polonskyi, P. Solař, and H. Biederman, "Fabrication of Cu nanoclusters and their use for production of Cu/plasma polymer nanocomposite thin films," *Thin Solid Films*, vol. 550, pp. 46–52, 2014.
- [91] A. Shelemin, O. Kylián, J. Hanuš, A. Choukourov, I. Melnichuk, A. Serov, D. Slavínská, and H. Biederman, "Preparation of metal oxide nanoparticles by gas aggregation cluster source," *Vacuum*, vol. 120, pp. 162–169, 2015.
- [92] A. Serov, A. Choukourov, A. Artemenko, A. Kuzminova, H. Biederman, and M. Hrabovsky, "Deposition of Fluorocarbon Plasma Polymer Nanoparticles and their Basic Properties," *Plasma Phys. Technol.*, pp. 75–77, 2015.
- [93] P. Solař, I. Melnichuk, A. Artemenko, O. Polonskyi, O. Kylián, A. Choukourov, D. Slavínská, and H. Biederman, "Nylon-sputtered plasma polymer particles produced by a semi-hollow cathode gas aggregation source," *Vacuum*, vol. 111, pp. 124–130, 2015.
- [94] O. Kylián, A. Kuzminova, M. Vaydulych, M. Cieslar, I. Khalakhan, J. Hanuš, A. Choukourov, D. Slavínská, and H. Biederman, "Core@shell Cu/hydrocarbon plasma polymer nanoparticles prepared by gas aggregation cluster source followed by in-flight plasma polymer coating," *Plasma Process. Polym.*, vol. 15, no. 1, pp. 1–7, 2018.
- [95] J. Hanuš, T. Steinhartová, O. Kylián, J. Kousal, P. Malinský, A. Choukourov, A. Macková, and H. Biederman, "Deposition of Cu/a-C:H Nanocomposite Films," *Plasma Process. Polym.*, vol. 13, no. 9, pp. 879–887, 2016.
- [96] J. Hanuš, H. Libenská, I. Khalakhan, A. Kuzminova, O. Kylián, and H. Biederman, "Localized surface plasmon resonance tuning via nanostructured gradient Ag surfaces," *Mater. Lett.*, vol. 192, pp. 119–122, 2017.

- [97] P. Solař, O. Polonskyi, A. Choukourov, A. Artemenko, J. Hanuš, H. Biederman, and D. Slavínská, "Nanostructured thin films prepared from cluster beams," *Surf. Coatings Technol.*, vol. 205, no. SUPPL. 2, pp. 42–47, 2011.
- [98] R. Pearse and A. Gaydon, "Identification of molecular spectra." Chapman and Hall, 1976.
- [99] T. R. Thomas, "Rough surfaces," *Longman Gr.*, vol. 153, 1982.
- [100] P. Solař, "Solarius Particles." 2012.
- [101] M. L. Watson, "Staining of Tissue Sections for Electron Microscopy with Heavy Metals," *J. Cell Biol.*, vol. 4, no. 4, pp. 475–478, 1958.
- [102] E. Suzuki, "High-resolution scanning electron microscopy of immunogold-labelled cells by the use of thin plasma coating of osmium," *J. Microsc.*, vol. 208, no. August, pp. 153–157, 2002.
- [103] V. der H. Paul, "X-ray photoelectron spectroscopy: an introduction to principles and practices," *John Wiley Sons*, 2011.
- [104] J. Moulder, "Handbook of X-ray photoelectron spectroscopy: a reference book of standard spectra for identification and interpretation of XPS data," 1992.
- [105] H. Fujiwara, "Spectroscopic Ellipsometry: principles and applications," 2007.
- [106] H. Tompkins and I. Eugene A., "Handbook of Ellipsometry," 2005.
- [107] A. Montaser, *Inductively coupled plasma mass spectrometry*. John Wiley & Sons, 1998.
- [108] X. Li and B. Bhushan, "A review of nanoindentation continuous stiffness measurement technique and its applications," *Mater. Charact.*, vol. 48, no. 1, pp. 11–36, 2002.
- [109] W. C. Oliver and G. M. Pharr, "Measurement of hardness and elastic modulus by instrumented indentation: Advances in understanding and refinements to methodology," *J. Mater. Res.*, vol. 19, no. 1, pp. 3–20, 2004.
- [110] Hysitron, "nanoDMA III User Manual," 2011.
- [111] O. Bakhtiari, S. Mosleh, T. Khosravi, and T. Mohammadi, "Preparation, Characterization and Gas Permeation of Polyimide Mixed Matrix Membranes," *J. Membr. Sci. Technol.*, vol. 1, no. 1, pp. 1–6, 2011.
- [112] H.-H. Perkampus, "UV-VIS Spectroscopy and its Applications," 2013.

- [113] N. Alissawi, T. Peter, T. Strunskus, C. Ebbert, G. Grundmeier, and F. Faupel, "Plasma-polymerized HMDSO coatings to adjust the silver ion release properties of Ag/polymer nanocomposites," *J. Nanoparticle Res.*, vol. 15, no. 11, 2013.
- [114] M. Strobel and C. S. Lyons, "An essay on contact angle measurements," *Plasma Process. Polym.*, vol. 8, no. 1, pp. 8–13, 2011.
- [115] F. M. Fowkes, "Attractive Forces At Interfaces," *Ind. Eng. Chem.*, vol. 56, no. 12, pp. 40–52, 1964.
- [116] D. K. Owens and R. C. Wendt, "Estimation of the surface free energy of polymers," *J. Appl. Polym. Sci.*, vol. 13, no. 8, pp. 1741–1747, 1969.
- [117] A. Shaw, P. Seri, C. A. Borghi, G. Shama, and F. Iza, "A reference protocol for comparing the biocidal properties of gas plasma generating devices," *J. Phys. D. Appl. Phys.*, vol. 48, no. 48, 2015.
- [118] E. Dolezalova, A. Shaw, F. Iza, M. Šimek, and G. Shama, "Study of plasma-induced inactivation of a reference micro- organism," 2014.
- [119] H. E. Wagner, R. Brandenburg, K. V. Kozlov, A. Sonnenfeld, P. Michel, and J. F. Behnke, "The barrier discharge: Basic properties and applications to surface treatment," *User Model. User-adapt. Interact.*, vol. 71, no. 3 SPEC., pp. 417–436, 2003.
- [120] A. Kuzminova, T. Kretková, O. Kylián, J. Hanuš, I. Khalakhan, V. Prukner, E. Doležalová, M. Šimek, and H. Biederman, "Etching of polymers, proteins and bacterial spores by atmospheric pressure DBD plasma in air," 2017.
- [121] T. Kretková, "Modifikace polymerních materiálů pomocí atmosférického plazmatu pro biolékařské aplikace," *Bakalářská práce*, 2011.
- [122] E. Gonzalez and R. F. Hicks, "Surface analysis of polymers treated by remote atmospheric pressure plasma," *Langmuir*, vol. 26, no. 5, pp. 3710–3719, 2010.
- [123] T. Homola, J. Matoušek, B. Hergelová, M. Kormunda, L. Y. L. Wu, and M. Černák, "Activation of poly(ethylene terephthalate) surfaces by atmospheric pressure plasma," *Polym. Degrad. Stab.*, vol. 97, no. 11, pp. 2249–2254, 2012.
- [124] D. Beamson, G. Briggse, "The XPS of Polymers Database.pdf." Manchester, UK, 2000.

- [125] M. J. Ariza, E. Rodríguez-Castellón, R. Rico, J. Benavente, M. Muñoz, and M. Oleinikova, "X-Ray Photoelectron Spectroscopy Analysis of Di-(2-ethylhexyl) Phosphoric Acid Activated Membranes.," *J. Colloid Interface Sci.*, vol. 226, no. 1, pp. 151–158, 2000.
- [126] R. Morent, N. De Geyter, T. Desmet, P. Dubruel, and C. Leys, "Plasma surface modification of biodegradable polymers: A review," *Plasma Process. Polym.*, vol. 8, no. 3, pp. 171–190, 2011.
- [127] F. Truica-Marasescu, P. Jedrzejowski, and M. R. Wertheimer, "Hydrophobic recovery of vacuum ultraviolet irradiated polyolefin surfaces," *Plasma Process. Polym.*, vol. 1, no. 2, pp. 153–163, 2004.
- [128] E. Bormashenko, G. Chaniel, and R. Grynyov, "Towards understanding hydrophobic recovery of plasma treated polymers: Storing in high polarity liquids suppresses hydrophobic recovery," *Appl. Surf. Sci.*, vol. 273, pp. 549–553, 2013.
- [129] M. H. Jung and H. S. Choi, "Photoresist etching using Ar/O₂ and He/O₂ atmospheric pressure plasma," *Thin Solid Films*, vol. 515, no. 4, pp. 2295–2302, 2006.
- [130] H. Puliyalil and U. Cvelbar, "Selective Plasma Etching of Polymeric Substrates for Advanced Applications," *Nanomaterials*, vol. 6, no. 6, p. 108, 2016.
- [131] N. S. Kasáľková, P. Slepíčka, Z. Kolská, P. Sajdl, L. Bačáková, S. Rimpelová, and V. Švorčík, "Cell adhesion and proliferation on polyethylene grafted with Au nanoparticles," *Nucl. Instruments Methods Phys. Res. Sect. B Beam Interact. with Mater. Atoms*, vol. 272, no. November 2017, pp. 391–395, 2012.
- [132] J. Liskova, O. Babchenko, M. Varga, A. Kromka, D. Hadraba, Z. Svindrych ZdenekBurdikova, and L. Bacakova, "Osteogenic cell differntation on H-terminated and O-terminated nanocrystalline diamond films," *Int. J. Nanomedicine*, vol. 10, pp. 1–16, 2015.
- [133] L. Bacakova, K. Walachova, V. Svorcik, and V. Hnatowicz, "Adhesion and proliferation of rat vascular smooth muscle cells (VSMC) on polyethylene implanted with O⁺ and C⁺ ions," *J. Biomater. Sci. Ed.*, vol. 12, no. 7, pp. 817–834, 2001.

- [134] F. Fumagalli, O. Kylián, L. Amato, J. Hanuš, and F. Rossi, “Low-pressure water vapour plasma treatment of surfaces for biomolecules decontamination,” *J. Phys. D. Appl. Phys.*, vol. 45, no. 13, p. 135203, 2012.
- [135] B. J. Park, D. H. Lee, J. C. Park, D. W. Han, I. S. Lee, S. O. Hyun, M. S. Chun, K. H. Chung, M. Aihara, and K. Takatori, “Sterilization using a microwave-induced argon plasma at atmospheric pressure,” *J. Microbiol. Biotechnol.*, vol. 10, no. 1, pp. 188–192, 2003.
- [136] S. Tseng, N. Abramzon, J. O. Jackson, and W. J. Lin, “Gas discharge plasmas are effective in inactivating *Bacillus* and *Clostridium* spores,” *Appl. Microbiol. Biotechnol.*, vol. 93, no. 6, pp. 2563–2570, 2012.
- [137] X. Deng, J. Shi, and M. Kong, “Physical mechanisms of inactivation of *Bacillus subtilis* spores using cold atmospheric plasmas,” *IEEE Trans. Plasma Sci.*, vol. 34, no. 4 II, pp. 1310–1316, 2006.
- [138] J. Shen, C. Cheng, S. Fang, H. Xie, Y. Lan, G. Ni, Y. Meng, J. Luo, and X. Wang, “Sterilization of *Bacillus subtilis* spores using an atmospheric plasma jet with argon and oxygen mixture gas,” *Appl. Phys. Express*, vol. 5, no. 3, 2012.
- [139] T. G. Klämpfl, G. Isbary, T. Shimizu, Y. F. Li, J. L. Zimmermann, W. Stolz, J. Schlegel, G. E. Morfill, and H. U. Schmidt, “Cold atmospheric air plasma sterilization against spores and other microorganisms of clinical interest,” *Appl. Environ. Microbiol.*, vol. 78, no. 15, pp. 5077–5082, 2012.
- [140] C. Hertwig, V. Steins, K. Reineke, A. Rademacher, M. Klocke, C. Rauh, and O. Schluter, “Impact of surface structure and feed gas composition on *Bacillus subtilis* endospore inactivation during direct plasma treatment,” *Front. Microbiol.*, vol. 6, no. AUG, pp. 1–12, 2015.
- [141] Y. F. Hong, J. G. Kang, H. Y. Lee, H. S. Uhm, E. Moon, and Y. H. Park, “Sterilization effect of atmospheric plasma on *Escherichia coli* and *Bacillus subtilis* endospores,” *Lett. Appl. Microbiol.*, vol. 48, no. 1, pp. 33–37, 2009.
- [142] R. Lamendola, R. d’Agostino, and F. Fracassi, “Thin film deposition from hexamethyldisiloxane fed glow discharges,” *Plasmas Polym.*, vol. 2, no. 3, pp. 147–164, 1997.

- [143] D. Hegemann, U. Vohrer, C. Oehr, and R. Riedel, "Deposition of SiO_x films from O₂/HMDSO plasmas," *Surf. Coatings Technol.*, vol. 116–119, pp. 1033–1036, 1999.
- [144] J. Kratochvíl, A. Kuzminova, O. Kylián, and H. Biederman, "Comparison of magnetron sputtering and gas aggregation nanoparticle source used for fabrication of silver nanoparticle films," *Surf. Coatings Technol.*, vol. 275, pp. 296–302, 2015.
- [145] S. Peng, J. M. McMahon, G. C. Schatz, S. K. Gray, and Y. Sun, "Reversing the size-dependence of surface plasmon resonances," *Proc. Natl. Acad. Sci.*, vol. 107, no. 33, pp. 14530–14534, 2010.
- [146] N. E. Blanchard, V. V. Naik, T. Geue, O. Kahle, D. Hegemann, and M. Heuberger, "Response of Plasma-Polymerized Hexamethyldisiloxane Films to Aqueous Environments," *Langmuir*, vol. 31, no. 47, pp. 12944–12953, 2015.
- [147] H. Dickert, K. Machka, and I. Braveny, "The uses and limitations of disc diffusion in the antibiotic sensitivity testing of bacteria," *Infection*, vol. 9, no. 1, pp. 18–24, 1981.
- [148] O. Kylián, J. Kratochvíl, M. Petr, A. Kuzminova, D. Slavínská, H. Biederman, and J. Beranová, "Ag/C: F Antibacterial and hydrophobic nanocomposite coatings," *Funct. Mater. Lett.*, vol. 10, no. 3, 2017.
- [149] A. Kuzminova, J. Beranova, O. Kylian, J. Hanus, and H. Biederman, "Ag/Al_xO_y nanocomposites prepared by means of gas aggregation source and RF magnetron sputtering of Al₂O₃ target," 27th Symposium on Plasma Physics and Technology, June 20–23, 2016, Prague, Czech Republic.
- [150] A. Kuzminova, A. Shelemin, J. Beranova, O. Kylian, J. Hanus, and H. Biederman, "Antibacterial activity of containing nanocomposites prepared by means of gas aggregation source," 16th Joint Vacuum Conference, June 6–10, 2016, Portoroz, Slovenia.
- [151] A. Kuzminova, J. Kratochvíl, O. Kylián, H. Langhansová, J. Lieskovská, J. Štěrbá, V. Straňák, and H. Biederman, "Antibacterial and non-fouling Cu/C:F nanocomposites deposited onto poly(ether-ether- ketone) foils," XXXIII International Conference on Phenomena in Ionized Gases, July 9–14, 2017, Lisbon, Portugal.

- [152] M. Petr, “Ultra tenké vrstvy nanášené magnetronovým naprašováním a jejich charakterizace,” 2016.
- [153] G. Schön, J. Tummavuori, B. Lindström, C. R. Enzell, C. R. Enzell, and C.-G. Swahn, “ESCA Studies of Ag, Ag₂O and AgO,” *Acta Chemica Scandinavica*, vol. 27, pp. 2623–2633, 1973.
- [154] R. N. Wenzel, “Resistance of Solid Surfaces To Wetting By Water,” *Ind. Eng. Chem.*, vol. 28, no. 8, pp. 988–994, 1936.
- [155] O. Kylián, O. Polonskyi, J. Kratochvíl, A. Artemenko, A. Choukourov, M. Drábik, P. Solař, D. Slavínská, and H. Biederman, “Control of wettability of plasma polymers by application of Ti nano-clusters,” *Plasma Process. Polym.*, vol. 9, no. 2, pp. 180–187, 2012.
- [156] B. D. Cassie, “Of porous surfaces,” *Physics (College. Park. Md.)*, vol. 40, no. 5, pp. 546–551, 1944.
- [157] Y. Leterrier, “Durability of nanosized oxygen-barrier coatings on polymers,” *Prog. Mater. Sci.*, vol. 48, no. 1, pp. 1–55, 2003.
- [158] S. Vasquez-Borucki, W. Jacob, and C. A. Achete, “Amorphous hydrogenated carbon films as barrier for gas permeation through polymer films,” *Diam. Relat. Mater.*, vol. 9, no. 12, pp. 1971–1978, 2000.
- [159] N. Schwarzer, “Coating design due to analytical modelling of mechanical contact problems on multilayer systems,” *Surf. Coatings Technol.*, vol. 133–134, pp. 397–402, Nov. 2000.

List of tables

Table 2.1 Polymers used in this study with their chemical structure.

Table 2.2 The polar and dispersive surface energies.

Table 3.1 Chemical composition of untreated and DBD plasma treated polymeric foils measured by XPS.

Table 3.2 RMS roughness of untreated and DBD treated polymeric foils.

Table 3.3 WCA of untreated and DBD plasma treated polymeric foils.

Table 3.4 Number of Saos-2 and HUVEC cells on untreated and DBD plasma treated PET foils.

Table 3.5 Number of survived bacterial spores and corresponding log reduction in dependence on the treatment time.

Table 3.6 Chemical composition of nanocomposites based on silver nanoparticles inside pHMDSO and SiO_x matrixes. Thickness of overcoat was 10 nm.

Table 3.7 Chemical composition of Ag nanoparticle before and after O₂ treatment. Nanoparticles were deposited on gold substrate.

List of abbreviations

PP	Polypropylene
PE	Polyethylene
LDPE	Low density polyethylene
HDPE	High density polyethelene
MDPE	Medium density polyethelene
LLDPE	Linear low density polyethelene
PET	Polyethylene terephthalate
PEN	Polyethylene naphthalate
PEEK	Polyether ether ketone
PMMA	Polymethyl methacrylate
PLA	Polylactic acid
AGM	Dielectric barrier discharge
PE-CVD	Plasma enhanced chemical vapor deposition
AGM	Activated growth model
HMDSO	Hexamethyldisiloxane
pHMDSO	Polymerized hexamethyldisiloxane
GAS	Gas aggregation source
NPs	Nanoparticles
OES	Optical emission spectroscopy
AFM	Atomic force microscopy
SEM	Scanning electron microscopy
XPS	X-ray photoelectron spectroscopy
ICP-MS	Inductively coupled plasma mass spectrometry
nanoDMA	Nano dynamic mechanical analysis
UV-VIS	Ultraviolet–visible spectroscopy
WCA	Water contact angle
CFU	Colony forming unit
PTFE	Polytetrafluoroethylene
LB	Luria-Bertani
PBS	Phosphate-buffered saline
LSPR	Localized surface plasmon resonance

Author's contribution

The author of the work performed all DBD plasma treatments of polymeric foils. She participated in the development, installation and adjustment of the experimental setups for deposition of thin films by PE-CVD method as well as for deposition of silver nanoparticles by means of gas aggregation source. The author prepared all samples for antibacterial tests, ion release measurements, wettability and permeability measurements. The following analyses of prepared samples were performed solely by the author: the contact angle measurements, AFM, UV-VIS, FTIR and permeability measurements. In the case of advanced surface characterization techniques and biological tests she collaborated with Mgr. Jan Hanuš PhD. (XPS), Mgr. Jaroslav Kousal PhD. (ellipsometry), doc. Ing. Andrey Shukurov PhD. (nanoDMA), Mgr. Ivan Khalakhan PhD. (SEM), RNDr. Jana Beranová PhD. (antibacterial tests) and RNDr. Marta Vandrovcová PhD. (cell tests). The author participated in processing and evaluation of obtained data. Furthermore, she worked together with Ing. Eva Doležalová PhD. to measure the bactericidal efficiency of DBD plasma.

List of publications

Reviewed international journals

1. **A. Kuzminova**, A. Shelemin, O. Kylián, M. Petr, J. Kratochvíl, P. Solař, and H. Biederman, "From super-hydrophilic to super-hydrophobic surfaces using plasma polymerization combined with gas aggregation source of nanoparticles," *Vacuum*, vol. 110, pp. 58–61, 2014.
2. **A. Kuzminova**, A. Shelemin, O. Kylián, A. Choukourov, H. Valentová, I. Krakovský, J. Nedbal, D. Slavínská, and H. Biederman, "Study of the effect of atmospheric pressure air dielectric barrier discharge on nylon 6,6 foils," *Polym. Degrad. Stab.*, vol. 110, pp. 378–388, 2014.
3. A. Serov, A. Choukourov, I. Melnichuk, A. Shelemin, **A. Kuzminova**, O. Kylián, J. Hanuš, J. Kousal, M. Drábik, D. Slavínská, and H. Biederman, "Poly(tetrafluoroethylene) sputtering in a gas aggregation source for fabrication of nano-structured deposits," *Surf. Coatings Technol.*, vol. 254, pp. 319–326, 2014.
4. **A. Kuzminova**, M. Vandrovcová, A. Shelemin, O. Kylián, A. Choukourov, J. Hanuš, L. Bačáková, D. Slavínská, and H. Biederman, "Treatment of poly(ethylene terephthalate) foils by atmospheric pressure air dielectric barrier discharge and its influence on cell growth," *Appl. Surf. Sci.*, vol. 357, pp. 689–695, 2015.
5. J. Kratochvíl, **A. Kuzminova**, O. Kylián, and H. Biederman, "Comparison of magnetron sputtering and gas aggregation nanoparticle source used for fabrication of silver nanoparticle films," *Surf. Coatings Technol.*, vol. 275, pp. 296–302, 2015.
6. **A. Kuzminova**, J. Beranová, O. Polonskyi, A. Shelemin, O. Kylián, A. Choukourov, D. Slavínská, and H. Biederman, "Antibacterial nanocomposite coatings produced by means of gas aggregation source of silver nanoparticles," *Surf. Coatings Technol.*, vol. 294, pp. 225–230, 2016.
7. M. Petr, O. Kylián, J. Hanuš, **A. Kuzminova**, M. Vaidulych, I. Khalakhan, A. Choukourov, D. Slavínská, and H. Biederman, "Surfaces With Roughness Gradient and Invariant Surface Chemistry Produced by Means of Gas Aggregation Source and Magnetron Sputtering," *Plasma Process. Polym.*, vol. 13, no. 6, pp. 663–671, 2016.

8. **A. Kuzminova**, T. Kretková, O. Kylián, J. Hanuš, I. Khalakhan, V. Prukner, E. Doležalová, M. Šimek, and H. Biederman, "Etching of polymers, proteins and bacterial spores by atmospheric pressure DBD plasma in air," vol. 50, art. no 135201, 2017.
9. O. Kylián, J. Kratochvíl, M. Petr, **A. Kuzminova**, D. Slavínská, H. Biederman, and J. Beranová, "Ag/C: F Antibacterial and hydrophobic nanocomposite coatings," *Funct. Mater. Lett.*, vol. 10, no. 3, art. no. 1750029, 2017.
10. J. Hanuš, H. Libenská, I. Khalakhan, **A. Kuzminova**, O. Kylián, and H. Biederman, "Localized surface plasmon resonance tuning via nanostructured gradient Ag surfaces," *Mater. Lett.*, vol. 192, pp. 119–122, 2017.
11. O. Kylian, A. Shelemin, P. Solar, A. Choukourov, J. Hanus, M. Vaidulych, **A. Kuzminova**, and H. Biederman, "Plasma polymers: From thin films to nanocolumnar coatings," *Thin Solid Films*, vol. 630, pp. 86–91, 2017.
12. M. Petr, O. Kylián, **A. Kuzminova**, J. Kratochvíl, I. Khalakhan, J. Hanuš, and H. Biederman, "Noble metal nanostructures for double plasmon resonance with tunable properties," *Opt. Mater.*, vol. 64, pp. 276–281, 2017.
13. A. Choukourov, P. Pleskunov, D. Nikitin, V. Titov, A. Shelemin, M. Vaidulych, **A. Kuzminova**, P. Solar, J. Hanuš, J. Kousal, O. Kylián, D. Slavínská, and H. Biederman, "Advances and challenges in the field of plasma polymer nanoparticles," *Beilstein J. Nanotechnol.*, vol. 8, no. 1, pp. 2002–2014, 2017.
14. O. Kylián, **A. Kuzminova**, M. Vaydulych, M. Cieslar, I. Khalakhan, J. Hanuš, A. Choukourov, D. Slavínská, and H. Biederman, "Core@shell Cu/hydrocarbon plasma polymer nanoparticles prepared by gas aggregation cluster source followed by in-flight plasma polymer coating," *Plasma Process. Polym.*, vol. 15, no. 1, pp. 1–7, 2018.
15. R. Štefaníková, T. Kretková, **A. Kuzminova**, J. Hanuš, M. Vaidulych, O. Kylián and H. Biederman, "Influence of atmospheric pressure dielectric barrier discharge on wettability and drying of poly(ether-ether-ketone) foils," *Polym. Degrad. Stab.*, vol. 150, pp. 114–121, 2018.
16. V. N. Popok, C.M. Jeppesen, P. Fojan, **A. Kuzminova**, J. Hanuš and O. Kylián, "Comparative study of antibacterial properties of polystyrene films with TiO_x and Cu nanoparticles fabricated using cluster beam technique," *Beilstein J. Nanotechnol.*, vol. 9, pp. 861–869, 2018.

Conference Proceedings and other Publications

1. **A. Kuzminova**, A. Shelemin, M. Petr, O. Kylian, and H. Biederman, "Barrier Coatings on Polymeric Foils for Food Packaging," WDS, pp. 128–133, 2013.
2. **A. Kuzminova**, J. Kratochvíl, A. Shelemin, O. Kylián, H. Biederman, and J. Beranová, "Preparation of Antibacterial Silver Containing Nanocomposites," WDS, pp. 102–107, 2014.
3. **A. Kuzminova**, A. Choukourov, A. Shelemin, O. Kylián, J. Hanuš, H. Biederman: Effect of DBD plasma treatment on properties of poly(ethylene terephthalate) foils, Book of abstracts of International Conference "Eco-sustainable Food Packaging Based on Polymer Nanomaterials", 26-28 February 2014, Roma, Italy.
4. H. Biederman, O. Kylián, J. Hanuš, O. Polonskyi, A. Choukourov, A. Shelemin, **A. Kuzminova**, D. Slavinska, L. Hanykova: Low pressure plasma coatings for food packaging, International Conference "Eco-sustainable Food Packaging Based on Polymer Nanomaterials", 26-28 February 2014, Roma, Italy.
5. **A. Kuzminova**, J. Kratochvíl, A. Shelemin, O. Kylián, J. Beranová, H. Biederman: Preparation of antibacterial silver containing nanocomposites, 23rd Week of Doctoral Students, 3-5 June, Prague, Czech Republic.
6. J. Kratochvíl, O. Kylián, **A. Kuzminova**, H. Biederman: Comparison of Ag nanocluster films deposited by sputter deposition and gas aggregation nanocluster source, 26th Symposium on Plasma Physics and Technology, 16-19 June 2014, Prague, Czech Republic.
7. **A. Kuzminova**, O. Kylián, A. Shelemin, J. Hanuš, H. Biederman: Plasma modification of polymeric foils by dielectric barrier discharge in air at atmospheric pressure, 26th Symposium on Plasma Physics and Technology, 16-19 June 2014, Prague, Czech Republic.
8. O. Kylián, J. Hanuš, M. Petr, **A. Kuzminova**, J. Kratochvíl, T. Steinhartova, A. Shelemin, H. Biederman: Low pressure plasma method for fabrication of super-hydrophobic fluorine-free coatings, 26th Symposium on Plasma Physics and Technology, 16-19 June 2014, Prague, Czech Republic.

9. M. Petr, O. Kylián, **A. Kuzminova**, J. Kratochvíl, J. Hanuš, P. Solař, T. Steinhartová, A. Shelemin, H. Biederman: From Superhydrophilic to Superhydrophobic Surfaces by Plasma Polymerization, 2nd German –Czech workshop on Nanoparticles from low temperature plasma and their applications, 23-24 May 2014, Prague, Czech Republic.
10. **A. Kuzminova**, J. Kousal, P. Kudrna, A. Shelemin, H. Biederman: Treatment of nylon by dielectric barrier discharge in air, ESCAMPIG XXII, 15-19 July 2014, Greifswald, Germany.
11. O. Kylián, J. Kratochvíl, **A. Kuzminova**, T. Steinhartová, A. Shelemin, M. Petr, P. Solař, J. Hanuš, A. Choukourov, H. Biederman: Nanoparticles, nanostructures and nanocomposites prepared by gas aggregation sources , 2nd German –Czech workshop on Nanoparticles from low temperature plasma and their applications, 23-24 May 2014, Prague, Czech Republic.
12. **A. Kuzminova**, A. Shelemin, J. Hanus, O. Kylian, A. Choukourov, H. Biederman: Treatment of polymeric foils by dielectric barrier discharge in air and its influence on their subsequent coating with silver, 14th International Conference on Plasma Surface Engineering, 15 – 19 September 2014, Garmisch-Partenkirchen, Germany.
13. O. Kylian, A. Shelemin, J. Kratochvil, **A. Kuzminova**, J. Hanus, A. Choukourov, H. Biederman: From super-hydrophilic to super-hydrophobic surfaces using combination of PECVD with gas aggregation source of nanoparticles, 14th International Conference on Plasma Surface Engineering, 15 – 19 September 2014, Garmisch-Partenkirchen, Germany.
14. A. Shukurov, A. Serov, I. Melnichuk, A. Shelemin, **A. Kuzminova**, O. Kylián, J. Hanuš, J. Kousal, H. Biederman: Nano-particles of fluorocarbon plasma polymer produced by an r. f. magnetron-based gas aggregation source, 14th International Conference on Plasma Surface Engineering, 15 – 19 September 2014, Garmisch-Partenkirchen, Germany.
15. M. Petr, **A. Kuzminova**, O. Kylian, H. Biederman: Optical properties of multilayered gold, silver and magnetron sputtered polytetrafluoroethylene nanocomposite coatings. 20th International Colloquium on Plasma Processes, 1-5 June 2015 in Saint-Etienne, France.

16. M. Petr, **A. Kuzminova**, A. Shelemin, J. Hanus, P. Solar, O. Kylian, H. Biederman: Super-hydrophobic and super-hydrophilic nanocomposite films. 20th International Colloquium on Plasma Processes, 1-5 June 2015 in Saint-Etienne, France.

17. M. Petr, O. Kylián, J. Kratochvíl, T. Steinhartová, J. Hanuš, **A. Kuzminova**, A. Choukourov, H. Biederman: Nanocomposite metal/plasma polymer films deposited by gas aggregation sources of nanoparticles combined with magnetron sputtering of polymers, 22nd International Symposium on Plasma Chemistry, 5-10 July 2015, Antwerp, Belgium.

18. Marta Vandrovcova, **A. Kuzminova**, O. Kylian, A. Choukourov, A. Shelemin, D. Slavinska, L. Bacakova, H. Biederman: The influence of plasma treated polymer on cell growth, 2015 EMN Biomaterials Meeting, 10-13 April 2015, Beijing, China.

19. **A. Kuzminova**, O. Kylián, J. Beranová, A. Choukourov, O. Polonskyi, H. Biederman: Antibacterial silver containing nanocomposites prepared by gas aggregation source of nanoparticles combined with PE-CVD, 22nd International Symposium on Plasma Chemistry, 5-10 July 2015, Antwerp, Belgium.

20. O. Kylián, **A. Kuzminova**, M. Vandrovcová, A. Choukourov, A. Shelemin, D. Slavínská, L. Bačáková, H. Biederman: Treatment of poly(ethylene terephthalate) foils by atmospheric pressure air dielectric barrier discharge and its influence on cell growth, 22nd International Symposium on Plasma Chemistry, 5-10 July 2015, Antwerp, Belgium.

21. **A. Kuzminova**, J. Hanus, A. Shelemin, O. Kylian and H. Biederman, Fabrication of metal oxide nanoparticles using gas aggregation source combined with an auxiliary oxygen RF plasma, 19th International Summer School on Vacuum, Electron and Ion Technologies, 21 – 25 September 2015, Sozopol, Bulgaria. Oral presentation

22. O. Kylián, **A. Kuzminova**, M. Vandrovcová, M. Bilek, A. Shelemin, J. Hanuš, A. Choukourov, L. Bačáková, D. Slavínská, H. Biederman: Atmospheric pressure plasma treatments for biomedical applications , Bioplasmas and Plasmas with Liquids, 13-16 September, Bertinoro, Italy.

23. A. Choukourov, J. Hanus, J. Kousal, O. Kylian, P. Solar, O. Polonskyim A. Shelemin, M. Vaidulych, **A. Kuzminova**, D. Slavinska, H. Biederman: Versatility of GASes for the production of nanoscale dispersed solids, 3rd German-Czech workshop “Nanoparticles from low temperature plasma and their applications”, May 19-20, 2016, Lubeck, Germany.

24. J. Hanus, **A. Kuzminova**, A. Shelemin, J. Kousal, O. Kylian, A. Choukourov, H. Biederman: In-flight modification of nanoparticles by auxiliary plasma, 3rd German-Czech workshop “Nanoparticles from low temperature plasma and their applications”, May 19-20, 2016, Lubeck, Germany.

25. **A. Kuzminova**, A. Shelemin, J. Beranova, O. Kylian, J. Hanus, H. Biederman: Antibacterial activity of containing nanocomposites prepared by means of gas aggregation source, 16th Joint Vacuum Conference, June 6-10, 2016, Portoroz, Slovenia. Oral presentation

26. J. Kratochvíl, M. Petr, **A. Kuzminova**, J. Hanuš, O. Kylián: Gradient Thin Films for Biomedical Applications, 25th Week of Doctoral Students, June 7–9, 2016, Prague, Czech Republic.

27. **A. Kuzminova**, J. Beranova, O. Kylian, J. Hanus, H. Biederman: Ag/AlxOy nanocomposites prepared by means of gas aggregation source and RF magnetron sputtering of Al₂O₃ target, 27th Symposium on Plasma Physics and Technology, June 20 –23, 2016, Prague, Czech Republic.

28. O. Kylian, **A. Kuzminova**, A. Shelemin, J. Hanus, M. Vaidulych, J. Kousal, A. Choukourov, H. Biederman: Plasma interaction with organic materials, Workshop on Application of Advanced Plasma Technologies in Agriculture, April 17-21, 2016, Ljubljana, Slovenia.

29. O. Kylian, A. Shelemin, P. Solar, A. Choukourov, J. Hanus, M. Vaidulych, D. Nikitin, **A. Kuzminova**, M. Petr, H. Biederman: Plasma polymers: from thin films to nanoparticles and nanostructured coatings, E-MRS Spring Meeting, May 2-6, 2016, Lille, France.

30. M. Petr, **A. Kuzminova**, L. Ploux, A. Marguier, V. Roucoules, O. Kylián , H. Biederman, Surfaces with roughness gradient and invariant surface chemistry for biological applications, 27th Symposium on Plasma Physics and Technology, June 20 –23, 2016, Prague, Czech Republic.

31. J. Kratochvíl, O. Kylian, **A. Kuzminova**, M. Petr, J. Hanus, D. Slavinska, H. Biederman: Application of Ag nanoparticles prepared by GAS for antibacterial nanocomposite coatings, Nanocluster Synthesis, Characterization & Applications, May 16-19, 2016, Okinawa, Japan.
32. **A. Kuzminova**, V. Prukner, E. Doležalová, O. Kylián, M. Šimek: Atmospheric pressure plasma treatment for inactivation of bacterial spores, 6th International Conference on Plasma Medicine, September 6-9, 2016, Bratislava, Slovakia.
33. **A. Kuzminova**, M. Petr, A. Shelemin, M. Vaidulych, P. Solař, J. Hanuš, A. Choukourov, O. Kylián, J. Kousal, D. Slavínská, M. Vandrovcová, L. Bačáková, J. Beranová, H. Biederman: Plasma Surface Modification for Biomedical Applications, 6th International Conference on Plasma Medicine, September 6-9, 2016, Bratislava, Slovakia.
34. O. Kylian, A. Shelemin, P. Solar, A. Choukourov, J. Hanus, M. Vaidulych, D. Nikitin, **A. Kuzminova**, M. Petr, H. Biederman: Nanostructured plasma polymers, 7th International Symposium on Plasma Nanoscience and Nanotechnology, October 16-20, 2016, Vravrona, Greece.
35. O. Kylian, M. Petr, **A. Kuzminova**, J. Hanus, H. Libenska, M. Vaidulych, J. Kratochvíl, H. Biederman: Plasma-based technique for production of surfaces with roughness and wettability gradients, 6th International Conference on Advanced Plasma Technologies, December 11-15, 2016, Siem Reap, Cambodia.
36. M. Šubr, **A. Kuzminova**, P. Praus, O. Kylián, M. Procházka: Silver nanoislands growing on magnetron-sputtered poly-tetrafluoroethylene film with gradient plasmon resonance for the surface-enhanced spectroscopies of biomolecules, 17th European Conference on the Spectroscopy of Biological Molecules, September 11-14, 2017, Amsterdam, Netherlands
37. **A. Kuzminova**, J. Kratochvíl, O. Kylián, H. Langhansová, J. Lieskovská, J. Štěrbá, V. Straňák, H. Biederman: Antibacterial and non-fouling Cu/C:F nanocomposites deposited onto poly(ether-ether-ketone) foils, XXXIII International Conference on Phenomena in Ionized Gases, July 9-14, 2017, Lisbon, Portugal.
38. O. Kylian, **A. Kuzminova**, J. Hanus, M. Vaidulych, A. Choukourov, M. Cieslar, D. Slavinska, H. Biederman: In-flight modification of metallic nanoparticles by low pressure RF plasma, XXXIII International Conference on Phenomena in Ionized Gases, July 9-14, 2017, Lisbon, Portugal.

39. O. Kylian, **A. Kuzminova**, M. Vaydulych, M. Cieslar, J. Hanus, P. Solar, A. Choukourov and H. Biederman: In-flight deposition of plasma polymer shells onto Cu nanoparticles produced by gas aggregation source, 15th International conference on advanced materials, August 27 - September 1, 2017, Kyoto, Japan.
40. J. Kratochvíl, D. Kahoun, H. Langhansová, J. Lieskovská, P. Fojtíková, J. Štěrbá, **A. Kuzminova**, J. Kousal, J. Hanuš, O. Kylián, V. Straňák, H. Biederman: Antibacterial thin films prepared by means of low temperature plasma, 8th International Conference on Innovations in Thin Film Processing and Characterization, October 23-27, 2017, Nancy, France.
41. O. Kylián, **A. Kuzminova**, M. Vaidulych, M. Petr, J. Hanuš, M. Šubr, M. Procházka, H. Biederman: Gradient surfaces produced by plasma-based techniques, 8th International Workshop on Polymer Metal Nanocomposites, September 12-15, 2017, Prague, Czech Republic.
42. **A. Kuzminova**, O. Kylián, M. Vaydulych, M. Cieslar, I. Khalakhan, J. Hanuš, H. Biederman: Fabrication of metal/polymer core-shell nanoparticles by low-pressure plasma, 8th International Workshop on Polymer Metal Nanocomposites, September 12-15, 2017, Prague, Czech Republic.
43. J. Kratochvíl, D. Kahoun, H. Langhansová, J. Lieskovská, P. Fojtikova, J. Štěrbá, **A. Kuzminova**, J. Kousal, J. Hanuš, O. Kylián, V. Straňák, H. Biederman: Antibacterial coatings based on plasma polymers and plasma polymer nanocomposites, 8th International Workshop on Polymer Metal Nanocomposites, September 12-15, 2017, Prague, Czech Republic.
44. P. Fojan, C.M. Jeppesen, V.N. Popok, **A. Kuzminova**, J. Hanus, O. Kylian, H. Biederman: Polystyrene Films with TiO_x Nanoparticles as Antibacterial Media, 8th International Workshop on Polymer Metal Nanocomposites, September 12-15, 2017, Prague, Czech Republic.